

**HUMAN MANUAL CONTROL AS AN
INFORMATION PROCESSING CHANNEL**

by

Mircea Florian Lupu

B.S. in Automation and Computer Engineering,

“Politehnica” University of Timisoara, Romania, 2007

M.S. in Electrical Engineering, University of Pittsburgh, 2010

Submitted to the Graduate Faculty of
Swanson School of Engineering in partial fulfillment
of the requirements for the degree of

Doctor of Philosophy

University of Pittsburgh

2013

UNIVERSITY OF PITTSBURGH
SWANSON SCHOOL OF ENGINEERING

This dissertation was presented

by

Mircea Florian Lupu

It was defended on

April 5, 2013

and approved by

Zhi-Hong Mao, PhD, Associate Professor
Department of Electrical and Computer Engineering

Luis F. Chaparro, PhD, Associate Professor
Department of Electrical and Computer Engineering

Patrick J. Loughlin, PhD, Professor
Department of Electrical and Computer Engineering

Mark S. Redfern, PhD, Professor
Department of Bioengineering

Mingui Sun, PhD, Professor
Department of Electrical and Computer Engineering

Dissertation Director: Zhi-Hong Mao, PhD, Associate Professor
Department of Electrical and Computer Engineering

Copyright © by Mircea Florian Lupu
2013

HUMAN MANUAL CONTROL AS AN INFORMATION PROCESSING CHANNEL

Mircea Florian Lupu, PhD

University of Pittsburgh, 2013

Human-machine interaction (HMI) can be modeled as information flows through bidirectional communication channels, where the human receives sensory information from the machine and sends command information back to the machine. The interaction between human and machine can thus be characterized by the dynamics of information exchange measured in bits per second (b/s).

The information-transmission rate (ITR) from human to machine is expected to depend on the complexity of the machine dynamics as well as human capabilities and limitations. We propose to investigate this relationship in order to provide a quantitative measure of human performance. The HMI task considered in our investigation is a one-dimensional manual control task of an unstable system. A set of experiments are conducted where human subjects maneuver a joystick in order to stabilize an inverted pendulum simulation. Two scenarios are analyzed: when time delay affects the feedback control system, and when the degree of instability of the task is increased.

Using information- and control-theoretic approaches, we identify the lower bound for the ITR of the controller, which is dependent on the dynamics of the control task. We suggest a method adopted from time series analysis to estimate the ITR from human experiments. We believe that the difference between these two quantities allows for the assessment of human performance and for the prediction of its limitations. Additionally, the association between the estimated ITR and the power spectrum of the control signal is discussed in order to create a more complete picture of human manual control abilities and limitations.

TABLE OF CONTENTS

PREFACE	xii
1.0 INTRODUCTION	1
1.1 Motivation	1
1.2 Objectives	3
1.3 Significance	6
2.0 LITERATURE REVIEW	8
3.0 TECHNICAL PRELIMINARIES	13
3.1 Shannon’s Information Theory	13
3.2 Entropy Rate of Time Series	17
3.3 Correlation Sum Estimation from Time Series	19
4.0 METHODS	22
4.1 Human Manual Control of an Unstable System	22
4.1.1 Characteristics of Human Motor Control	22
4.1.2 Unstable System Description	24
4.1.3 Human Controller Model	26
4.2 Minimum Required Information Rate to Stabilize a Feedback Control System	27
4.2.1 Fundamental Lower Bound of Information Rate	27
4.2.2 Lower Bound of Information Rate for LTI Controllers	29
4.3 An Upper Bound of Information Rate at the “Limits of Controllability”	30
4.4 An Upper Bound of Information Rate from Human Experiments	32
4.4.1 Human Subjects Participation	32
4.4.2 Difficulties Computing the Mutual Information Rate	34

4.4.3	An Upper Bound for $I_\infty(\mathbf{y}; \mathbf{u})$	36
4.4.4	Equivalence between Shannon's Entropy Rate and the Entropy Rate of Dynamical Systems	37
4.4.5	Quantifying Intermittent Control with $h_q(m, \epsilon)$	40
4.4.6	Numerical Estimation of $h_q(m, \epsilon)$ using $q = 2$	42
4.5	Bandwidth Limitations in Feedback Control Systems	44
4.5.1	Design Trade-Offs in Feedback Control Systems	44
4.5.2	Bandwidth Constraints of Feedback Systems	47
4.5.3	Power Spectrum and Information-Transmission Rate	49
5.0	RESULTS	51
5.1	Lower Bounds of $I_\infty(\mathbf{y}; \mathbf{u})$	51
5.2	Estimation of $I_\infty(\mathbf{y}; \mathbf{u})$ using h_2 from Experiments	52
5.3	Power Spectrum Analysis of Manual Control	60
6.0	DISCUSSION	66
6.1	Information-Transmission Rate to Measure Human Performance	66
6.1.1	On Lower Bound and Upper Bound	66
6.1.2	Information-Transmission Rate and Human Performance	68
6.1.3	Comparison with Other Related Studies	69
6.1.4	On Bi-Directional Information Transmission in HMI	71
6.2	Effects of Bandwidth and Power Spectrum on Information Transmission	72
6.2.1	Effect of Time Delay	72
6.2.2	Why is the Bandwidth of Manual Control restricted to 2 Hz ?	73
6.2.3	Effect of Degree of Instability	73
6.3	On Intermittency in the Control of Unstable Systems	77
6.3.1	Balancing an Inverted Pendulum with Intermittent Control	77
6.3.2	Identifying Intermittent Control	79
6.3.3	Intermittent Control and the Correlation Entropy h_2	82
6.3.4	Limitations of the h_2 Estimation Method	82
6.4	Is Manual Control Stochastic or Deterministic?	83
7.0	CONCLUSION	88

APPENDIX A. INVERTED PENDULUM DYNAMICS	90
APPENDIX B. EXPERIMENTAL DATA	93
BIBLIOGRAPHY	95

LIST OF TABLES

1	Relationship between Shannon's entropy rate and the entropy rate of dynamical systems for discrete- and continuous dynamics.	38
2	Average values for τ used for the delay vectors.	54
3	Estimated information-transmission rate [b/s] for 12 subjects.	58
4	Reported information-transmission rates from [1].	71
5	Description of the inverted pendulum parameters.	91
6	Duration of recorded data [seconds] for 12 subjects.	93
7	Values of τ [samples] for 12 subjects.	94

LIST OF FIGURES

1	Hypothesis about the variation of the information-transmission rates with: (a) time delay, and (b) the degree of instability of the task (the arrows mark the direction of increase). The ITR can vary between an upper bound (solid line) and the lower bound (double line) required for feedback stability, ITR_{min} . This range is denoted by the dotted vertical line within the dark shaded area. The light shaded area marks the available bandwidth size.	4
2	Communication system according to Shannon [2].	8
3	Human-in-the-loop (HIL) system: the human operator generates one degree of freedom control commands to stabilize the inverted pendulum.	24
4	Parameters of the inverted pendulum: θ is the pendulum angle; L is the length of the pendulum, and x is the displacement of the bottom tip.	25
5	Human-in-the-loop (HIL) system: the manual command \mathbf{v} generated by the deterministic function K is contaminated by the remnant \mathbf{d} before delivery to the plant P	27
6	Pulse-like control signals in stabilizing highly unstable systems by the human.	31
7	Experiment setup: human operators had to maneuver a joystick to stabilize a planar inverted pendulum simulated on a computer screen. The graphical user interface (GUI) was adapted from [3].	33
8	Coarse-grained entropy rate $h_q(m, \epsilon)$ of a stochastic signal (dotted line), a deterministic signal (dashed line), and a deterministic signal with measurement noise (solid line). Figure adapted from [4].	39

9	Intermittent control in the trajectory of the pendulum angle (top), and the corresponding velocity of the control movements (bottom). Example of a predicted profile (a), and an actual profile from experiments (b) (Subject H , 5 m long pendulum, no time delay).	41
10	An LTI feedback control system with controller K and plant P : \mathbf{r} - reference signal, \mathbf{y} - output signal, \mathbf{d} - disturbance related to human movement, \mathbf{s} - disturbance of the overall system, \mathbf{n} - measurement noise.	45
11	Magnitudes of the sensitivity function and the complementary sensitivity function on log-log scale (base 10) that reflect feedback design trade-offs. The sensitivity amplification areas in the sensitivity function and the complementary sensitivity function are marked.	46
12	Probing stationarity: mean and standard deviation of the displacement x of the bottom tip of the pendulum (a), and its increment x_d (b). Ten non-overlapping segments of data are shown from subject D when a 400 ms time delay was considered.	53
13	Entropy rate estimation of $h_2(\mathbf{u})$ with no time delay. The curves correspond to the embedding dimensions 1 (circles) to 10 (stars).	55
14	Entropy rate estimation of $h_2(\mathbf{u})$ with 100 ms (a), 200ms (b), 400 ms (c), and 600 ms (d) time delay. The curves correspond to the embedding dimensions 2 (circles) to 10 (stars).	56
15	Entropy rate estimation of $h_2(\mathbf{u})$ for different pendulum lengths: 12 m (a), 8 m (b), 5 m (c), and 3 m (d). The curves correspond to embedding dimensions 2 (circles) to $m = 10$ (stars).	57
16	The variation of the information-transmission rate (ITR) with time delay (a), and with the pendulum length (b): estimated upper bound of the ITR of the human controller (solid), lower bound of the ITR according to Theorem 1 (dashed), and lower bound of the ITR according to Theorem 2 (dotted). . . .	59

17	Power spectrum of the control signal \mathbf{u} : when different time delays affected the control task (a), and when different degrees of instability were considered (b). The vertical line marks the bandwidth up to which 90% of the power was distributed.	61
18	Estimated bandwidth of the power spectrum of the closed-loop system: when different time delays affected the task (top), and when different pendulum lengths were considered (bottom).	62
19	Power spectrum of the closed-loop system: when different time delays affected the control task (a), and when different degrees of instability were considered (b). The vertical line marks the bandwidth up to which 90% of the power was distributed.	63
20	Entropy rate H_{PS} computed using the power spectrum: when different time delays affected the task (top), and when different pendulum lengths were considered (bottom).	65
21	Example of power spectrum with lower bandwidth ($f_1 < f_2$), which yields a higher information-transmission rate ($ITR_1 > ITR_2$): illustration of ITR vs. bandwidth (a); and the frequency distribution in the power spectra of the two control signals (b).	75
22	Power spectra of both the velocity of the inverted pendulum angle (a) and the velocity of the hand movement (b) exhibit peaks in the range of 0.5 – 1 Hz (adapted from [5]).	80
23	(a) The power spectrum of $\Delta z/l$ -fluctuations on log-log scale is characterized by two power law regimes with exponents $-1/2$ (upper line) and -2.5 (lower line). (b) Normalized laminar-phase probability distribution, $P(\delta t)$. The dashed line represents a power law with exponent $-3/2$. Figures adapted from [6].	81
24	Inverted pendulum system.	91

PREFACE

This work could not have been accomplished without the motivation and inspiration provided by my advisor, Dr. Zhi-Hong Mao. I would like to thank him for his full support, and for sharing his contagious optimistic and dynamic view on the extraordinary combined fields of control theory, human interaction, and information theory.

I would also like to thank my PhD committee members, each of whom has enriched this work in a unique way. Dr. Chaparro has had a significant impact on my development as a graduate student and has made my experiences as a teaching assistant very enjoyable. Dr. Loughlin's critical eye and insightful comments about my research have always challenged me to improve my work and pay attention to detail. Dr. Redfern's passion for bioengineering and his tremendous experience have fueled my desire to understand and explain human motor control using techniques from the wonderful world of engineering. Dr. Sun has taught me to appreciate the relevance of my work in real applications and has always reminded me how important it is not to lose sight of the big picture.

I would also like to express my humble gratitude to my family who has supported and encouraged my every decision. I would especially like to thank my wife Ana, whose patience and encouragement has enriched my work.

This effort would not have been as pleasant without my lab colleagues and wonderful friends who helped to make Pittsburgh a great place to call "home".

1.0 INTRODUCTION

1.1 MOTIVATION

The main goal of automation is to reduce human workload in various applications. For example, the manufacturing industry benefits from automatic control systems that are able to perform tasks much faster and more precisely than humans. The responsibilities of human operators seem to have shifted from active intervention to passive roles such as supervision and maintenance. However, a set of modern applications in control systems opens up new challenges for human involvement in operating machinery. Examples of such applications can be found in a variety of fields:

1. *Biomedical*: In telesurgery, the doctor performs surgery on a patient from a remote location. Surgical tasks are performed by a robotic system [7] that is manipulated by the surgeon. Since the well known transatlantic telesurgery from 2001 [8] investigations in remote surgery have focused mainly on introducing more sensory information for the surgeon such as force feedback and reducing the impact of time delay of the communication channel that bridges the surgeon and the patient [9, 10, 11]. Despite this, not much research has been conducted on the capabilities and limitations of the human operator given the time delay and limited sensory information.
2. *Industrial*: In underground mining, remotely-controlled robots are used to explore and map inaccessible or dangerous locations for humans [12, 13]. They can also be utilized in rescue operations [14, 15]. Similar remotely-operated robots were deployed to survey the damages of the nuclear reactors of the Fukushima Dai-1 plant after the tsunami that hit Japan in March 2011 [16].

3. *Military*: Remotely human-controlled robots have been successfully used in military bomb detection and diffusion operations. The development of unmanned aircraft systems (UAS) has also grown considerably in recent years. The UAS can carry out military operations such as remote sensing, transportation or even destroying enemy targets without endangering human lives.
4. *Space*: The exploration of Mars with the help of remote-controlled space vehicles [17] proved to be an immense success when two special built space vehicles, Opportunity and Spirit, were deployed on Mars in 2004. More recently, another rover called Curiosity [18] successfully landed on Mars equipped with instruments designed for analyzing the rock collected from the Mars' surface. Being remotely controlled from human operators on Earth, they deliver important insights into the harsh environment of Mars.

The complexity of human-machine interaction (HMI) has to be addressed in such applications because humans are no longer merely users but rather indispensable active components of these systems. Therefore, it is important to understand human capabilities and assess their limitations in such human-in-the-loop (HIL) control systems. A human operator of the Fukushima Dai-1 remotely-controlled robots warned about “the challenges that many robot developers may take for granted, such as the difficulty of handling the controls while wearing five pairs of gloves or seeing the user interface from behind a bulky mask. Which means that the controls and interfaces need to be made even easier to operate” [19].

In most HMI applications human control is exerted manually through hand movements. The hand has proven to be an efficient tool in operating machinery due to its many degrees of freedom. Manual control applications may require discrete or continuous hand movements, or a combination of both. Discrete hand movements are achieved via hand gestures, while continuous manual control relies on manual commands that have to be delivered continuously to sustain a desired outcome of the system. However, there is no consistent measure to assess human performance across both strategies among any type of HMI task. The computation of this measure should be independent of the type of manual control used, and its quantitative value should be dependent on the dynamics and variations in the task (i.e. varying time delay). The capacity and the limitations of human manual control can thus be predicted after estimating this measure of performance.

1.2 OBJECTIVES

The main objective of this study is to analyze human capabilities in feedback control systems by suggesting a measure for human performance compatible with both discrete- and continuous-type manual control. This goal is to be achieved through the following tasks:

1. *Quantitatively evaluate human performance in manual control tasks by analyzing the human operator as an information channel.* A coherent combination of tools from control theory, information theory, and time series analysis is to be used to estimate the information-transmission rate (ITR) measured in bits per second (b/s) that a human operator exchanges in a feedback control system.
2. *Analyze the efficiency of human performance and estimate its capacity and limitations.* Recent studies [20, 21] have investigated a method of analyzing the rate of information flow in a feedback control system. These studies enable the computation of the minimum information-transmission rate required by any controller to stabilize the system. A comparison between this theoretical lower bound and the information-transmission rate estimated in Task 1 can provide insight into both the quality of human control and its limitations. For example, it may be possible to obtain the variation of the ITR with time delay, then to extrapolate the ITR curve for different time delays and to estimate the maximum amount of time delay for stable control of the system. Moreover, the maximum achievable information-transmission rate can provide an estimation of the capacity of human manual control.
3. *Identify the information-transmission capabilities of the human controller relative to the bandwidth and the frequency distribution in the power spectrum of its control commands.* Our previous study [22] investigated the bandwidth constraints imposed on the controller by the dynamics of the feedback system. These constraints imply that the bandwidth of the control commands satisfies a lower bound if the controlled plant is unstable and an upper bound if any time delay affects the feedback system. Combining these results with the analysis from Task 1 and 2, we can infer the ITR-capabilities of the human controller relative to these bandwidth requirements.

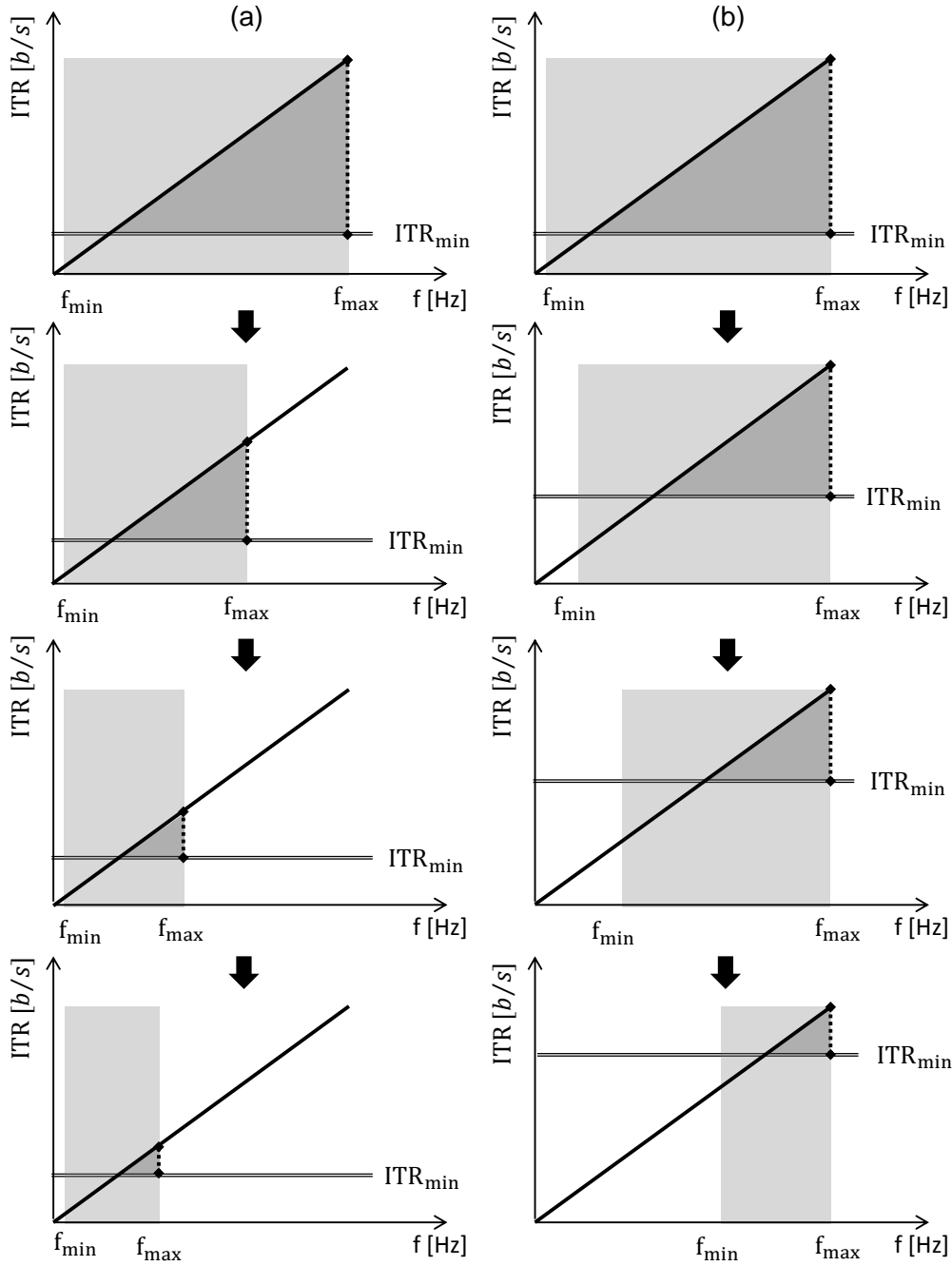


Figure 1: Hypothesis about the variation of the information-transmission rates with: (a) time delay, and (b) the degree of instability of the task (the arrows mark the direction of increase). The ITR can vary between an upper bound (solid line) and the lower bound (double line) required for feedback stability, ITR_{min} . This range is denoted by the dotted vertical line within the dark shaded area. The light shaded area marks the available bandwidth size.

Our hypothesis is illustrated in Fig. 1. Let the plant be an unstable system such that lower bounds for both the frequency bandwidth ($f_{min} > 0$) and the information-transmission rate (ITR_{min}) are assumed. When the task is not affected by time delay and when the degree of instability of the plant does not make the control task challenging, the human has some freedom to choose control commands according to his/her skill, attention etc. Let f_{min} and f_{max} be the lower bound and the upper bound of the bandwidth size of the control signal, respectively. This range is denoted by the light shaded area. Let the information-transmission rate vary (dark shaded area) between the lower bound defined by ITR_{min} (double thin line) and an upper bound (solid line) that represents the maximum capability of the human operator to deliver information. The range of information-transmission rates accessible for human operators is delimited by a vertical dotted line.

When time delay affects the feedback system [Fig. 1, column (a)], we predict that the human operator will adjust the control strategy to generate control signals in a lower frequency bandwidth in order to maintain stability according to [22]. Consequently, the range of possible information-transmission rates is expected to decrease and is also reduced to smaller values that are very close to the lower bound (ITR_{min}). Thus, the ability of the human operator to deliver information is assumed to decrease with increasing time delay.

When the degree of instability of the task is increased (i.e. larger magnitude of unstable poles of the plant) [Fig. 1, column (b)], we expect the lower bound of the frequency (f_{min}) to increase [22], such that the human controller would have to adapt to deliver faster corrective movements. Furthermore, ITR_{min} is assumed to increase with the degree of instability, such that the human operator is expected to generate a higher rate of information in order to stabilize the feedback system. Consequently, the range of possible information-transmission rates will vary within larger values, but its size will decrease with the degree of instability.

The dark shaded area is observed to gradually decrease with the level of difficulty of the task reflected by larger time delays and higher degrees of instability. The range of ITRs accessible for human controllers reduces correspondingly, implying that human operators will not be able to generate enough information to stabilize the closed-loop system. Our study aims to estimate the ITR of the human controller and to analyze this hypothesis. Furthermore, we propose a method to predict if and when a critical situation will occur.

1.3 SIGNIFICANCE

Our research is expected to provide a quantitative indication of human capabilities in HIL control systems contributing to our understanding and predictability of the fundamental limitations of human controllers. These limitations can be used to:

- discard impossible designs or specifications that are beyond the capabilities of the human controller;
- determine the controllability of a system or achievability of a task;
- prove the optimality of certain designs;
- provide an understanding of the intrinsic factors that restrict human operator performance (e.g. cognitive workload, muscular delay, motor noise).

This investigation can deliver important insights for the allocation of responsibilities between human and machine [23]. It will allow us to address questions such as: How efficiently can a human control a machine? How can an HMI interface be designed to maximally benefit from the human performance [24, 25, 26]? For example, in safety-critical situations, if human performance reduces below a lower bound of the information-transmission rate, certain automatic control systems could take over to avoid dangerous outcomes.

Studying the human operator as an information processor [27] in a variety of tasks that involve human participation can help us to derive a standardized measure of human performance. As we will see in the next section, other studies have also reported on the use of information measures for human operators performing certain tasks [28, 29, 30, 31] or for specific body parts such as the hand [32] or arm [33]. Previous studies have computed the information exchange between human and machine by means of specific methods that do not apply in other circumstances. For example, Fitt's law was extensively used to quantify the information-transmission rate for discrete-type tasks, but it cannot be directly applied for sustained control such as balancing an inverted pendulum. Our investigation is different because it addresses a general framework which can be used to estimate the information-transmission capabilities of the human operator independent of the adopted control strategy and the machine dynamics.

Finally, our analysis of performance is individualized to each human operator, and may enable the classification of human controllers according to their capabilities. Furthermore, human operators can be matched with the control task with which they achieve their best performance. Additionally, different stages of improvement during training can be tracked by evaluating the capabilities of the human controller to deliver information in an HMI task.

2.0 LITERATURE REVIEW

Human-machine interaction can be modeled as information flows through bi-directional communication channels [34], where the human receives sensory information from the machine and sends command information back to the machine. The interaction between human and machine can then be characterized by dynamics of information exchange measured in bits per second (b/s).

First introduced by Shannon [2], information theory has been applied to characterize performances of human sensory- and motor systems since the 1950's [35, 36, 37, 38]. Classical information theory describes the functionality of a communication system (Fig. 2), where an information source produces a message, the transmitter encodes the message and sends it over the channel, and the receiver reconstructs the message that is subsequently sent to the destination. The channel capacity is defined as the maximum amount of information that a communication channel can transmit correctly without error per channel use.

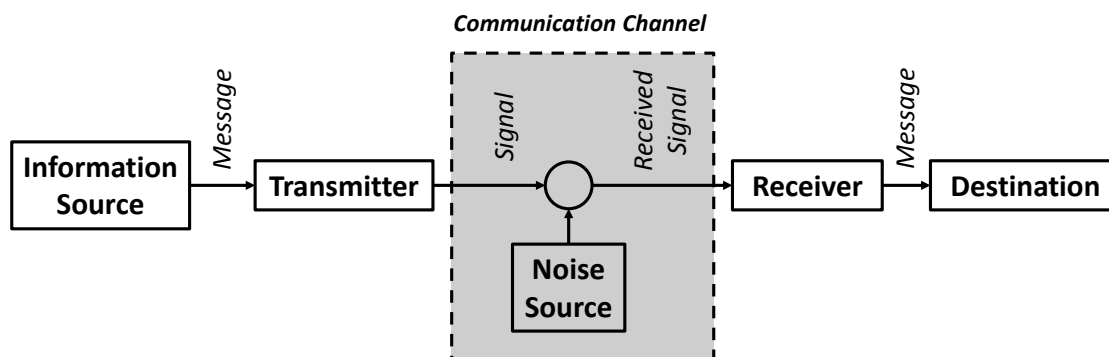


Figure 2: Communication system according to Shannon [2].

Based on the analogy with the communication channel, the Hick - Hyman law [28, 29] assesses the cognitive information capacity in choice-reaction experiments. In this case, the channel is the sensory-perceptual system, and the destination is the appropriate action [39]. The amount of time T required by a person to make a decision as a result of n possible choices can be predicted by $T = b \log_2(n + 1)$, where $1/b$ is measured in b/s and is known as the rate of gain of information.

For movement control, Fitts [30] proposed the famous Fitts law about speed/accuracy trade-offs: “The performance capacity of the human motor system plus its associated visual and proprioceptive feedback mechanisms, when measured in information units, is relatively constant over a considerable range of task conditions” ([30, p. 381]). Essentially, the law states that there is a linear relationship between task difficulty ID and movement time MT , which is denoted by $IP = ID/MT$. The index of difficulty $ID = \log_2(2A/W)$ specifies the relationship between the amplitude of the distance between two stationary targets (A) and the width of the targets where the movement must terminate (W). Fitts’ data suggested that the information-processing rate (IP) in a one-dimensional discrete movement was approximately 10 b/s [30, 40].

The information-theoretic approach was also applied to various tracking tasks. In a set of tracking experiments [31, 41], the observed maximum rate of human information processing via one dimensional movement was limited by about 9 b/s for continuous tracking and 11 b/s for discrete tracking. These experiments imply that human operators can achieve a higher information rate using discrete actions rather than continuous movements.

For multiple dimensional movements using the hand, researchers only studied some limited aspects of its information processing. For example, it was estimated that the information-processing rate of the thumb and index finger in a pinch-grip movement was 4.5 b/s [42], and in playing piano the maximum rate of information-transmission from visual input to finger movements was about 25 b/s [43]. Shannon estimated the entropy of the English language to be 1.3 bits per character, and human operators type at an average speed of 250 characters per minute [44], which indicates an information-transmission rate of 5.4 b/s in typing. A similar result was achieved when using continuous gestures on a data entry interface [44] where an information-transmission rate of 4.8 b/s was reported.

These studies encourage the use of information rates for characterizing human performance, especially in the interaction with machines. However, the information rates were derived for either specific simple discrete-movement tasks (e.g. reaching, typing), or for tracking tasks where human manual control was evaluated relative to its response to various sinusoidal signals. Instead, our investigation focuses on estimating the information-exchange rate between human operator and machine in a feedback control system. The dynamics of the controlled system may be unstable, and require the human operator to *continuously* generate control commands (e.g. piloting a plane through a turbulence zone). In such interactive HMI tasks, the information-transmission rates from human to machine should depend on the complexity of machine dynamics. Our study aims to investigate this dependency *quantitatively* by directly measuring the human response in such control tasks by analyzing the time series generated by the human controller.

Our motivation to experimentally estimate the information-transmission rate is accentuated by recent research [20, 21, 45], which coherently connects control- and information-theoretic concepts to determine the information flow rate through general dynamic feedback systems. A minimum bound on the information-transmission rate of any type of controller can be derived such that the overall feedback system is stable. We will show that this bound depends on the degree of instability of the task. Moreover, if the overall feedback system is linear time-invariant (LTI), then we can determine that any time delay and/or nonminimum-phase zeros of the plant have to be factored into this lower bound.

Our investigation uses a similar analogy to the communication system used by Shannon (Fig. 2). While Hick and Hyman considered the channel to be represented by the human sensory-perceptual system, our approach is similar to Fitt’s approach and considers the entire *human sensorimotor system* to be the communication channel. The human controller is thus assumed to be able to convey information and to obey afferent limitations similar to a communication channel.

The information transmitted by the human is reflected in his or her ability to generate motor commands effectively to perform a control task. In order to determine a quantitative measurement of this ability, the human response has to be analyzed. In practice, the human output is observed as a time series that records an apparently continuous variable measured

at discrete-time intervals, while the information-transmission rate is estimated by the mutual information rate. Following the “naive” histogram method [4, 46] (i.e. box counting approach) there are two main difficulties associated with the estimation of this quantity.

First, the data has to be properly quantized for the approximation of the probability distributions. If the data is quantized too coarsely, then some important information may be lost in the estimation of the probability distribution. On the other hand, if the resolution of the data is too fine (assuming that high frequency sampling is available), then characteristics of the noise present in the data would be more prominent than those of the signal [47]. What would be the best way to quantize the data in order to obtain a representative result? Because the mutual information rate involves two different sets of data samples for its computation, how should one set of data be quantized relative to the other? We aim for a numerical evaluation of this quantity that is robust relative to the choice of the quantization method.

Second, the approximation of high-dimensional probability distributions implies computation complexity, and will most probably be vulnerable to a biased estimation of the mutual information rate due to sparsity of the data [48, 49]. For the estimation of entropy and mutual information, which require the approximation of one- and two-dimensional probability distributions, some studies have shown methods to correct this bias [50, 51, 52, 53]. However, no similar solutions were reported for the mutual information rate which involves higher-dimensional probability distributions. Some authors suggest approximating probability distributions using kernel functions [54, 55] or adaptive partitioning of the data [49, 56, 57, 58]. Although these methods avoid high-dimensional probability distribution estimation, they only provide a qualitative measurement rather than a quantitative numerical value.

Despite a recent abundance of information-theoretic approaches to a broad set of applications [59], the estimation of information-theoretic quantities has proven to be application oriented and does not address our challenges. Most applications are in biomedical signal processing [54, 55, 60, 61] and in analyzing correlations in the stock market [62, 63]. These methods focus mainly on extracting causal interdependencies between time series (i.e. which time series influences which), and the single numerical values of quantities such as entropy, transfer entropy [47], and mutual information rate are not very informative. A vast majority of these methods are summarized in [64] with their advantages and disadvantages.

Concepts from information theory were adapted to illustrate important characteristics of dynamical systems. Kolmogorov [65] and Sinai [66] applied the entropy rate for dynamical systems to measure the uncertainty of the evolution of the state trajectory over time. In this case, the numerical value of the entropy of a time series is important for two reasons: it provides information about the topology of the attractor in the phase space [59], and the value of its reciprocal is the time scale for predictability of the system [4]. The Hausdorff dimension and the Kolmogorov-Sinai entropy are important quantities used to characterize dynamical systems, particularly to assess chaotic behavior. The value of the Hausdorff dimension renders the dimension of the attractor in the phase space of the system, while the Kolmogorov-Sinai entropy can characterize the level of disorder in a dynamical system [4]. Therefore, the quantitative value for these measurements is of great relevance to understanding the behavior of a system.

Grassberger et al. [67, 68, 69] provided a method to estimate these quantities using *correlation integrals*. This method captures the characteristics of a time series by assuming that the data was generated by a dynamical system, and by analyzing the evolution of the trajectory of the state in the phase space. The state vector of the system is approximated from the time series, and partitioning of the phase space is considered rather than quantizing the data samples. The computation of high-dimensional joint probability distributions is avoided by using a neighbor-search algorithm over the states. The quantization problem described earlier is also solved because the characteristics of the dynamical system are evaluated at different length scales of the neighborhood size of the phase-space partition. Similar methods are summarized by Gaspard and Wang [70] who refer to the entropy of a dynamical system over different length scales as “coarse grained dynamical entropy”. Because this method is designed for estimating the entropy rate from any arbitrary time series, we decided to use this approach in our study in order to estimate the entropy rate of the human output. We will present the underlying assumptions and limitations needed to apply this method for our investigation.

3.0 TECHNICAL PRELIMINARIES

To analyze human performance in HIL control systems we will use a multidisciplinary approach that comprehensively combines control theory, information theory, time series analysis, and non-invasive human experiments. We start by discussing technical preliminaries from information theory and time series analysis.

3.1 SHANNON'S INFORMATION THEORY

This section introduces the notation and definitions for the information-theoretic terms that are used throughout the study. The main references for this section are [2, 71], while more detailed mathematical formulations can be found in [72].

Let \mathbf{x} and \mathbf{y} be random variables or vectors that take values in the ranges \mathcal{X} and \mathcal{Y} , respectively. Let \mathcal{P} be a **partition** of the alphabet \mathcal{X} such that a finite collection of disjoint sets E_i satisfies $\bigcup_i E_i = \mathcal{X}$.

Given $\mathbf{x} \in \mathcal{X}$ and $\mathbf{y} \in \mathcal{Y}$, we can define the **mutual information** between two random variables as the measure of information that one random variable contains about the other. According to a general definition ([71, p. 252] or [72, p. 9]), the mutual information, $I : (\mathbf{x}, \mathbf{y}) \rightarrow \mathbf{R}_+ \cup \{\infty\}$, between two random variables is given by

$$I(\mathbf{x}; \mathbf{y}) = \sup \sum_i \sum_j P_{\mathbf{xy}}(E_i \times F_j) \log \frac{P_{\mathbf{xy}}(E_i \times F_j)}{P_{\mathbf{x}}(E_i)P_{\mathbf{y}}(F_j)} \quad (3.1)$$

where the supremum is taken over all finite partitions $\{E_i\}$ of \mathcal{X} and $\{F_j\}$ of \mathcal{Y} . Throughout this study we assume log to the base 2 such that the mutual information is measured in *bits*.

Furthermore, we adopt the convention $0 \log 0 = 0$. It should be noted that no assumptions were made on \mathcal{X} and \mathcal{Y} (i.e. discrete or continuous), and they may be different.

The quantity $H(\mathbf{x}) = I(\mathbf{x}; \mathbf{x})$ is called the **entropy**, and it is a measure of uncertainty about the random variable \mathbf{x} . Depending on the probability space, the mutual information and the entropy can be expressed as follows:

- If \mathcal{X} and \mathcal{Y} are countable, and $P_{\mathbf{x}, \mathbf{y}}$ is the joint probability mass function, then

$$I(\mathbf{x}; \mathbf{y}) = \sum_{x \in \mathcal{X}} \sum_{y \in \mathcal{Y}} P_{\mathbf{xy}}(x, y) \log \frac{P_{\mathbf{xy}}(x, y)}{P_{\mathbf{x}}(x)P_{\mathbf{y}}(y)} \quad (3.2)$$

$$H(\mathbf{x}) = - \sum_{x \in \mathcal{X}} P_{\mathbf{x}}(x) \log P_{\mathbf{x}}(x). \quad (3.3)$$

- If $\mathcal{X} = \mathbb{R}^q$ and $\mathcal{Y} = \mathbb{R}^s$, and the joint probability density $p_{\mathbf{xy}}$ is well-defined, then

$$I(\mathbf{x}; \mathbf{y}) = \int_{\mathbb{R}^s} \int_{\mathbb{R}^q} p_{\mathbf{xy}}(x, y) \log \frac{p_{\mathbf{xy}}(x, y)}{p_{\mathbf{x}}(x)p_{\mathbf{y}}(y)} dx dy \quad (3.4)$$

$$h(\mathbf{x}) = - \int_{\mathbb{R}^q} p_{\mathbf{x}}(x) \log p_{\mathbf{x}}(x) dx. \quad (3.5)$$

Without loss of generality we consider the latter case to define the **joint entropy** $h(\mathbf{x}, \mathbf{y})$ and the **conditional entropy** $h(\mathbf{x}|\mathbf{y})$:

$$h(\mathbf{x}, \mathbf{y}) = - \int_{\mathbb{R}^s} \int_{\mathbb{R}^q} p_{\mathbf{xy}}(x, y) \log p_{\mathbf{xy}}(x, y) dx dy$$

$$h(\mathbf{y}|\mathbf{x}) = - \int_{\mathbb{R}^s} \int_{\mathbb{R}^q} p_{\mathbf{xy}}(x, y) \log p_{\mathbf{xy}}(y|x) dx dy.$$

The entropy $h(\mathbf{x})$ of continuous random variables, also referred to as **differential entropy**, can be related to the entropy $H(\mathbf{x})$ of discrete random variables. By assuming that the range \mathcal{X} can be divided into bins of length ϵ then, according to [71, Theorem 8.3.1, p. 248]:

$$H(\mathbf{x}_\epsilon) + \log \epsilon \rightarrow h(\mathbf{x}), \quad \text{as } \epsilon \rightarrow 0 \quad (3.6)$$

where $H(\mathbf{x}_\epsilon)$ is the entropy of the quantized version of the continuous random variable \mathbf{x} .

The mutual information between \mathbf{x} and \mathbf{y} can then be rewritten in different ways:

$$\begin{aligned}
I(\mathbf{x}; \mathbf{y}) &= h(\mathbf{x}) + h(\mathbf{y}) - h(\mathbf{x}, \mathbf{y}) & (3.7) \\
&= h(\mathbf{x}) - h(\mathbf{x}|\mathbf{y}) \\
&\approx H(\mathbf{x}_\epsilon) + \log \epsilon - H(\mathbf{x}_\epsilon|\mathbf{y}_\epsilon) - \log \epsilon \\
&= H(\mathbf{x}_\epsilon) - H(\mathbf{x}_\epsilon|\mathbf{y}_\epsilon) \\
&= I(\mathbf{x}_\epsilon; \mathbf{y}_\epsilon), \quad \text{when } \epsilon \rightarrow 0. & (3.8)
\end{aligned}$$

A **communication channel** is denoted by the triple $(\mathcal{X}, p(y|x), \mathcal{Y})$ consisting of an input alphabet \mathcal{X} , an output alphabet \mathcal{Y} , and the transition probability $p(y|x)$ that the value y is received given that x was transmitted over the channel. The transmission of information over a communication channel is quantified by the mutual information, which estimates the rate of bits per channel use that can be successfully transmitted with an arbitrarily small probability of error [2].

It should be noted that the entropy, joint entropy, conditional entropy, and the mutual information are functionals of probability distributions and do not depend on the specific values of $x \in \mathcal{X}$ and $y \in \mathcal{Y}$. They satisfy the following properties (refer to [71] for proofs):

1. $I(\mathbf{x}; \mathbf{y}) \geq 0$, with equality if only if \mathbf{x} and \mathbf{y} are independent.
2. The entropy of a discrete random variable (3.3) is always nonnegative.
3. The differential entropy (3.5) can be negative for certain probability distributions, and it may not exist if the cumulative distribution function $P(x) = \text{Prob}(\mathbf{x} \leq x)$ is not absolutely continuous such that $p(x) = P'(x)$.
4. The chain rule for the mutual information:

$$I(\mathbf{x}, \mathbf{y}; \mathbf{z}) = I(\mathbf{x}; \mathbf{z}) + I(\mathbf{y}; \mathbf{z}|\mathbf{x}). \quad (3.9)$$

5. The data processing inequality [71, p. 35] establishes:

$$I(\mathbf{x}; g(\mathbf{y})) \leq I(\mathbf{x}; \mathbf{y}). \quad (3.10)$$

for any measurable (linear or nonlinear) function $g(\cdot)$ of the data \mathbf{y} .

Let $\mathbf{x}(k)$ be a stochastic process, and we call it **asymptotically stationary** if the following conditions are simultaneously satisfied:

1. $\lim_{k \rightarrow \infty} E[\mathbf{x}(k)] = 0$;
2. $\lim_{k \rightarrow \infty} E[\mathbf{x}(k)^T \mathbf{x}(k)] < \infty$;
3. $\lim_{k \rightarrow \infty} E[\mathbf{x}(k + \gamma)^T \mathbf{x}(k)]$ exists for any $\gamma \in \mathbb{N}$;

where $E(\cdot)$ is the expected value operator.

Given a time sequence of random variables $\mathbf{x}^{n-1} = \{\mathbf{x}(0), \mathbf{x}(1), \dots, \mathbf{x}(n-1)\}$, which we refer to as a **time series**, we are interested in determining the average sufficient information (in bits) to describe the sequence. For independent identically distributed (i.i.d.) random variables, the sequence of length n can be described by $n \cdot h(\mathbf{x})$ bits of information. However, if the random variables are not i.i.d., then the entropy of the sequence scales with n by the **entropy rate**, which is defined as

$$h_\infty(\mathbf{x}) = \limsup_{n \rightarrow \infty} \frac{h(\mathbf{x}^{n-1})}{n} \quad (3.11)$$

when the limit exists. The entropy rate can also be defined using the conditional entropy:

$$h'_\infty(\mathbf{x}) = \limsup_{n \rightarrow \infty} h(\mathbf{x}(n) | \mathbf{x}(n-1), \mathbf{x}(n-2), \dots, \mathbf{x}(0)) \quad (3.12)$$

when the limit exists. While the former definition indicates the average number of bits per time sample needed to describe the n random variables, the latter definition computes the average number of bits needed to represent the current time sample given the past. For stationary stochastic processes these two quantities are equal such that $h_\infty(\mathbf{x}) = h'_\infty(\mathbf{x})$.

The **mutual information rate** is defined as the rate at which the mutual information scales with the length n of the time sequences corresponding to two random variables:

$$\begin{aligned} I_\infty(\mathbf{x}; \mathbf{y}) &= \limsup_{n \rightarrow \infty} \frac{I(\mathbf{x}^{n-1}, \mathbf{y}^{n-1})}{n} \\ &= \limsup_{n \rightarrow \infty} \frac{1}{n} \left[\int_{\mathbf{R}^{ns}} \int_{\mathbf{R}^{nq}} p_{\mathbf{xy}}(\mathbf{x}^{n-1}, \mathbf{y}^{n-1}) \log \frac{p_{\mathbf{xy}}(\mathbf{x}^{n-1}, \mathbf{y}^{n-1})}{p_{\mathbf{x}}(\mathbf{x}^{n-1}) p_{\mathbf{y}}(\mathbf{y}^{n-1})} d\mathbf{x} d\mathbf{y} \right] \end{aligned} \quad (3.13)$$

As a universal measure of the rate at which information is transmitted reliably over an arbitrary communication medium [21, 71, 73], the mutual information rate, also referred to as **information-transmission rate (ITR)** in our investigation, is used to assess the performance of the human controller in a feedback control system.

3.2 ENTROPY RATE OF TIME SERIES

Introduced by Shannon [2] for communication channels, the entropy rate was later extended by Kolmogorov [65] and Sinai [66] to quantify the complexity of dynamical systems. The utilization of this adapted entropy rate in our study is motivated by many robust and less computationally-expensive numerical methods that were developed to estimate it [69, 70]. We will discuss later how the entropy rate applied to dynamical systems is equivalent with Shannon's entropy rate under certain assumptions, and how it will be used to approximate the mutual information rate. A brief introduction to dynamical systems is presented next. The entropy rate of dynamical systems is defined in a general framework using the order- q Renyi entropies [74]. For a rigorous mathematical definition, please refer to [4, 65, 66, 75].

Dynamical systems are characterized by the evolution of a trajectory (also called orbit) in some vector space (state space or phase space) such that the exhibited dynamics of the system is a consequence of the evolution of this trajectory in the state space over time. If the system is purely *deterministic*, then the evolution of the system is well established by solving the system or integrating the system given some initial conditions. Moreover, if the set of initial conditions drives the system to the same asymptotic behavior, then the trajectory is considered to evolve to a *basin of attraction*. The dynamical system is called *dissipative* in this case, and the subset of the phase space where the trajectory is eventually attained (called *attractor*) is invariant under dynamical evolution. Simple attractors may be fixed points or limit cycles, but other attractors may exhibit very complicated geometrical structures. The latter are called *strange attractors* or *fractals* (i.e. the name refers to the dimension of the attractor which is a positive fractional number, rather than a natural number) and may lead to chaos. *Chaos* is established when a dynamical system shows sensitivity to initial conditions. That is, two arbitrarily close initial conditions generate two significantly different future trajectories of the system. The exponential rate of divergence is represented by the largest *Lyapunov exponent*.

If the signal generated by a dynamical system follows some probability distribution, and the transition between the observed numbers is well-defined, then one can make inferences about the internal states of the system and their evolution over time. The entropy rate

suggested by Kolmogorov and Sinai provides insight about the average information needed to describe a state with a certain accuracy, or how much information is gained about future observations given past measurements. The analysis is also linked to prediction capabilities, because the entropy rate scales inversely with the time scale of prediction.

Without loss of generality, consider a discrete-time dynamical system with a D -dimensional continuous phase space, and assume that the state of the system $\mathbf{x}(t)$ is measured at finite time intervals τ (the time t is assumed such that the state trajectory is already located on the attractor). If the phase space is covered by a partition \mathcal{P}_ϵ of disjoint cells $\{\alpha_i\}_{i=1}^{n_c}$ of size ϵ^D , then the joint probability distribution $p(\alpha_{l_1}^{t_1}, \alpha_{l_2}^{t_2}, \dots, \alpha_{l_m}^{t_m})$ is defined as the probability that the state of the system successively visits the partition cells $(\alpha_{l_1}, \alpha_{l_2}, \dots, \alpha_{l_m})$, with $l_i \in \{1, 2, \dots, n_c\}$, at times $t_i = t + (i - 1)\tau$. In the particular case of a time series, where scalar measurements are observed, the partitions are intervals on the real axis. The order- q Renyi block entropy of block size m can then be formulated as

$$H_q(m, \epsilon) = \frac{1}{1 - q} \log \sum_{\mathcal{P}_\epsilon} p^q(\alpha_{l_1}^{t_1}, \alpha_{l_2}^{t_2}, \dots, \alpha_{l_m}^{t_m}) \quad (3.14)$$

The **order- q generalized entropy** is then defined as the information needed to predict in which cell the trajectory will be at time t_{m+1} given the trajectory up to time t_m :

$$h_q(m, \mathcal{P}_\epsilon) = H_q(m + 1, \mathcal{P}_\epsilon) - H_q(m, \mathcal{P}_\epsilon) = \frac{H_q(m, \mathcal{P}_\epsilon)}{m} \quad (3.15)$$

$$h_q = \sup_{\mathcal{P}_\epsilon} \lim_{m \rightarrow \infty} h_q(m, \mathcal{P}_\epsilon) \quad (3.16)$$

It should be noted that h_q with a positive finite index $0 < q < \infty$ denotes the entropy rate for dynamical systems, as opposed to h which refers to the differential entropy, and h_∞ which implies the differential entropy rate.

The **Kolmogorov-Sinai entropy**, denoted by h_{KS} , is obtained for the particular case when the limit $q \rightarrow 1$ is taken in (3.16). It should be mentioned that the supremum over all finite partitions in (3.16) is taken implicitly if the partition is chosen to be a *generating partition* [66]. A method that illustrates how to choose generating partitions can be found in [76]. The entropy rate of dynamical systems is known to be invariant over the range of

generating partitions (i.e. they are not unique). Consequently, when $h_q(m, \epsilon)$ is evaluated relative to the size of the partition cells ϵ , the entropy rate may be invariant over a range of ϵ values, also called *plateau*.

3.3 CORRELATION SUM ESTIMATION FROM TIME SERIES

We will consider the dynamical system from the previous section that is characterized by some state trajectory. If the phase space is covered by partition cells of size ϵ , then the order- q generalized correlation sum computes the probability that two states of the system at different times are closer than a threshold ϵ

$$C_q(\epsilon) = K \sum_{i=1}^M \left[\sum_{j=1, j \neq i}^M \Theta(\epsilon - \|\mathbf{x}(i) - \mathbf{x}(j)\|) \right]^{q-1} \quad (3.17)$$

where $K = 1/[M(M-1)^{q-1}]$ is a normalizing factor, M is the number of states, $\|\cdot\|$ is a norm, and $\Theta(\cdot)$ is the Heaviside step function: $\Theta(x) = 0$, if $x \leq 0$, and $\Theta(x) = 1$, otherwise.

When analyzing a time series, the states of the system are not known, but instead the scalar measurements $\{u(k)\}_{k=1}^N$ are available, where N is the length of the time series. Therefore, only a projection of the internal states of the system onto an interval on the real axis is observed:

$$u(k) = s(\mathbf{x}(k\Delta t)) + \eta(k) \quad (3.18)$$

where $u(k)$ is the scalar measurement of some observation function $s(\cdot)$ of the current state of the system $\mathbf{x} \in \mathbb{R}^q$ at a fixed sampling time Δt contaminated with some measurement noise, η .

A reconstruction of the phase space is therefore required [59, ch. 1]. Takens' delay embedding theorem [77] suggests that the evolution of the delay vector

$$\mathbf{u}(k) = [u(k), u(k - \tau), \dots, u(k - (m - 1)\tau)]^T \quad (3.19)$$

for $k = (m - 1)\tau + 1, \dots, N$, reflects the same dynamics of the unknown state vector (in the sense of mapping onto each other by a uniquely invertible smooth map) for embedding

dimensions $m \geq 2D$, where D is the dimension of the attractor in the phase space. Consequently, the state of the original system in (3.17) is substituted by its vector approximation:

$$C_q(m, \epsilon) = K \sum_{i=1}^M \left[\sum_{j=1, j \neq i}^M \Theta(\epsilon - \|\mathbf{u}(i) - \mathbf{u}(j)\|) \right]^{q-1} \quad (3.20)$$

In practice, the dimension m is estimated using the *false nearest neighbor* algorithm [78, 79]. The time lag τ between successive samples is an important parameter when over- or under-sampling the data. If both τ and the sampling period are too small, the elements of the delay vector are clustered together and little information is gained about the phase space of the system. Additionally, a small value of τ may be useless if the variation of the signal during the time interval $m\tau$ covered by the delay vector is smaller than the noise level. However, if τ is too large, then the elements of the delay vector may not be correlated at all, and the estimation of the correlation sum is strongly biased. Studies suggest that a “good” choice of the lag τ is the $1/e$ -crossing of the normalized autocorrelation function [4, 59], or the first minimum of the delayed mutual information [49, 56, 57]. The latter is preferable because it also captures nonlinear correlations in the data.

The q -order Renyi entropy of block size m , $H_q(m)$ in (3.14), scales with the generalized correlation sum $C_q(m, \epsilon)$ (3.20) such that

$$C_q(m, \epsilon) \propto \epsilon^{(q-1)D_q} e^{(1-q)H_q(m)} \quad (3.21)$$

where D_q is the generalized dimension [4, ch. 6], which is constant for ϵ -values inside the plateau. For this range of ϵ -values it can be derived that

$$h_q(m, \epsilon) = H_q(m+1) - H_q(m) = \frac{1}{q-1} \log \frac{C_q(m, \epsilon)}{C_q(m+1, \epsilon)} \quad \text{bits/sample.} \quad (3.22)$$

Furthermore, the dependency of $h_q(m, \epsilon)$ on the embedding dimension m reveals important information about the dynamical system. The rate of convergence of $m \rightarrow \infty$ is proven to relate to the strength of correlations in the system [67], thus providing insight into the size of the memory of the system.

Careful interpretation of the $h_q(m, \epsilon)$ curve is required. Establishing a plateau in the scaling curve should be done by inspection rather than by an automatic algorithm [4, ch. 6].

The result can be affected by the noise in the signal, especially if the length scale for ϵ is not larger than three times the noise level. Another artifact is observed for length scales smaller than the resolution of the data. While the former case may not exhibit any plateau, the latter suffers from lack of neighbors and exhibit fluctuations. Another aspect that influences the estimation of $h_q(m, \epsilon)$ is the finite number of samples in the time series. For a consistent estimation, it has been suggested [4, ch. 9.7] that the minimum length of the time series should satisfy $N_{min} > \epsilon^{-D}$, where D is the dimension of the attractor.

4.0 METHODS

4.1 HUMAN MANUAL CONTROL OF AN UNSTABLE SYSTEM

4.1.1 Characteristics of Human Motor Control

The interaction of humans in HIL systems, not necessary unstable systems, is defined by the complex synergy of three main components:

- perception of the the sensory input from the environment (i.e. visual, vestibular, and/or proprioceptive information);
- formulation of the command signal by the central nervous system (CNS): response programming, selection, and execution;
- implementation of movement by the muscular-skeletal system (i.e. muscle contraction).

Investigations on human motor control have shown that these components account for the observation of two main classes of movements: discrete and continuous [80, 81]. **Discrete movements**, also referred to as ballistic movements, are pre-planned at the neuromuscular level, and they are executed ballistically without sensory feedback information (i.e. open-loop). They have a recognizable start and end. Examples include throwing, rapid reaching and pointing, saccadic eye movements, etc. **Continuous movements** imply sustained control, where ongoing (continuous) regulation is executed as the response to ever-changing information from sensory feedback. Examples include tracking tasks, steering a vehicle, postural control, windsurfing, controlling the sail, etc. An important characteristic that distinguishes continuous control from discrete control is the difficulty to identify discrete actions that have a beginning and an end. Depending on the control task, humans choose between one strategy or the other. Their interplay builds up the repertoire of human movements.

However, certain tasks such as playing the piano, typing on a keyboard, writing, dancing, and even speech, are characterized by discrete actions that can be executed consecutively in a smooth and continuous manner. Therefore, continuous movements were initially challenged to be serial and discrete in nature. Even early investigations by Craik [82] and Vince [83] on human tracking of unpredictable discrete stimuli showed that, although the human operator can be modeled as a servo system, the control movements were intermittent rather than continuous. This interaction between closed-loop (sensory feedback dependent) and open-loop (sensory feedback independent) control strategy led researchers to consider another class of control movements: **intermittent control**.

Intermittency in motor control is characterized by continuous assimilation of sensory information and serial production of ballistic movements [80, 84, 85]. Depending on how familiar the human is with the task, movements can be executed almost continuously. Intermittent control is therefore situated between the two extremes represented by continuous and discrete control, because control actions are continuous-time trajectories, but they are triggered intermittently [86]. Moreover, this hypothesis is consistent with the property of the CNS to group information into chunks [23, 84]: the movement trajectory may be encoded into a finite set of possible sub-movements which are pre-learned and executed continuously.

An important characteristic of intermittent control is the time interval between the completion of the current control command and the beginning of the next. Particularly, the *refractory period* (also referred to as intermittent interval) accounts for the time interval associated with response programming and selection of each movement. Using experiments where the discrete response to stimuli was analyzed, it was possible to estimate the refractory period to 250-500 ms [82, 83, 87, 88, 89, 90, 91, 92]. Therefore, voluntary movement is restricted to 2-3 actions per second corresponding to a low-frequency bandwidth of 1-2 Hz.

Next, we focus our attention on the specific task of controlling an unstable system. Investigations on human control strategies of unstable systems support the opinion that stabilizing control commands resemble on-off intermittency in the sense that serial actions are pre-planned using accumulated sensory feedback and executed ballistically [91, 93, 94, 95, 96]. For human experiments on intermittent control of unstable systems, we refer to the studies by Cabrera et al. [6, 97, 98], Loram et al. [5, 86, 88, 99], and Gawthrop et al. [100, 101, 102].

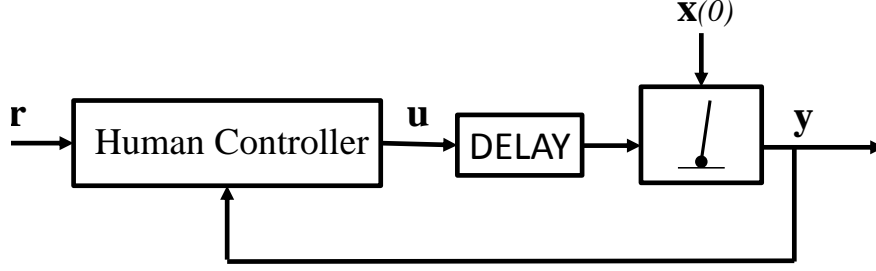


Figure 3: Human-in-the-loop (HIL) system: the human operator generates one degree of freedom control commands to stabilize the inverted pendulum.

4.1.2 Unstable System Description

Among various HMI tasks, stabilizing unstable systems (e.g., unstable aircraft [103], missile guidance, booster rockets, postural control [104]) is of special interest to researchers because this family of tasks challenges the human sensorimotor control system. One such task has also been shown to provide a reliable measure of neurological capabilities [105].

In our investigation, the performance of the human is analyzed during manual control of an unstable system. In the HIL system shown in Fig. 3 the human subject has to perform a balancing task involving a planar inverted pendulum simulation. The equation of the inverted pendulum system [106, 107], which is illustrated in Fig. 4, is given by:

$$\frac{mL^2}{3} \frac{d^2\theta}{dt^2} + \frac{mL}{2} \cos\theta \frac{d^2x}{dt^2} = \frac{mgL}{2} \sin\theta \quad (4.1)$$

where m is the mass of the pendulum (uniform rod), L is the length of the pendulum (in m), θ is the angle of the pendulum relative to the vertical position (in rad), x is the displacement of the bottom tip of the pendulum, and $g = 9.81$ is the gravitational acceleration (in m/s^2). The complete derivation of this equation is provided in appendix A. The control variable of the inverted pendulum system is the displacement x applied to the bottom tip of the pendulum. The output of the inverted pendulum system is the angle θ , which is to be kept as small as possible.

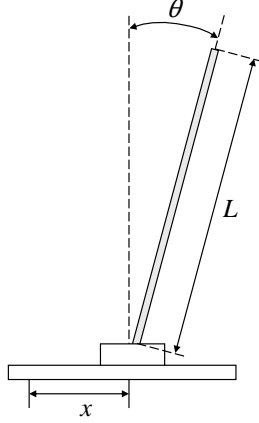


Figure 4: Parameters of the inverted pendulum: θ is the pendulum angle; L is the length of the pendulum, and x is the displacement of the bottom tip.

In order to obtain the unstable pole of the plant, we first derive the linearized version of the inverted-pendulum dynamics. For small values of θ (for which we have that $\sin \theta \approx \theta$ and $\cos \theta \approx 1$), the transfer function of the inverted pendulum can be computed as

$$H(s) = \frac{\Theta(s)}{X(s)} = \frac{-\frac{\alpha}{g}s^2}{s^2 - \alpha} = \frac{-\frac{\alpha}{g}s^2}{(s + \sqrt{\alpha})(s - \sqrt{\alpha})} \quad (4.2)$$

where $\alpha = 3g/2L$. The linearized dynamics of the inverted pendulum system yields two poles, one of which is real and positive. This unstable pole varies inversely with the length of the pendulum: $\lambda_u = \sqrt{3g/2L}$, and its magnitude reflects the **degree of instability** of the system. It should be noted that the poles of a transfer function are equivalent to the eigenvalues of the state matrix if the linear equation is rewritten in state-space representation. Therefore, these two terms are used interchangeably because they refer to the same quantity.

We investigate two representative scenarios of human manual control in which the difficulty of the control task is increased:

1. when introducing various amounts of time delay in the feedback system. This scenario is expected to reproduce the difficulties of manual control through a network communication channel that may induce a certain (possibly unknown) amount of time delay. Practical applications include teleoperation and telesurgery.

2. when changing the degree of instability of the task by varying the pendulum length (without time delay). The time constant of the control task decreases proportionally with the pendulum length, and therefore faster responses are required from the human controller to stabilize the inverted pendulum.

The purpose of considering these two scenarios is to observe the limitations of human operators by possibly determining the maximum time delay and the highest degree of instability of the task that a human can successfully control. Moreover, the variation of the information-transmission rate with time delay and degree of instability is expected to reflect the human performance.

4.1.3 Human Controller Model

The model of the human controller has to exhibit intermittent control in order to be consistent with experimental observations. Our approach of modeling the human operator follows the design proposed by McRuer [108, 109, 110]. Specifically, the human controller consists of a quasi-linear system and a remnant element (Fig. 5). Hence, the control command \mathbf{u} is based on two components:

$$\mathbf{u} = \mathbf{v} + \mathbf{d} \tag{4.3}$$

where \mathbf{v} represents the component that is linearly correlated to the perceived sensory signals \mathbf{r} and \mathbf{y} ; and \mathbf{d} , also called the “remnant”, represents all the output content that cannot be described by the linear element. Without loss of generality, we assume the reference signal of the feedback system \mathbf{r} to be zero.

The source of the remnant is impossible to identify unambiguously. However, it has been shown [110] that it can be caused by multiple factors such as noise related to sensing capabilities and implementation of movement, nonlinear operations, and non-steady behavior such as learning abilities. In accordance with the observed characteristics of manual control, the remnant accounts for the multiplicative noise component [111, 112].

The human sensorimotor system is modeled as an information channel, and the ITR from human to machine is characterized by the rate of information conveyed from \mathbf{y} to \mathbf{u} and measured by $I_\infty(\mathbf{y}; \mathbf{u})$.

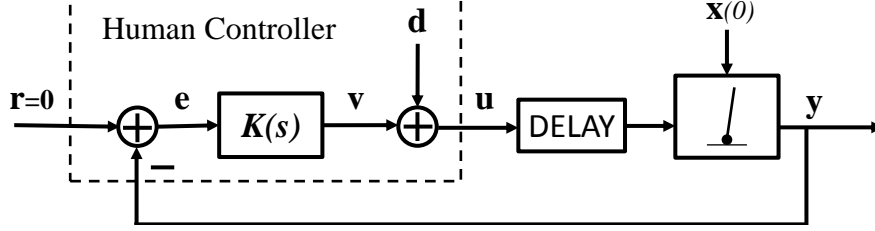


Figure 5: Human-in-the-loop (HIL) system: the manual command \mathbf{v} generated by the deterministic function K is contaminated by the remnant \mathbf{d} before delivery to the plant P .

4.2 MINIMUM REQUIRED INFORMATION RATE TO STABILIZE A FEEDBACK CONTROL SYSTEM

Consider the HIL system illustrated in Fig. 5, where the human performs a control task described by the plant P . Assume that the dynamics of the task can be described by the discrete-time state-space equation:

$$\begin{aligned} \mathbf{x}(k+1) &= A\mathbf{x}(k) + B\mathbf{u}(k - r_d) \\ \mathbf{y}(k) &= C\mathbf{x}(k) \end{aligned} \quad (4.4)$$

where \mathbf{x} is the state vector of the plant; \mathbf{u} and \mathbf{y} are the input- and output vector of the plant; r_d represents any time delay included in the plant dynamics (e.g. due to a transmission link in a network channel); and A , B , and C are the state-, input-, and output matrix, respectively.

4.2.1 Fundamental Lower Bound of Information Rate

The following theorem establishes the connection between the information rate $I_\infty(\mathbf{y}; \mathbf{u})$ and the stability properties of the closed-loop system in Fig. 5. The unstable plant P is said to be *stabilized in the mean-square sense* if, through feedback control, the state vector \mathbf{x} satisfies the following expression:

$$\sup_k E [\mathbf{x}(k)^T \mathbf{x}(k)] < \infty \quad (4.5)$$

where $E(\cdot)$ denotes the expected value and $'$ means transpose.

Theorem 1: For the HIL control system indicated in Fig. 5, if the human controller stabilizes the unstable plant in the mean-square sense, then

$$I_\infty(\mathbf{y}; \mathbf{u}) \geq \sum_{i=1}^p \log |\lambda_i| \quad (4.6)$$

where A is the state matrix of the plant and λ_i , $i = 1, 2, \dots, p$, are the unstable eigenvalues of A . The lower bound of the ITR in a feedback system is thus shown to be dependent on the degree of instability of the plant.

Proof: According to [21, Theorem 4.2, p. 1608], the following inequality holds for the feedback control system in Fig. 5:

$$h_\infty(\mathbf{u}) \geq h_\infty(\mathbf{d}) + \liminf_{n \rightarrow \infty} \frac{I(\mathbf{x}(0); \mathbf{u}^n)}{n} \quad (4.7)$$

where $\mathbf{u}^{n-1} = [\mathbf{u}(0), \dots, \mathbf{u}(n-1)]$. Inequality (4.7) states that the entropy rate of the control input \mathbf{u} is no less than the entropy rate of the noise \mathbf{d} given the non-negativity property of the mutual information rate. This result only assumes that the feedback system is causal. Additionally, if the human controller stabilizes the plant in the mean-square sense as defined by (4.5), then according to [20, Lemma 4.1, p. 61] the following is also satisfied:

$$\liminf_{n \rightarrow \infty} \frac{I(\mathbf{x}(0); \mathbf{u}^n)}{n} \geq \sum_{i=1}^l \max\{0, \log |\lambda_i(A)|\} \quad (4.8)$$

where $\lambda_i(A)$, $i = 1, \dots, l$, are the total number of eigenvalues of A , the state matrix of the unstable plant. The left-hand side of (4.8) quantifies the minimum information-transmission rate required for stabilization of the closed-loop system. As indicated in [21, Lemma 4.3, p. 1608], the results of (4.7) and (4.8) can be summarized as

$$h_\infty(\mathbf{u}) \geq h_\infty(\mathbf{d}) + \sum_{i=1}^p \log |\lambda_i|. \quad (4.9)$$

where $|\lambda_i|$, $i = 1, 2, \dots, p$, represents the magnitude of only the unstable eigenvalues of A .

Additionally, it can be shown that the ITR satisfies the following inequalities:

$$I_\infty(\mathbf{y}; \mathbf{u}) \geq I_\infty(\mathbf{v}; \mathbf{u}) \quad (4.10)$$

$$= h_\infty(\mathbf{u}) - h_\infty(\mathbf{u}|\mathbf{v}) \quad (4.11)$$

$$= h_\infty(\mathbf{u}) - h_\infty(\mathbf{v} + \mathbf{d}|\mathbf{v}) \quad (4.12)$$

$$= h_\infty(\mathbf{u}) - h_\infty(\mathbf{d}|\mathbf{v})$$

$$\geq h_\infty(\mathbf{u}) - h_\infty(\mathbf{d}) \quad (4.13)$$

where the inequality (4.10) follows from (3.10): $I_\infty(\mathbf{v}; \mathbf{u}) = I_\infty(K(\mathbf{y}); \mathbf{u}) \leq I_\infty(\mathbf{y}; \mathbf{u})$ according to the assumption that K is causal and deterministic; (4.11) was obtained from the mutual information rate formula (3.7); in (4.12) the command \mathbf{u} was substituted according to (4.3); and in (4.13) we used the property that conditioning reduces entropy [71, Theorem 2.6.5, p.29]: $h(\mathbf{d}|\mathbf{v}) \leq h(\mathbf{d})$. By following (4.9), we finally obtain (4.6). ■

4.2.2 Lower Bound of Information Rate for LTI Controllers

It should be noted that the lower bound for $I_\infty(\mathbf{y}; \mathbf{u})$, which was established in (4.6), depends only on the degree of instability of the plant P given by the unstable eigenvalues. While we assumed the plant to be linear time invariant (LTI), the controller can be nonlinear and/or time variant due to the remnant component. The next theorem considers the particular case of an LTI controller, and it shows that the lower bound for $I_\infty(\mathbf{y}; \mathbf{u})$ must also depend on time delay and nonminimum-phase zeros of the plant, if they exist. Let us first define the *Blaschke product* containing the unstable eigenvalues of the discrete-time plant P :

$$B(z) = \prod_{i=1}^n \frac{z - \lambda_i}{1 - z\lambda_i}.$$

We can then introduce the following quantity:

$$\beta_k \triangleq \frac{1}{k!} \frac{d^k}{dz^k} B(z) \Big|_{z=0}.$$

Theorem 2: Consider the HIL control system indicated in Fig. 5, where the transfer function representation of the plant P has unstable poles: λ_i , $i = 1, 2, \dots, p$, nonminimum-phase zeros: ζ_l , $l = 1, 2, \dots, z$, and relative degree $d \geq 1$. If an LTI controller represented by a proper rational function stabilizes the feedback system, then

$$I_\infty(\mathbf{y}; \mathbf{u}) \geq \frac{1}{2} \log \left(\prod_{i=1}^p |\lambda_i|^2 + \delta + \eta \right) \quad (4.14)$$

where

$$\begin{aligned} \delta &= \begin{cases} 0, & \text{if } d = 1 \\ \sum_{k=1}^{d-1} |\beta_k|^2, & \text{if } d > 1 \end{cases} \\ \eta &= \sum_{l=1}^z \sum_{i=1}^z \frac{\gamma_l \bar{\gamma}_i}{\zeta_l \bar{\zeta}_i - 1} \\ \gamma_l &\triangleq (1 - |\zeta_l|^2) \left(B^{-1}(\zeta_l) - \sum_{k=0}^{d-1} \frac{\beta_k}{\zeta_l^k} \right) \prod_{k=1, k \neq l}^q \frac{1 - \zeta_l \bar{\zeta}_k}{\zeta_l - \zeta_k}. \end{aligned} \quad (4.15)$$

Proof: For the detailed proof refer to [113, p. 1401]. ■

It can be noted that the minimum information-transmission rate to stabilize an overall LTI feedback system increases not only with the magnitude and the number of the unstable poles, but also with the amount of time delay r_d , which is reflected by the relative degree d for discrete-time systems, and the nonminimum-phase zeros of the plant.

4.3 AN UPPER BOUND OF INFORMATION RATE AT THE “LIMITS OF CONTROLLABILITY”

In this section, we derive an upper bound of the information-transmission rate that refers to the situation when the control task is near the limits of controllability. By “the limit of controllability” we refer to the situation when the human operator is required to produce control movements in a quick manner in order to compensate for the high degree of instability of the plant. We assume that the human sensorimotor system is challenged to exhibit as much information as possible to stabilize the system, while being restricted to a “bang-bang” control strategy. We derived that the rate of information transmission from human to

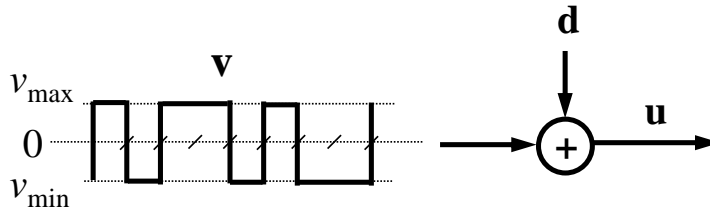


Figure 6: Pulse-like control signals in stabilizing highly unstable systems by the human.

machine in manual control of an unstable system with one degree of freedom (e.g. balancing of an inverted pendulum restricted in a plane) is limited to 4 b/s.

To explain the derivation, we considered the human-machine system in Fig. 5, and we investigated the rate of information transmission $I_\infty(\mathbf{v}; \mathbf{u})$ as an indication of the human control performance. We based our computation on two main assumptions.

First, the human was assumed to utilize discrete rather than continuous control strategies in stabilizing highly unstable systems, such that the control commands exhibit a pulse-like force pattern [107, 114]. Furthermore, as the task difficulty increased, each control output was approximated by a three-level switch operation (Fig. 6) to encode a left movement, right movement, or no action [114]. Therefore, the intended control command \mathbf{v} carries $\log_2 3 \approx 1.6$ bits of information for each control output. The information contained in a sequence of control actions is less than or equal to the sum of information carried by individual actions (equal when the control actions are independent of each other). Hence, the rate of information carried by \mathbf{v} is no more than 1.6 bits per control action:

$$H_\infty(\mathbf{v}) \leq 1.6 \text{ bits per action.}$$

Second, the control actions are assumed to be triggered at relatively constant intervals of no less than 0.4 seconds [115, 114, 5]. Thus, we can obtain the rate of information per unit time:

$$H_\infty(\mathbf{v}) \leq 1.6/0.4 = 4 \text{ b/s.}$$

According to the definition of the mutual information rate (3.7) and the non-negativity property of the discrete entropy rate, $H_\infty(\mathbf{v}|\mathbf{u}) \geq 0$, we have that

$$I_\infty(\mathbf{v}; \mathbf{u}) = H_\infty(\mathbf{v}) - H_\infty(\mathbf{v}|\mathbf{u}) \leq H_\infty(\mathbf{v}) \leq 4 \text{ b/s}. \quad (4.16)$$

We emphasize that the upper bound of the information-transmission rate estimated by 4 b/s refers to the maximum amount of information that the human controller generates using a three-level switch assuming the task to be near the limits of controllability. For more detailed information about this study, please refer to our previous work [116].

However, we are interested in approximating the information-transmission rate of human controllers by relaxing this assumption. Specifically, we want to estimate the information rate directly from the time series that represents the control signal generated by humans. Therefore, we conducted our own experiments for different levels of difficulty of the task by testing different degrees of instability and by including different amounts of time delay.

4.4 AN UPPER BOUND OF INFORMATION RATE FROM HUMAN EXPERIMENTS

In this section we focus on quantifying the information-transmission rate, $I_\infty(\mathbf{y}; \mathbf{u})$, directly from our own human experiments. We first describe the experimental setup, and then introduce the method of estimating the information-transmission rate using tools from time series analysis.

4.4.1 Human Subjects Participation

Twelve voluntary human subjects were recruited to participate in this study, aged between 20 and 35 years old. The subjects had to perform the task of balancing an inverted pendulum restricted in a plane. The linearized dynamics of the inverted pendulum was simulated in Matlab following the protocol by Bodson [3]. The human controller received visual feedback through a graphical user interface (GUI) from the computer screen. The control signal was exerted with one degree of freedom using a Logitech ATK3 joystick (Fig. 7).



Figure 7: Experiment setup: human operators had to maneuver a joystick to stabilize a planar inverted pendulum simulated on a computer screen. The graphical user interface (GUI) was adapted from [3].

The following scenarios were tested in which the difficulty of the control task was increased:

1. various amounts of time delay in the feedback system: a pendulum length of 20 m was used for the following amounts of time delay: 0, 100, 200, 400, and 600 ms;
2. different degrees of instability of the task (by varying the pendulum length) without time delay: the pendulum lengths considered are 20, 12, 8, 5, and 3 m.

The subjects were instructed to keep the inverted pendulum as close as possible to the upright vertical position ($\theta \approx 0$), and they were told that this deviation was the measure of performance. When the task would become too difficult to control, they were encouraged to adopt any strategy in order to avoid the falling of the inverted pendulum.

Before the experiment, each subject was allowed a short training session in order to accommodate to the task and gain confidence in their ability to stabilize the inverted pendulum. We observed that most of the subjects were able to perform the control task after a few minutes of practice, and they improved slowly afterward.

For the experiment, ten trials were recorded for each time delay and each pendulum length, corresponding to the scenarios mentioned above. The duration of a trial was 60 seconds, unless the pendulum was dropped before this time elapsed and the trial was terminated. A trial was marked as “successful” if the subject succeeded in stabilizing the inverted pendulum for the entire 60 seconds. Both successful and unsuccessful trials counted for the analysis of the experimental data in order to reflect the human capabilities and limitations for each considered situation.

The human subjects were paid volunteers, and the experiments were approved by the University of Pittsburgh Institutional Review Board (IRB) with ID: PRO11110083.

4.4.2 Difficulties Computing the Mutual Information Rate

As a component of a feedback control system, the controller is expected to generate command signals to ensure the stability of the closed-loop system. The capability of the controller to convey information is measured by the mutual information rate (3.13):

$$\begin{aligned}
I_\infty(\mathbf{y}; \mathbf{u}) &= \limsup_{n \rightarrow \infty} \frac{I(\mathbf{y}^{n-1}; \mathbf{u}^{n-1})}{n} & (4.17) \\
&= \limsup_{n \rightarrow \infty} \frac{h(\mathbf{y}^{n-1})}{n} + \limsup_{n \rightarrow \infty} \frac{h(\mathbf{u}^{n-1})}{n} - \liminf_{n \rightarrow \infty} \frac{h(\mathbf{y}^{n-1}, \mathbf{u}^{n-1})}{n} \\
&= \limsup_{n \rightarrow \infty} \frac{h(\mathbf{u}^{n-1})}{n} - \liminf_{n \rightarrow \infty} \frac{h(\mathbf{u}^{n-1} | \mathbf{y}^{n-1})}{n}
\end{aligned}$$

where the mutual information is defined using finite partitions as in (3.1) for the time series $\mathbf{y}^{n-1} = \{\mathbf{y}(k)\}_{k=0}^{n-1}$ and $\mathbf{u}^{n-1} = \{\mathbf{u}(k)\}_{k=0}^{n-1}$, with $\mathbf{y} \in \mathbb{R}^s$, $\mathbf{u} \in \mathbb{R}^q$. By assuming that the input \mathbf{y} and the output \mathbf{u} of the controller can be measured with an arbitrarily high sampling frequency (i.e. great resolution), the following difficulties are encountered when computing the mutual information rate direct numerically:

- The joint probability distributions are unknown, and they would have to be estimated from the finite number of data samples obtained from the measurements. This could introduce a bias in the estimation, especially if the “naive” box counting method is considered for probability distribution estimation [48, 49, 50, 51, 52, 64].

- The computation of infinite limits involves additional difficulties due to finitely many data samples and limited computational resources.
- The time series is recorded at a fixed sampling frequency, and the observed samples have to be assigned to the discrete sequences \mathbf{y}^{n-1} and \mathbf{u}^{n-1} : if data is oversampled, then even a large sequence may not contain enough information to characterize the system due to redundancies; if the data is undersampled, then very important properties of the system may be lost when estimating the joint probability distributions.
- The computation of the joint entropy rate $h_\infty(\mathbf{y}, \mathbf{u})$ and the conditional entropy rate $h_\infty(\mathbf{u}|\mathbf{y})$ is also difficult because the signals are of different types: how does one scale the observables of one signal relative to the other? One of the signals may dominate the resulting entropy rate estimation, thus generating a biased result.

Instead of computing $I_\infty(\mathbf{y}; \mathbf{u})$ according to (4.17) with the challenges mentioned above, we hypothesize that the human sensorimotor system can be modeled as a dynamical system. Consequently, we can apply numerical methods to estimate the entropy rate of the manual control signal \mathbf{u} as introduced in section 3.2. We pursued this approach because we only have to focus on estimating the probability distribution of one time series rather than evaluate the joint probability distribution of \mathbf{y} and \mathbf{u} . The numerical method to estimate the entropy rate of a time series using the correlation sum formulation (3.22) has proven to be a robust method in time series analysis [4]. Moreover, it provides techniques to mitigate difficulties related to both oversampling/undersampling and quantizing the recorded time series.

Furthermore, *studying the human controller as a dynamical system* can provide additional insight about the “internal states” of the human sensorimotor system. It is difficult, if not impossible, to determine these states in practice. However, the entropy rate of a time series is able to provide the average information needed to encode a state with a certain accuracy, or how much information is gained about present observations of the human output given past measurements.

However, an important gap has to be addressed between $I_\infty(\mathbf{y}; \mathbf{u})$, which represents the desired quantity to be estimated, and the entropy rate of the control signal h_q , which would be the actual estimated quantity. We will prove in the next section that the latter is an upper bound of the former under certain assumptions.

4.4.3 An Upper Bound for $I_\infty(\mathbf{y}; \mathbf{u})$

To establish an upper bound for $I_\infty(\mathbf{y}; \mathbf{u})$, we first consider the relationship between the mutual information rate of continuous random variables and their quantized version (3.8):

$$I_\infty(\mathbf{y}; \mathbf{u}) = \sup_{\epsilon} I_\infty(\mathbf{y}_\epsilon; \mathbf{u}_\epsilon). \quad (4.18)$$

By quantizing a continuous random variable, we obtain a discrete random variable with a finite alphabet. The next theorem provides an upper bound for the mutual information of discrete random variables, $I_\infty(\mathbf{y}_\epsilon; \mathbf{u}_\epsilon)$, given that \mathbf{y} is a deterministic function of \mathbf{u} . In other words, the upper bound of the information-transmission rate can be defined by the entropy rate of the control signal given that the plant dynamics are known.

Theorem 3: Consider the feedback control system in Fig. 5, where the plant is a causal LTI system. The following relationship holds for the mutual information rate of two discrete random variables (also applies to the quantized version of two continuous variables):

$$I_\infty(\mathbf{y}_\epsilon; \mathbf{u}_\epsilon) \leq H_\infty(\mathbf{u}_\epsilon). \quad (4.19)$$

Proof: For the discrete-time plant P in Fig. 5 the output \mathbf{y} can be determined by the input \mathbf{u} and the fixed initial condition $\mathbf{x}(0)$ such that

$$\mathbf{y}(k+1) = P(k, \mathbf{u}^k, \mathbf{x}(0)), \quad k \in \mathbb{N} \quad (4.20)$$

where \mathbf{u} and $\mathbf{x}(0)$ are independent of each other. The following relationships can then be established:

$$I_\infty(\mathbf{y}_\epsilon; \mathbf{u}_\epsilon) = I_\infty(P(\mathbf{u}_\epsilon, \mathbf{x}(0)); \mathbf{u}_\epsilon) \quad (4.21)$$

$$\leq I_\infty(\mathbf{u}_\epsilon, \mathbf{x}(0); \mathbf{u}_\epsilon) \quad (4.22)$$

$$= I_\infty(\mathbf{u}_\epsilon; \mathbf{u}_\epsilon) + I_\infty(\mathbf{x}(0); \mathbf{u}_\epsilon | \mathbf{u}_\epsilon) \quad (4.23)$$

$$= H_\infty(\mathbf{u}_\epsilon) + I_\infty(\mathbf{x}(0); \mathbf{u}_\epsilon) \quad (4.24)$$

$$= H_\infty(\mathbf{u}_\epsilon) \quad (4.25)$$

where (4.21) was obtained by substituting (4.20); the data processing inequality (3.10) was applied to obtain the inequality (4.22); the mutual information chain rule (3.9) yields (4.23);

then (4.24) follows by definition of the entropy for discrete random variables; (4.25) is obtained by assuming the initial condition $\mathbf{x}(0)$ of the plant and the control signal \mathbf{u} independent of each other. ■

The final element to bridge the gap between the information-transmission rate, $I_\infty(\mathbf{y}; \mathbf{u})$, and the entropy rate of dynamical systems is the equivalence between Shannon’s entropy rate for discrete variables, $H_\infty(\mathbf{u}_\epsilon)$, and the entropy rate for dynamical systems, which is established in the next section.

4.4.4 Equivalence between Shannon’s Entropy Rate and the Entropy Rate of Dynamical Systems

The entropy rate of dynamical system was introduced in section 3.2 using the general formulation $h_q(m, \epsilon)$ given by expression (3.15). This method implies that the continuous phase space of the dynamical system be coarse grained with a finite partition of ϵ -size cells. By assigning a unique symbol to each cell, the evolution over time of the trajectory in the phase space corresponds to a sequence of finitely many symbols. Therefore, coarse graining the phase space generates a discrete random variable such that the entropy for dynamical systems is applied to a finite alphabet. In order to obtain Shannon’s definition of the entropy rate (3.11), we have to take the limit $q \rightarrow 1$ such that:

$$H_\infty(\mathbf{u}_\epsilon) = \lim_{m \rightarrow \infty} \lim_{q \rightarrow 1} h_q(m, \epsilon) \quad (4.26)$$

Therefore, the entropy rate of dynamical systems that depends on the size of the partition is, by definition, equivalent to Shannon’s entropy rate for discrete random variables [75].

Gaspard and Wang [70] referred to $h_q(m, \epsilon)$ as *coarse-grained dynamical entropy* and ϵ -entropy per unit time based on its scaling with the resolution ϵ . They emphasized the advantages of evaluating $h_q(m, \epsilon)$ relative to different values of ϵ , such as observing a convergence to a constant entropy rate (“plateau”) over a range of ϵ -values. It should be noted that in expression (4.26) both Shannon’s entropy rate and the entropy rate of dynamical systems depend on ϵ . How do these two entropy rates vary with ϵ ? Do they yield the same behavior? To address these questions, we have to discuss the general relationship between Shannon’s entropy rate formula and the entropy rate of dynamical systems. These

two quantities depend on both the type of the system (deterministic or stochastic) and the alphabet (continuous range or enumerable finite elements) as it is illustrated in Table 1. Their compatibility depends strictly on these properties.

The entropy rate definition by Claude Shannon [2] applies to **stochastic processes** characterized by probability measures. According to expression (3.6), we know that, for *continuous* random variables, the differential entropy rate h_∞ is a finite constant (positive or negative) and the entropy rate H_∞ diverges to infinity with $\epsilon \rightarrow 0$. However, for *discrete* random variables, the entropy rate H_∞ has a constant nonnegative value, while the differential entropy rate h_∞ diverges to minus infinity.

The Kolmogorov-Sinai entropy h_{KS} is a specific case of the entropy rate of **dynamical systems**, and it is defined as:

$$h_{KS} = \lim_{q \rightarrow 1} \lim_{\epsilon \rightarrow 0} \lim_{m \rightarrow \infty} h_q(m, \epsilon) \quad (4.27)$$

where the supremum over all ϵ -size partitions from the definition (3.16) was replaced with the limit $\epsilon \rightarrow 0$. By relaxing this limit, we are able to assess the general variation of the entropy rate of dynamical systems, $h_q(m, \epsilon)$, relative to the ϵ -scale in order to understand the convergence and divergence of h_{KS} for the deterministic- and the stochastic case, respectively. These results are summarized in Table 1 with the corresponding Shannon's entropy rates. Moreover, the Kolmogorov-Sinai entropy is considered to be an important tool to classify dynamical systems as we will illustrate next.

Table 1: Relationship between Shannon's entropy rate and the entropy rate of dynamical systems for discrete- and continuous dynamics.

	Stochastic	Deterministic
Discrete	$0 \leq h_{KS} = H_\infty < \infty$ $h_\infty \rightarrow -\infty$	$0 \leq h_{KS} = H_\infty < \infty$ $h_\infty \rightarrow -\infty$
Continuous	$h_{KS} = h_\infty - \log \epsilon$ $H_\infty, h_{KS} \rightarrow \infty$ $-\infty < h_\infty < \infty$	$0 \leq h_{KS} < \infty$ H_∞, h_∞ - undefined relation to h_{KS}

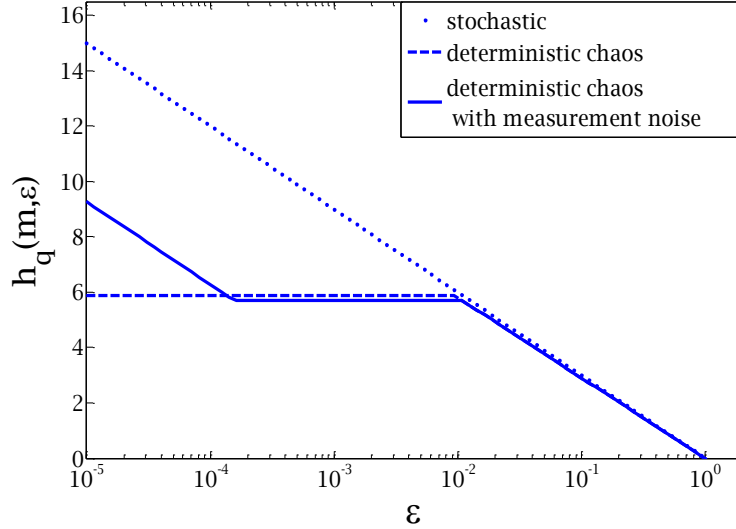


Figure 8: Coarse-grained entropy rate $h_q(m, \epsilon)$ of a stochastic signal (dotted line), a deterministic signal (dashed line), and a deterministic signal with measurement noise (solid line). Figure adapted from [4].

If the trajectory of the dynamical system evolves in *continuum*, then the typical shapes of the entropy rate, $h_q(m, \epsilon)$, are shown in Fig. 8 relative to different ϵ -length scales:

- If ϵ is comparable to the range of observables, then we obtain trivially that $h_q(m, \epsilon) = 0$.
- For deterministic systems (dashed curve), $h_q(m, \epsilon)$ scales to a finite constant for small values of ϵ and sufficiently large m . It was shown [67, 69, 70] that this value is a good numerical approximation to the Kolmogorov-Sinai entropy: $h_q(m, \epsilon) \approx h_{KS}$. The value of this constant is nonnegative, and it classifies the dynamical system according to the degree of “chaoticity” [117, p.24]: $h_{KS} = 0$ for classical dynamical systems; and $0 < h_{KS} < \infty$ for chaotic systems.
- For stochastic systems (or deterministic systems with m not sufficiently large) the entropy rate diverges to infinity: $h_q(m, \epsilon) \rightarrow \infty$ for $\epsilon \rightarrow 0$ (dotted curve). This result is not surprising, since the relationship between Shannon’s entropy rate and the entropy rate of dynamical systems in this case is established by: $h_q(m, \epsilon) = h(m) - \log \epsilon$, where h is a

constant value for the differential entropy (3.6). It should be noted that the expression only holds if the stochastic process has an *absolutely continuous probability measure*. For a detailed mathematical proof refer to [118, 119].

- For a deterministic system with measurement noise (solid curve), $h_q(m, \epsilon)$ exhibits a plateau in an intermediate range of ϵ and then scales like $-\log \epsilon$ for $\epsilon \rightarrow 0$. This case illustrates the sensitivity of the method relative to the noise level in the system.

It seems that the convergence of the dynamical entropy rate $h_q(m, \epsilon)$ to a plateau in the continuous case implies that the system is deterministic (possibly chaotic for positive values), rather than stochastic. However, if the state space is covered by *finitely many* states, the entropy rate of dynamical systems (and, implicitly, the Kolmogorov-Sinai entropy due to the independence to ϵ) is applied to discrete dynamics, and it converges to a nonnegative constant value that equals Shannon’s entropy rate (i.e. first row in Table 1). This is indeed the case under which our expression (4.26) holds. Therefore, in order to ensure the applicability of this expression to manual control, we have to assume that the repertoire of control movements consists of a finite set of possible actions that can be associated with the states of the phase space. We will show in the next section that the preference (or rather the necessity) of human operators to adopt intermittent control, which is characteristic for stabilizing unstable systems, is consistent with our assumption.

4.4.5 Quantifying Intermittent Control with $h_q(m, \epsilon)$

We observed in section 4.1.1 that human controllers exhibit intermittent control when stabilizing an unstable system: serial actions are pre-planned using accumulated sensory feedback and executed ballistically without sensory feedback [91, 93, 94, 95, 96]. These characteristics of intermittent control seem to be apparent in the trajectory of the velocity of the control actions, which is illustrated in Fig. 9 together with the trajectory of the pendulum angle. The time interval between consecutive control movements represents the time delay associated with the processing of sensory information, response selection (refractory period), and execution of the movement through muscle contraction. It is apparent that control movements are indeed triggered at discrete time intervals.

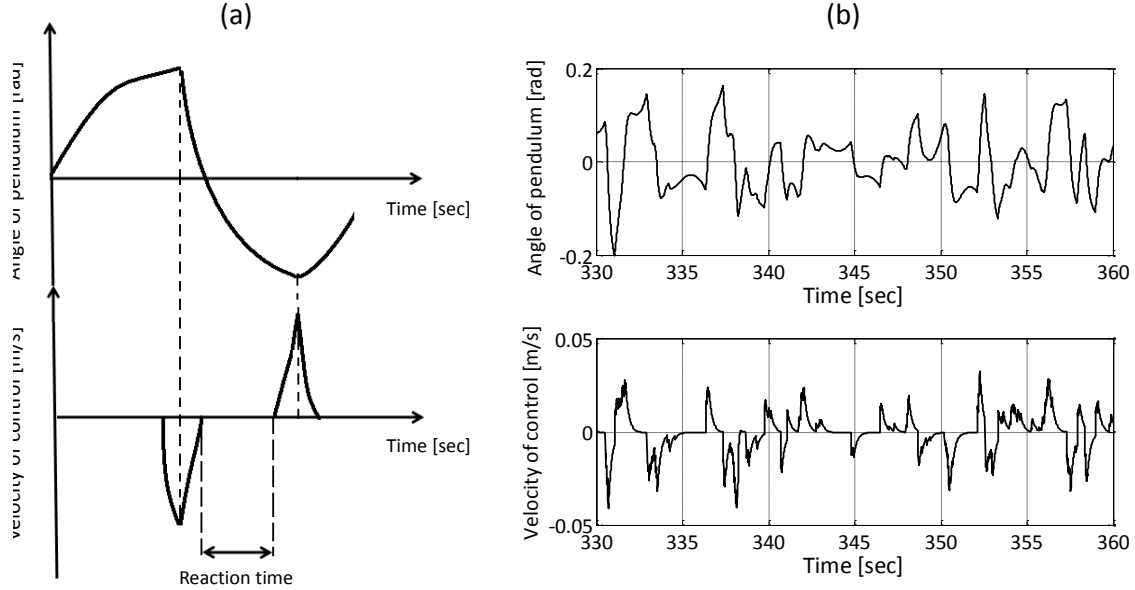


Figure 9: Intermittent control in the trajectory of the pendulum angle (top), and the corresponding velocity of the control movements (bottom). Example of a predicted profile (a), and an actual profile from experiments (b) (Subject H , 5 m long pendulum, no time delay).

The human controller is restricted by the task complexity to generate fast control commands with which he/she is very familiar. Therefore, the control actions are executed ballistically (open loop), and they must originate from a set of pre-learned movements. This set is assumed to be finite, and intra-movement variations could be explained by the state-dependent noise. We can associate these reflex-type control movements with the states of a dynamical system, and the transition between states is determined by neuromuscular planning and execution of the movement. Therefore, the human controller can be assumed to act as a stochastic dynamical system with finitely many states. Furthermore, studies [120, 121] showed that intermittency in manual control exhibits a continuous but non-differentiable trajectory. Therefore, discrete-type movements of human operators seem evident in the control of unstable systems. The equivalence between Shannon's entropy rate and the entropy rate of dynamical systems from expression (4.26) is thus established because of the discrete-type dynamics of the human output.

Applying the entropy rate formula for dynamical systems, $h_q(m, \epsilon)$, to quantify the complexity of manual control appears adequate. The time series that we observe from the output of the human controller represents the trajectory of the velocity of movements. The exact states of the dynamical system are unknown, but they can be reconstructed using delay vectors $\mathbf{u} = [u(k), u(k - \tau), \dots, u(k - (m - 1)\tau)]^T$, where $k = (m - 1)\tau + 1, \dots, N$. The entropy of block size m (3.14) quantifies the amount of information needed to predict the next state given the history of the past states. Or, similarly, it estimates the average amount of information required to encode a state represented by a control action. The entropy rate $h_q(m, \epsilon)$ as in equation (4.29) provides the rate of information measured in bits per second.

4.4.6 Numerical Estimation of $h_q(m, \epsilon)$ using $q = 2$

Recall from expression (3.22) that the entropy rate can be computed using the correlation sum for the range of ϵ -values that resemble a plateau:

$$h_q(m, \epsilon) = \frac{1}{q - 1} \log \frac{C_q(m, \epsilon)}{C_q(m + 1, \epsilon)} \quad \text{bits/sample.} \quad (4.28)$$

It should be noted that, beyond the variation with ϵ and m , the general formulation of the entropy rate using order- q Renyi entropies is also dependent on q . Although taking $q \rightarrow 1$ yields Shannon's entropy rate, the accuracy of this estimate is strongly dependent on the quality and the amount of data samples. Following the protocol of Grassberger and Procaccia [69], we compute $h_q(m, \epsilon)$ using the order $q = 2$, because it is by far the easiest to estimate: the correlation sum only requires the computation of the arithmetic average over the number of neighbors. Moreover, choosing $q = 2$ was shown to be a numerically robust method and not to introduce a bias in the estimation of the correlation sum because of finite statistics [4, ch. 11]. When a plateau can be observed in the plot of $h_2(m, \epsilon)$ versus ϵ , the value of this plateau, h_2 , is related to Shannon's entropy rate by the relationship: $h_2 \leq h_1$ [4, ch. 11]. Moreover, h_2 is known to provide a very good numerical approximation of Shannon's entropy rate [67, 68, 69, 70].

The entropy rate $h_2(m, \epsilon)$, also called *correlation entropy*, can then be computed in terms of bits per second:

$$h_2(m, \epsilon) = \frac{1}{\tau} \log \frac{C_2(m, \epsilon)}{C_2(m+1, \epsilon)} \quad \text{b/s} \quad (4.29)$$

where τ is the lag in the delay vector, and m is the embedding dimension. The correlation sum $C_2(m, \epsilon)$ can be defined such that it accounts for temporal correlations between delay vectors:

$$C(m, \epsilon) = \frac{2}{(M - n_{min})(M - n_{min} - 1)} \sum_{i=1}^M \sum_{j=i+n_{min}+1}^M \Theta(\epsilon - \|\mathbf{u}(i) - \mathbf{u}(j)\|). \quad (4.30)$$

The delay vectors in the correlation sum may not be drawn randomly (i.e. statistically independent) from a corresponding probability distribution. A bias is introduced when delay vectors at successive times are also close in phase space due to the continuous time evolution [4, ch. 6]. In order to avoid such undesired temporal correlations between adjacent vectors, Theiler [122] suggested excluding the pairs of delay vectors that are closer than $n_{min}\Delta t$ seconds to each other, where Δt is the sampling frequency of the time series. The time interval $n_{min}\Delta t$ can be obtained using the space-time separation plot.

The computation of $h_2(m, \epsilon)$ from the time series representing manual control actions was performed with the help of the software package TISEAN (TIme SEries ANalysis) [123, 124].

To summarize, we iterated the difficulties of estimating the mutual information rate from a limited amount of data. We illustrated the computational advantages of estimating the entropy rate of the time series, $h_2(m, \epsilon)$ (4.29), which is assumed to numerically approximate Shannon’s entropy rate of the quantized version of a continuous trajectory represented by the time series (4.26). We proved in the previous section that the latter represents an upper bound to the mutual information rate (Theorem 3).

Therefore, if $h_2(m, \epsilon)$ plotted versus ϵ scales to a plateau for increasing m , then its value approximates an upper bound for $I_\infty(\mathbf{y}; \mathbf{u})$ such that it quantifies the “best” human performance. We will evaluate this upper bound relative to the minimum thresholds established in (4.6) and (4.14) for any controller (not necessary LTI), and an LTI controller, respectively.

4.5 BANDWIDTH LIMITATIONS IN FEEDBACK CONTROL SYSTEMS

The performance of a feedback control system is directly reflected by the shape of its frequency response. A desired performance can be obtained when a certain shape is imposed upon the sensitivity function and the complementary sensitivity function. However, some limitations exist and certain trade-offs have to be considered, especially when the dynamics encountered in the closed-loop system include unstable poles, nonminimum phase zeros and/or time delay.

This section discusses the restrictions imposed on the bandwidth of a closed-loop system based on these limitations and trade-offs when a desired performance is required. The purpose of this study is to understand the behavior of the human controller when time delay and unstable poles are present in the feedback loop. A more detailed description of this investigation can be found in our previous work [22].

4.5.1 Design Trade-Offs in Feedback Control Systems

The first limitations and trade-offs in feedback control design were established by Bode [125], who introduced the Bode sensitivity integral. Later, Horowitz [126] investigated the application of the sensitivity integral in feedback system design. Freudenberg and Looze [127, 128] extended these results to band-limited systems with unstable poles, nonminimum phase zeros, and time delay. A dual result to Bode's sensitivity integral using the complementary sensitivity integral was established by Middleton and Goodwin [129, 130, 131].

Consider the closed-loop system in Fig. 10 which includes the plant P and a controller K , both LTI. The sensitivity function, $S(\cdot)$, and the complementary sensitivity function, $T(\cdot)$, are defined as following:

$$\begin{aligned} S(s) &= \frac{1}{1 + L(s)} \\ T(s) &= \frac{L(s)}{1 + L(s)} \end{aligned} \tag{4.31}$$

where “ s ” is the Laplace variable, and $L(s) = P(s)K(s)$ is the open-loop transfer function. The complementary sensitivity function is equivalent to the closed-loop transfer function.

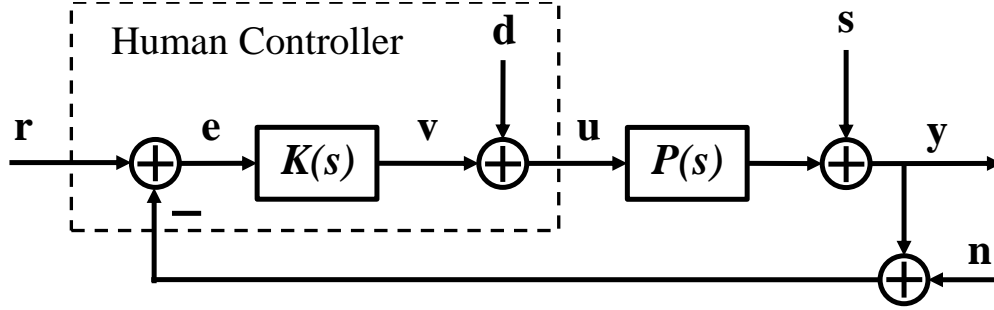


Figure 10: An LTI feedback control system with controller K and plant P : \mathbf{r} - reference signal, \mathbf{y} - output signal, \mathbf{d} - disturbance related to human movement, \mathbf{s} - disturbance of the overall system, \mathbf{n} - measurement noise.

The shapes of both the sensitivity function and the complementary sensitivity function influence directly the performance of the closed-loop system:

1. $|S(j\omega)| \ll 1$ is desirable to:
 - appropriately track the reference signal \mathbf{r} ;
 - reject disturbances \mathbf{d} and \mathbf{s} ;
 - minimize the sensitivity to additive variations of the plant dynamics.
2. $|T(j\omega)| \ll 1$ is required for:
 - rejection of measurement noise \mathbf{n} ;
 - robustness to unstructured uncertainties.
3. $S(j\omega) + T(j\omega) = 1$ should be satisfied by definition for any frequency.

Due to the latter constraint, both $|S(j\omega)|$ and $|T(j\omega)|$ cannot be made small at the same time. Therefore, a *trade-off* exists between the first two sets of properties at any frequency. Practice shows that good tracking performance and disturbance rejection are required at low frequencies, and that stability robustness and measurement noise rejection must be ensured at high frequencies [127, 128]. The typical shapes of $|S(j\omega)|$ and $|T(j\omega)|$ to reflect these design trade-offs are illustrated in Fig. 11.

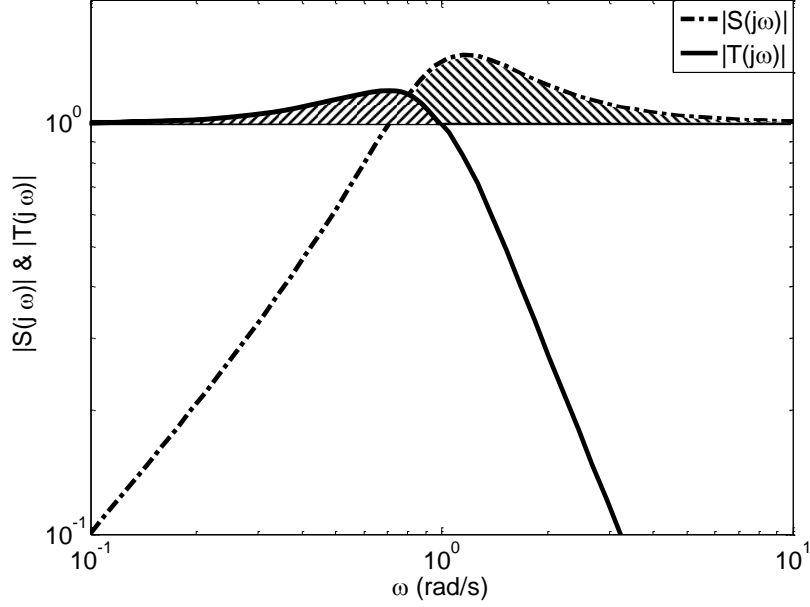


Figure 11: Magnitudes of the sensitivity function and the complementary sensitivity function on log-log scale (base 10) that reflect feedback design trade-offs. The sensitivity amplification areas in the sensitivity function and the complementary sensitivity function are marked.

Bode's sensitivity integral [125] introduces an additional trade-off in the feedback control design. Let $L(s)$ be an open-loop transfer function that is rational and stable with relative degree of at least two. Then, if the feedback control system is stable, the sensitivity function satisfies Bode's sensitivity integral:

$$\int_0^{\infty} \log |S(j\omega)| d\omega = 0. \quad (4.32)$$

The negative values of the sensitivity magnitude on a logarithmic scale at certain frequencies represent desirable *sensitivity reduction* of the feedback system. Bode's integral shows that the area corresponding to this frequency range has to equal the area corresponding to the *sensitivity amplification*. Hence, regardless of the design of the controller, any sensitivity improvement in a frequency range requires a sensitivity deterioration in another frequency range. More recent studies show that Bode's integral also holds for nonlinear systems [132, 133] and time-varying systems [134].

Let $L(s)$ be an open-loop transfer function that is rational **with unstable poles** $\{p_i : i = 1, \dots, N_p\}$ and has relative degree of at least two. Then, if the associated closed-loop system is stable, the sensitivity function satisfies [127]

$$\int_0^\infty \log |S(j\omega)| d\omega = \pi \sum_{i=1}^{N_p} \operatorname{Re}(p_i). \quad (4.33)$$

Bode's sensitivity integral formula for unstable systems shows that the area of the sensitivity amplification ($\log |S(j\omega)| > 0$) is larger than the area of sensitivity reduction ($\log |S(j\omega)| < 0$) by a constant that varies with the number and magnitude of the unstable poles of the open-loop system.

The dual of Bode's sensitivity integral shows that the trade-off described by the sensitivity integral is worsened if the open-loop system has nonminimum phase zeros (i.e. zeros located in the open right half of the s -plane) and/or time delay. Let $L(s)$ be an open-loop transfer function of the form $L(s) = \tilde{L}(s)e^{-s\tau}$, where $\tilde{L}(s)$ is rational with nonminimum phase zeros $\{z_i : i = 1, \dots, N_z\}$, and τ is the time delay. If $L(s)$ has at least one pole at the origin and the closed-loop system is stable, then the complementary sensitivity function satisfies [129]

$$\int_0^\infty \log |T(j\omega)| \frac{d\omega}{\omega^2} = \pi \sum_{i=1}^{N_z} \operatorname{Re} \left(\frac{1}{z_i} \right) + \frac{\pi}{2} \tau - \frac{\pi}{2} K_v^{-1}. \quad (4.34)$$

where $K_v = \lim_{s \rightarrow \infty} sL(s)$ is the velocity constant of the system.

4.5.2 Bandwidth Constraints of Feedback Systems

In real applications, physical systems exhibit unexpected behavior beyond a certain bandwidth due to unmodeled nonlinear dynamics, digital control implementations, hardware elements, power limitations and others. Stein [103] defined the "available bandwidth" as the frequency up to which the physical system resembles the frequency response of the nominal model. Beyond this frequency, the magnitude corresponding to the frequency response of the closed-loop system should roll off rapidly to guarantee robust stability. Therefore, the available bandwidth is always finite, which implies that the integrals (4.32) - (4.34) have to be satisfied for a limited bandwidth.

Middleton [130] suggested approximate bounds on the sensitivity function and the complementary sensitivity function (not shown here), that comply with the general trade-offs illustrated in Fig. 11, in order to impose a *certain desired performance* of the closed-loop system. Substituting these bounds into the sensitivity integral (4.33) and the complementary sensitivity integral (4.34) yields the following inequalities [130, Lemma 13 & 14])

$$\sup_{\omega \in \mathbb{R}} |S(j\omega)| \geq e^{\frac{\pi}{2\omega_c} \sum_{i=1}^{N_p} \text{Re}(p_i)} \quad (4.35)$$

$$\sup_{\omega \in \mathbb{R}} |T(j\omega)| \geq 0.25e^{2\omega_c \left[\frac{\tau}{2} + \sum_{i=1}^{N_z} \text{Re}\left(\frac{1}{z_i}\right) \right]} \quad (4.36)$$

where ω_c is the bandwidth (in rad/sec) of the closed-loop system corresponding to the half-power frequency (i.e. $|T(j\omega_c)| = 1/\sqrt{2}$). For performance purposes we can restrict the peaks of the sensitivity function and the complementary sensitivity function to be $\sqrt{2}$. When expressed in terms of the bandwidth ω_c , the inequalities (4.35) and (4.36) become

$$\omega_c \geq 4.5 \sum_{i=1}^{N_p} \text{Re}(p_i) \quad (4.37)$$

$$\omega_c \leq 0.9 \left[\frac{\tau}{2} + \sum_{i=1}^{N_z} \text{Re}\left(\frac{1}{z_i}\right) \right]^{-1} \quad (4.38)$$

The bandwidth of the feedback system seems to have a lower bound (4.37) set by the unstable poles of the open-loop system (i.e. f_{min} from section 1.2) and an upper bound (4.38) determined by the nonminimum phase zeros and/or time delay of the open-loop system (i.e. f_{max} from section 1.2). Similar bounds can also be established in the time domain by probing the feedback system with a step response [130, 131].

To establish the relationship between the bandwidth of the open-loop system and the bandwidth of the closed-loop system, we recall expression (4.31) such that:

- $|L(j\omega)| \gg 1 \Rightarrow |T(j\omega)| \approx 1;$
- $|L(j\omega)| \ll 1 \Rightarrow |T(j\omega)| \ll 1;$
- $|L(j\omega)| \approx 1$ and $\angle L(j\omega) \approx \pm 180 \Rightarrow |T(j\omega)| \gg 1.$

Therefore, the roll-off frequency of the open-loop system can be assumed to be close to the roll-off frequency of the feedback system. Moreover, if we assume the bandwidth of the plant to be larger than that of the controller, then the bandwidth of the open-loop system $|L(j\omega)|$ is directly related to the bandwidth of the controller. Therefore, we can apply the inequalities for the lower bound (4.37) and the upper bound (4.38) to the bandwidth of the controller in order to achieve the desired performance.

It should be noted that these inequalities are generated relative to the performance requirement set by the bounds of the sensitivity function and the complementary sensitivity function. Therefore, less restrictive performance of the feedback system will relax these bandwidth inequalities, while a performance with higher expectations will make them tighter.

4.5.3 Power Spectrum and Information-Transmission Rate

Beyond bandwidth limitations in manual control, we believe that the shape of the power spectrum of the control signal can provide additional insight into the variation of the information-transmission rates when time delay and higher degrees of instability affect the task. Therefore, we would like to address the following questions: is there any relationship between the power spectrum of the control signal and the information-transmission rate? Specifically, can we predict the variation of the information rate of manual control with time delay and degree of instability, based on the frequency distribution of the power spectrum? This analysis is supported by previous studies using tracking tasks [31, 135], which reported that optimal human performance is related not only to the bandwidth of the controller, but also to the frequency distribution in the power spectrum of the control signal.

The information-transmission rate is determined by two main components: the uncertainty of choosing a control action from a set of possible commands, and the rate at which these actions are executed. We propose a new information-theoretic formula that relates both of these quantities to the power spectrum of the control signal. We suggest computing the following weighted entropy rate:

$$h_{PS} = - \int_0^{\infty} f |U(f)|^2 \log_2 |U(f)|^2 df$$

where the power spectrum of the control signal $|U(f_i)|^2$ is a continuous function of the frequency distribution f . For computational purposes, we calculate the weighted entropy rate H_{PS} that applies to the quantized version of the power spectrum and has a finite number of frequency components:

$$H_{PS} = - \sum_{i \in F} f_i |U(f_i)|^2 \log_2 |U(f_i)|^2 \quad (4.39)$$

where F represents the set of all frequency points in the power spectrum $|U(f_i)|^2$. The weighted entropy rate H_{PS} reflects the uncertainty of choosing a control action corresponding to a frequency component (i.e. a periodic movement of a certain frequency) related to its frequency of execution. Because the power spectrum is a continuous function, the value of H_{PS} depends on the number of frequency points, similarly as in expression (3.6). Therefore, H_{PS} can only be used to illustrate a qualitative rather than a quantitative dependency of the information-transmission rate with time delay and degree of instability of the task. Moreover, nonlinear correlations between the samples of the control signal are lost when computing the power spectrum.

5.0 RESULTS

5.1 LOWER BOUNDS OF $I_\infty(\mathbf{y}; \mathbf{u})$

The lower bounds of the information-transmission rate of the controller, defined by $I_\infty(\mathbf{y}; \mathbf{u})$, were established in Theorem 1 for *any* deterministic controller, and in Theorem 2 for an *LTI* controller.

According to Theorem 1, the lower bound is a fixed quantity that depends only on the unstable poles of the open-loop system. Before evaluating expression (4.6), the differential equation that represents the dynamics of the inverted pendulum (4.1) was initially linearized for small variations of the pendulum angle θ , and then rewritten in the continuous state-space representation (4.2). By discretization with the sampling period Δt , the state matrix A of the discrete-time state space representation (4.4) was obtained:

$$A = e^{A_c T_s} \tag{5.1}$$

where A_c is the state matrix of the continuous state space representation with unstable pole $\lambda_u = \sqrt{3g/2L}$. By applying the eigendecomposition theorem for the state matrix A , it can be shown that the unstable pole of the discrete-time plant is $\lambda = e^{\lambda_u \Delta t}$. The minimum rate of information to stabilize the feedback control system (4.6) can then be derived as follows:

$$\begin{aligned} \sum_{i=1}^p \log |\lambda_i| &= \log |e^{\lambda_u \Delta t}| \text{ bits/sample} \\ &= \lambda_u \cdot \Delta t \cdot \log e \text{ bits/sample} \\ &= \frac{1}{\Delta t} \cdot \lambda_u \cdot \Delta t \cdot \log e \text{ bits/second} \\ &= \sqrt{\frac{3g}{2L}} \cdot \log e \text{ b/s} \end{aligned}$$

The lower bound of the ITR varies with the degree of instability of the plant, which is inversely related to the pendulum length. Therefore, smaller pendulum lengths imply a larger degree of instability, and consequently the controller is required to deliver information at a higher rate to stabilize the feedback system.

Theorem 2 considers the special case when the controller is an LTI system. The inequality (4.14) was shown to include in the lower bound of the ITR not only unstable poles, but also nonminimum phase zeros and any time delay from the open-loop path. It should be noted that the inverted pendulum in our study does not have nonminimum phase zeros ($\eta = 0$). However, different amounts of time delay are introduced in order to evaluate the performance of the human controller. Therefore, the lower bound of the ITR (4.14) is shown to increase with both the degree of instability of the plant and the amount of time delay:

$$\begin{aligned} \frac{1}{2} \log \left(\prod_{i=1}^p |\lambda_i|^2 + \delta + \eta \right) &= \frac{1}{2} \log \left(|e^{\lambda_u \Delta t}|^2 + \delta \right) \text{ b/sample} \\ &= \frac{1}{\Delta t} \cdot \frac{1}{2} \log \left(|e^{\lambda_u \Delta t}|^2 + \delta \right) \text{ b/s} \end{aligned}$$

where

$$\delta = (1 - e^{2\lambda_u \Delta t})^2 \sum_{k=1}^{d-1} e^{2\lambda_u \Delta t(k-1)} \quad (5.2)$$

is a monotonic increasing function of d , the relative degree of the transfer function. For $\delta = 0$ (i.e. no time delay in this study), the lower bound coincides with the one from Theorem 1.

5.2 ESTIMATION OF $I_\infty(\mathbf{y}; \mathbf{u})$ USING h_2 FROM EXPERIMENTS

We have seen in section 4.4 that the information-transmission rate of the controller is described by the mutual information rate $I_\infty(\mathbf{y}, \mathbf{u})$, and its numerical computation involves many difficulties mainly due to finite statistics. However, we are able to estimate the entropy rate of the time series using h_2 defined in (4.29). Based on the observation that human manual control exhibits intermittency when stabilizing unstable systems (4.4.5) and thus generates discrete control movements, we established the equivalence of h_2 with Shannon's entropy rate, H_∞ . We proved in Theorem 3 (4.19) that the latter quantity represents

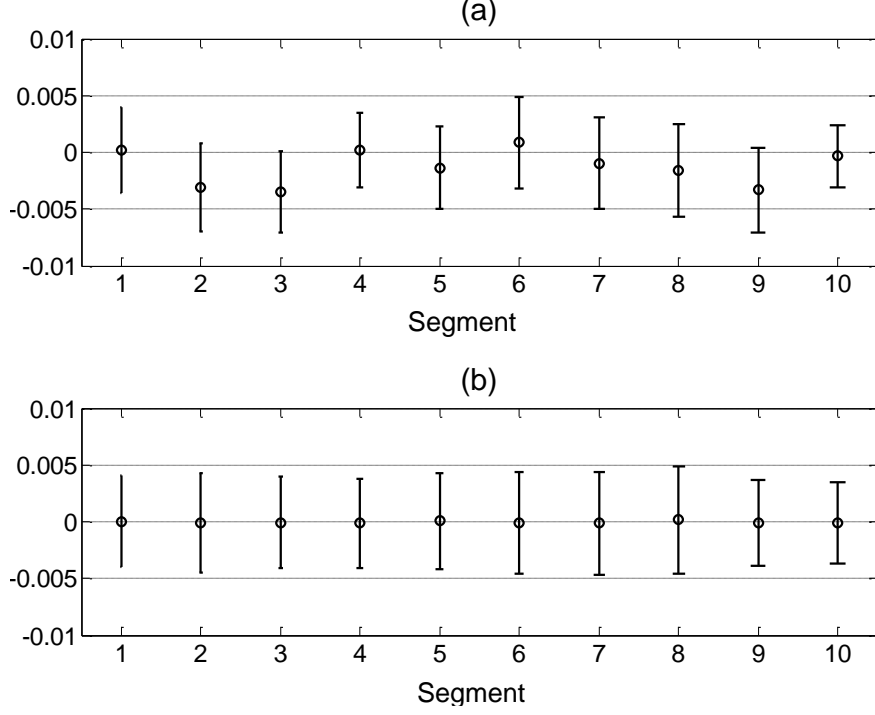


Figure 12: Probing stationarity: mean and standard deviation of the displacement x of the bottom tip of the pendulum (a), and its increment x_d (b). Ten non-overlapping segments of data are shown from subject D when a 400 ms time delay was considered.

an upper bound of $I_\infty(\mathbf{u}, \mathbf{y})$. Therefore, the following inequality holds when applied for the manual control sequence \mathbf{u} :

$$I_\infty(\mathbf{u}, \mathbf{y}) \leq h_2(\mathbf{u}). \quad (5.3)$$

In the human experiments described in section 4.1, the recorded control signal is the displacement x of the bottom tip of the pendulum. In order to apply our method for entropy rate estimation, the time series must be tested for stationarity. We regard the asymptotic stationarity conditions mentioned in section (3.1). The autocorrelation function is assumed to be independent of the lag, and we proceed with the verification of the mean and variance conditions. After testing for a constant mean and constant variance, we observe that the stationarity conditions are not met for the measured variable x to be considered stationary [Fig. 12(a)]. Therefore, we turn to a common practice by using *increments* (also

called returns) to render a stationary signal from a non-stationary signal [4, p. 279]. For discrete-time signals, this procedure implies taking the difference between adjacent samples: $x_d(n) = x(n+1) - x(n)$. The new signal is assumed stationary, and its mean and standard deviation are shown in Fig. 12(b) for 10 non-overlapping segments of the time series. We can now proceed with computing the entropy rate of the velocity of the generated joystick movements: $\mathbf{u}^N = \{x_d(k)\}_{k=1}^N$.

The estimation of the entropy rate $h_2(m, \epsilon)$ was performed using the TISEAN software package [4]. The control signal was recorded with a sampling period of $\Delta t = 10$ ms, which corresponds to a sampling frequency of 100 Hz. The time series corresponding to the ten trials of each tested scenario were concatenated in order to obtain a larger time series. Thus, more data samples were used for each subject and each scenario for the entropy estimation method in order to generate a representative result. These concatenated time series were then normalized to the interval $[0, 1]$, and a maximum embedding dimension of $m = 10$ was proven sufficient using the false nearest neighbors algorithm. The lag τ of the delay vector (3.19) was estimated by determining the first minimum of the delayed mutual information [4]. The values obtained for τ are given in appendix B, and the average values are shown in Table 2.

The entropy rate $h_2(m, \epsilon)$ is illustrated in Fig. 13 as a function of the embedding dimension m and the ϵ -scaling for a long pendulum (i.e. 20 m) and no time delay. With increasing m , the entropy rate settles to a plateau for smaller values of ϵ . The value of this plateau reflects the estimated entropy rate of the human control signal. The entropy rate plots when time delays are present in the open-loop system are shown in Fig. 14. Similarly, entropy rate plots for different pendulum lengths, corresponding to various degrees of instability of the task, are illustrated in Fig. 15.

Table 2: Average values for τ used for the delay vectors.

Pendulum length [m]	20					12	8	5	3
Time delay [ms]	0	100	200	400	600	0			
τ [samples]	15	17	16	17	20	15	14	14	15

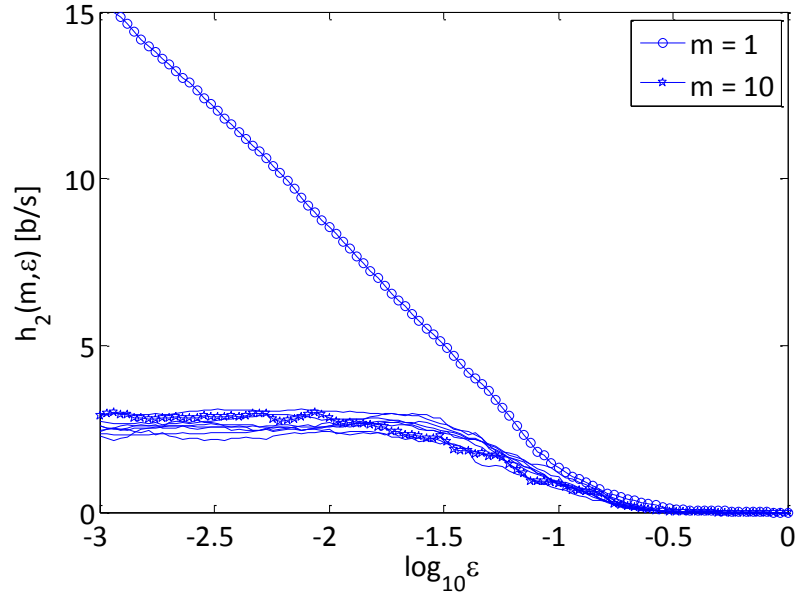


Figure 13: Entropy rate estimation of $h_2(\mathbf{u})$ with no time delay. The curves correspond to the embedding dimensions 1 (circles) to 10 (stars).

The estimated information-transmission rates using the entropy rate method are listed in Table 3 for successful readings. We define a “successful reading” when a plateau can be identified in the coarse-grained entropy plot, $h_2(m, \epsilon)$. It can be observed that some subjects encountered difficulties balancing the inverted pendulum with large time delay and high degree of instability. In these situations the pendulum was dropped in less than 60 seconds, and the limited amount of recorded data was not sufficient to generate a successful entropy-rate reading. The latter situation was marked with “-” in Table 3.

The results in Fig. 16 illustrate the successfully estimated information rates that were averaged over all subjects for each considered scenario. The information-transmission rate was observed to decrease with the amount of time delay in the feedback system [Fig. 16(a)]. The curve that describes the variation of the information-transmission rate with time delay intersects the lower bound set by Theorem 2 for a time delay of approximately 400 ms. However, this curve is always above the lower bound set by Theorem 1 for any amount of time delay.

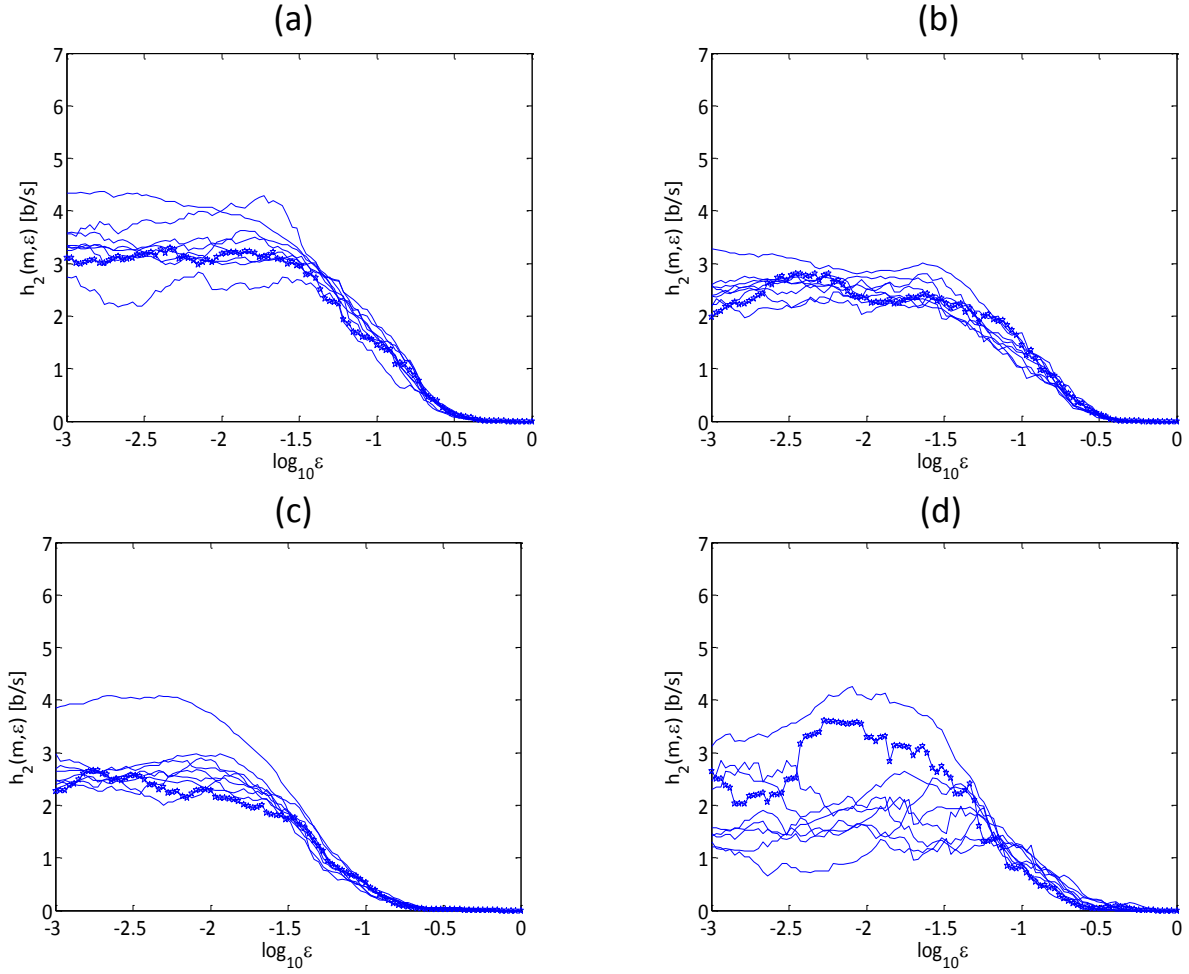


Figure 14: Entropy rate estimation of $h_2(\mathbf{u})$ with 100 ms (a), 200ms (b), 400 ms (c), and 600 ms (d) time delay. The curves correspond to the embedding dimensions 2 (circles) to 10 (stars).

For manual control tasks with higher degrees of instability, the minimum information-transmission rate required for feedback stabilization established by Theorem 1 suggests that the human controller should ramp up its capabilities to convey information when the degree of instability increases. The successfully estimated information-transmission rates reflect this tendency. The information-rate curve was observed to increase accordingly with the level of instability of the task [Fig. 16(b)].

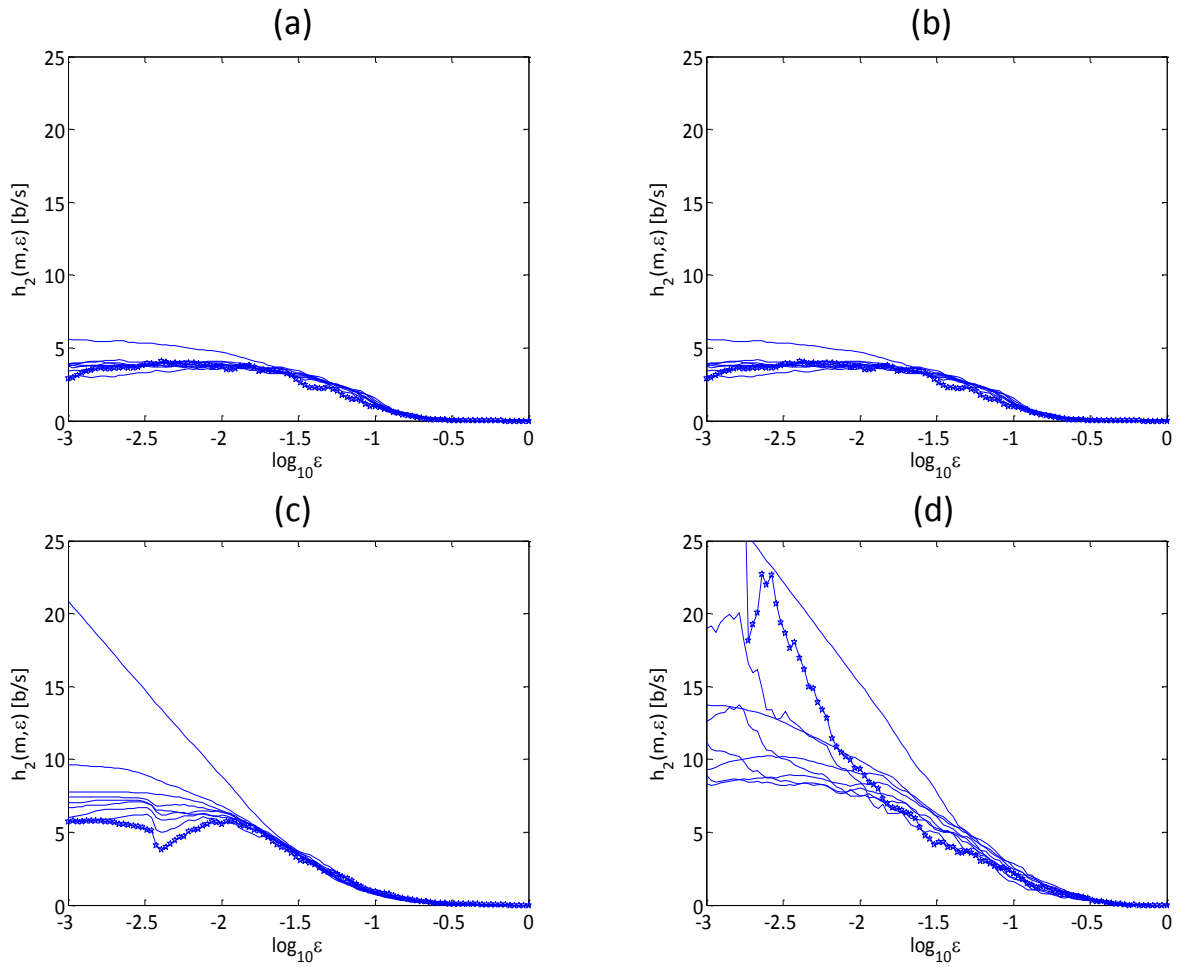


Figure 15: Entropy rate estimation of $h_2(\mathbf{u})$ for different pendulum lengths: 12 m (a), 8 m (b), 5 m (c), and 3 m (d). The curves correspond to embedding dimensions 2 (circles) to $m = 10$ (stars).

Table 3: Estimated information-transmission rate [b/s] for 12 subjects.

Pendulum length [m]	20					12	8	5	3
	0	100	200	400	600	0			
Subject A	6	5	6	2.6	5	5	7	-	-
Subject B	3.8	2.9	2.1	-	-	5.4	5.5	-	-
Subject C	2	2.5	2.6	2.7	2	3.8	4	5	7.8
Subject D	2.8	3.1	2.8	2.3	2.5	3.5	6.7	7.6	-
Subject E	2.7	2.2	2.5	2	2.8	3.8	4.2	5	-
Subject F	2.4	2.3	2.5	2	1.7	3	3.8	5	8.5
Subject G	4	3.9	4.4	3.2	-	4.7	6	-	-
Subject H	3	3.4	3.4	2	1.3	3.8	4.1	6	8.5
Subject I	3.2	3.1	2.6	2.5	-	4.5	5.3	6.8	-
Subject J	2.6	3.2	2.6	2.6	1.5	4	6.2	7	8.6
Subject K	2.5	2.7	2.2	3	1.5	4	4.1	5.8	-
Subject L	2.8	2.7	2.8	2.7	-	4.5	6.2	6.6	-
Average	3.15	3.08	3.04	2.51	2.29	4.17	5.26	6.09	8.35

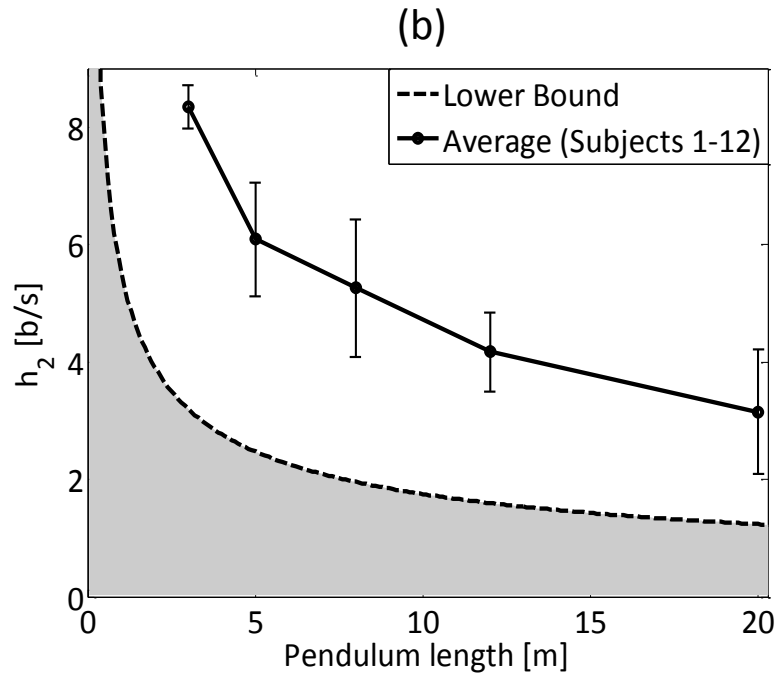
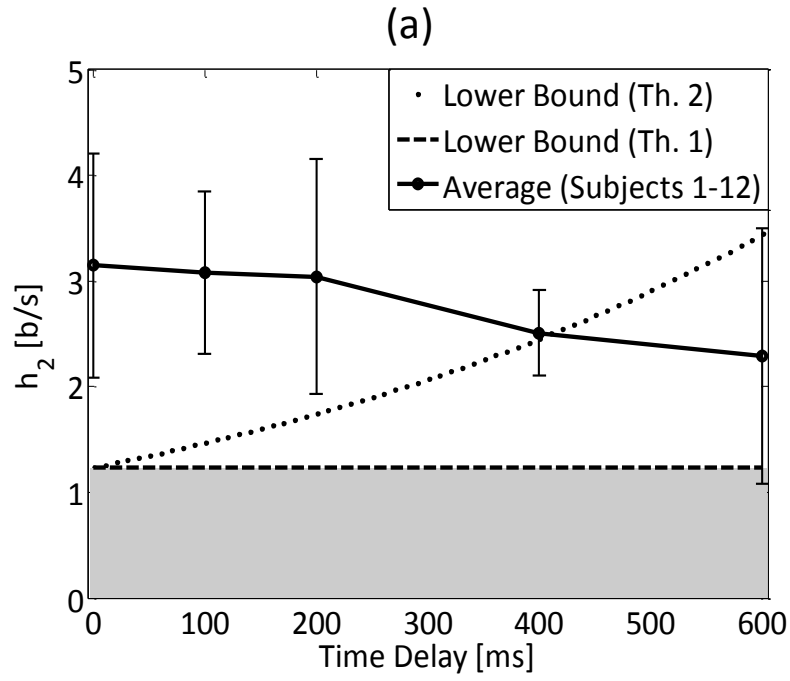


Figure 16: The variation of the information-transmission rate (ITR) with time delay (a), and with the pendulum length (b): estimated upper bound of the ITR of the human controller (solid), lower bound of the ITR according to Theorem 1 (dashed), and lower bound of the ITR according to Theorem 2 (dotted).

5.3 POWER SPECTRUM ANALYSIS OF MANUAL CONTROL

It is important to analyze the frequency response of the human controller for each tested scenario in order to illustrate how humans adapt their manual control strategy to satisfy the bandwidth constraints from section 4.5. Moreover, we would like to investigate if there are any correlations between the frequency response and the estimated information-transmission rate of manual control.

The power spectrum of the control signal contains information about both the size of the bandwidth and the distribution of the frequency components. Therefore, we derived the averaged power spectrum in order to observe the adjustment of the control strategy relative to time delay and the degree of instability of the task over all subjects. The averaged power spectrum corresponding to each scenario was obtained using the following procedure:

1. Obtain the magnitude of the frequency response of the control signal (using FFT);
2. Compute the power spectrum by squaring the magnitude from the previous step;
3. Normalize relative to the maximum value of the power spectrum;
4. Average across all subjects for each scenario;
5. Normalize relative to the maximum value of the power spectrum.

The normalized averaged power spectrum of the control signal for different time delays is illustrated in Fig. 17(a), and for different pendulum lengths is shown in Fig. 17(b). The frequency up to which 90% of the power was concentrated is marked by vertical lines in Fig. 17, in order to evaluate the “available bandwidth” of the controller. This is a common application of Parseval’s theorem when the signal is not band-limited [136].

The shape of the power spectrum, when no time delay affected the control task considering the lowest degree of instability (i.e. largest pendulum length of 20 m), resembles a *low-pass filter* response. When time delay was included in the system, the dominant frequencies are observed to shift toward lower frequencies. When stabilizing the inverted pendulum with higher degree of instability, the power spectrum exhibited a peak around 0.5 Hz, implying that the human generated mostly periodic movements. This dominant peak is observed to shift toward higher frequencies with the degree of instability of the task.

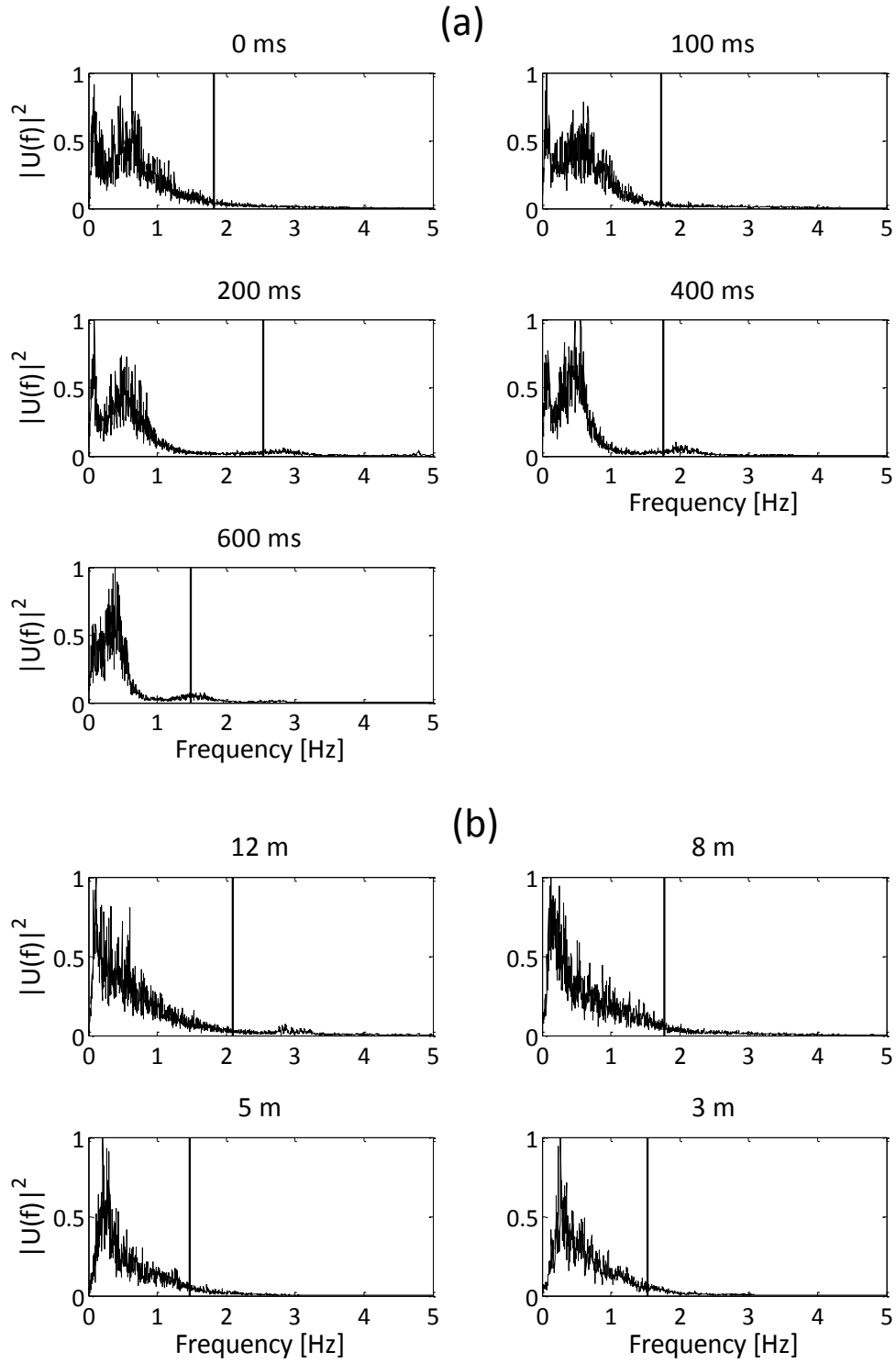


Figure 17: Power spectrum of the control signal \mathbf{u} : when different time delays affected the control task (a), and when different degrees of instability were considered (b). The vertical line marks the bandwidth up to which 90% of the power was distributed.

Manual Control and Bandwidth Limitations of Feedback Systems

In order to verify our predictions from section 4.5, we have to associate the frequency response of the controller with that of the plant to obtain the bandwidth ω_c of the closed-loop system. The inequalities (4.37) and (4.38) reflect our expectation of how ω_c should vary with time delay and the degree of instability of the task, respectively.

The frequency response of the plant has a high-pass filter characteristic (not shown), and the resulting power spectrum of the closed-loop system is shown in Fig. 19 for each scenario. We considered the frequency up to which 90% of the power is concentrated as a bandwidth-like parameter (vertical lines in Fig. 19). This “available bandwidth” is summarized in Fig. 18. It should be noted that the choice of other measures of the bandwidth gives different values for the bandwidth, but the trend maintains its consistency.

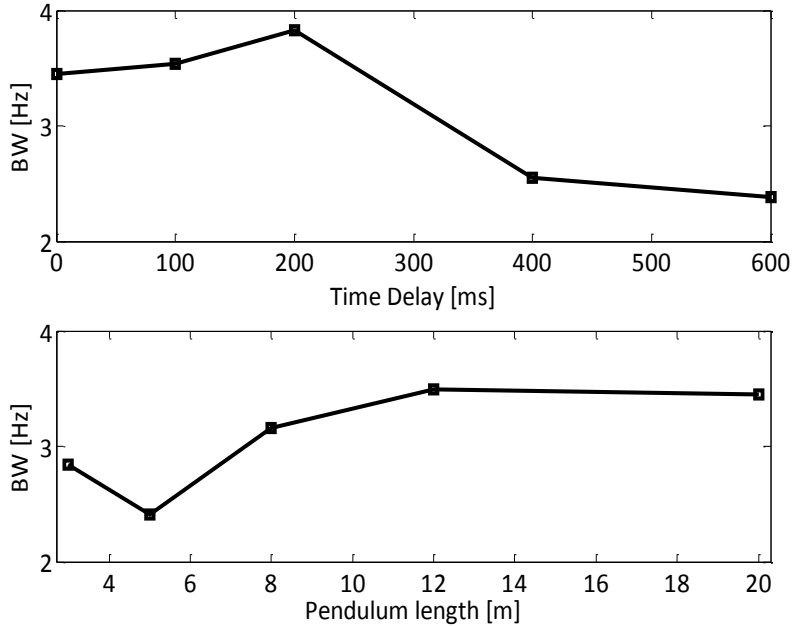


Figure 18: Estimated bandwidth of the power spectrum of the closed-loop system: when different time delays affected the task (top), and when different pendulum lengths were considered (bottom).

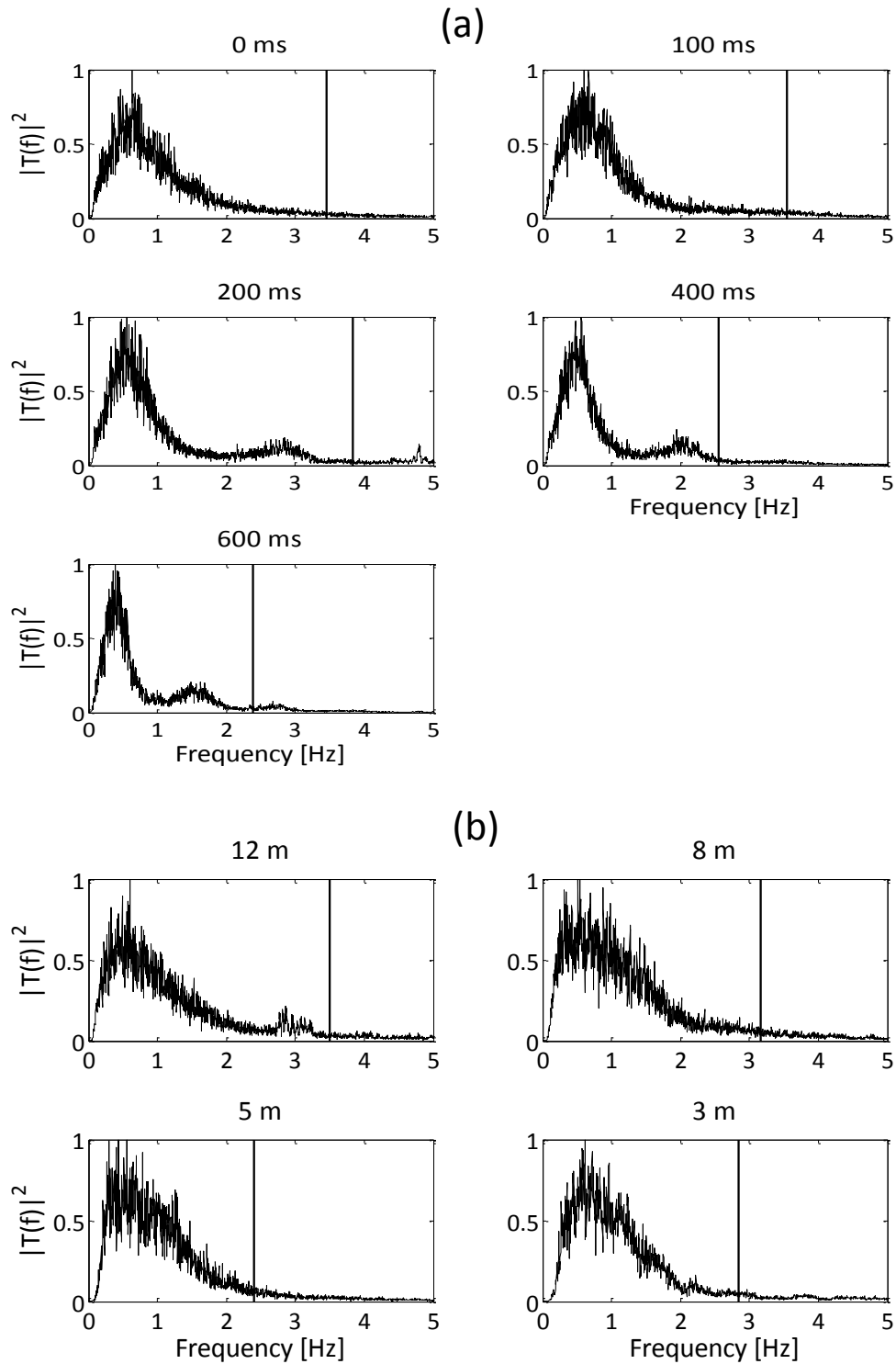


Figure 19: Power spectrum of the closed-loop system: when different time delays affected the control task (a), and when different degrees of instability were considered (b). The vertical line marks the bandwidth up to which 90% of the power was distributed.

Some expectations from our analysis in section 4.5 seem to be consistent with our results shown in Fig. 17 and Fig. 19. Firstly, the human adapted to lower-frequency control commands when time delay was present in the system [Fig. 17(a)] as predicted by inequality (4.38). Secondly, the human was expected to make fast movements relative to the degree of instability of the task, which can be inferred from inequality (4.37). We observed that the human adjusts to this requirement because the peak in the power spectrum [Fig. 17(b)] shifted to higher frequencies for higher degrees of instability. However, the available bandwidth did not increase as expected, which may reflect the effort of the human to minimize the effect of state-dependent noise related to fast movements.

We recall that the inequalities (4.37) and (4.38) are based on two main assumptions: the feedback system is LTI, and the frequency response of the closed-loop system (i.e. complementary sensitivity function) has a low-pass filter shape. While the former assumption may seem doubtful because human behavior is unlikely LTI, the latter may be challenged by the results in Fig. 19, where the power spectra resemble a band-pass filter.

Shape of Power Spectrum and Information-Transmission Rate

The weighted entropy rate, H_{PS} , described by equation (4.39) is evaluated in order to illustrate if we can predict the variation of the information-transmission rate with time delay and degree of instability from the frequency distribution of the power spectrum of the control signal (Fig. 20). The entropy rates computed using the power spectrum provide a consistent prediction of the variation of the estimated information rates with time delay (Fig. 16). However, the fluctuation of the information rates with the degree of instability was not consistent for high degree of instability values.

The average power spectrum of manual control from Fig. 17(a) showed how manual control was restricted to lower bandwidths relative to the amount of time delay in the system. Human controllers seemed to abandon fast actions when time delay was present. Therefore, they adopted a control strategy based on a *smaller* set of possible movements exerted in a *low-frequency bandwidth*. Therefore, the information rate is expected to decrease with time delay, and H_{PS} was able to successfully predict this result [Fig. 20 (top)].

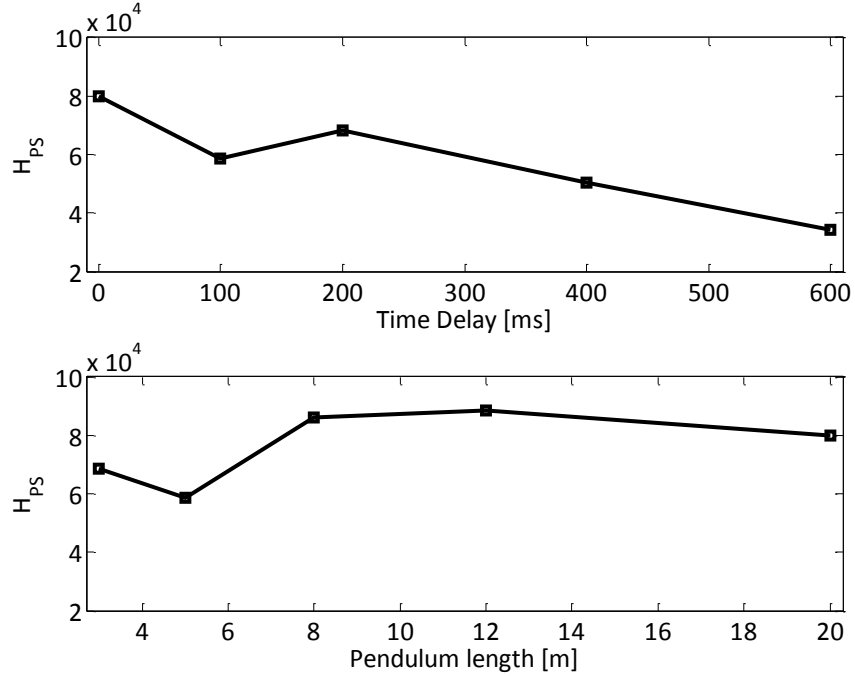


Figure 20: Entropy rate H_{PS} computed using the power spectrum: when different time delays affected the task (top), and when different pendulum lengths were considered (bottom).

When the degree of instability of the task was increased, the human adjusted correspondingly by delivering higher frequency movements more consistently [Fig. 17(b)]. While the overall bandwidth seemed to decrease up to a certain point (Fig. 18), the frequency distribution within this bandwidth showed that the rate of generating control actions increased slightly. The product of these two quantities that influence the information rate is represented by H_{PS} , which was observed to increase initially, but decreased for higher values of the degree of instability [Fig. 20 (bottom)]. The difference between this result and the estimated information rates (Fig. 16) may be explained by two factors. First, the power spectra was derived as an average over all subjects, while the information rate is averaged only over successful readings of the entropy rate (as shown in Table 3). Second, the nonlinear correlations in the control signal were lost when computing the power spectrum.

6.0 DISCUSSION

6.1 INFORMATION-TRANSMISSION RATE TO MEASURE HUMAN PERFORMANCE

The main goal of our investigation is to propose a measure of performance for human operators when they perform a manual control task in a feedback-control system. We analyze the human controller as a communication channel and characterize its performance by dynamics of information exchange measured in bits per second (b/s). This quantity is represented by the mutual information rate (3.1), also referred to as information-transmission rate (ITR).

6.1.1 On Lower Bound and Upper Bound

Current advances in networked control theory proposed by Martins and Dahleh [20, 21] have established the connection between the information-transmission rate and the degree of instability of a dynamic system. This interdisciplinary method that combines information- and control-theoretic approaches enables the derivation of a lower bound of the information-transmission rate of the human controller.

We determine the lower bound of the ITR that refers to the minimum rate of information to be conveyed by *any* deterministic controller (not necessary LTI) in order to stabilize an unstable plant. We aimed to derive a very conservative lower bound. It should be noted that, if the plant under consideration was stable, the tight lower bound of the information-transmission rate required for stabilization would be indeed 0 b/s for any deterministic controller. Now that the plant yields unstable poles, the minimum information-transmission rate required for stabilization depends on both the number and magnitude of the unstable

poles [Theorem 1, (4.6)]. For the specific case of an *LTI* controller, the lower bound would also increase if time delays and nonminimum-phase zeros were to be factored into the plant dynamics [Theorem 2, (4.14)]. Therefore, the lower bound of the ITR that we derived is related to the dynamics of the performed task.

Computing the mutual information rate directly involves many difficulties related to sampling and quantizing the input- and output signal of the human controller in order to approximate the high-dimensional probability distributions [refer to expression (4.17)]. Instead, we proposed to estimate the entropy rate of the control command $H_\infty(\mathbf{u})$, which we showed to represent an upper bound of the mutual information rate [Theorem 3, (4.19)].

First, we estimated an upper bound of the information rate that reflects the maximum amount of information that the human controller generates through “bang-bang” control when the task is near the limits of controllability (section 4.3). By “the limit of controllability” we refer to a situation when the human operator is required to generate control movements in a quick manner in order to compensate for the high degree of instability of the plant. We assume that, in this scenario, the human sensorimotor system is challenged to exhibit as much information as possible to stabilize the system. The bang-bang characteristics are modeled using a three-level switch for: left, right, and no action. Thus, the entropy rate $H_\infty(\mathbf{u})$ of the discrete control variable was shown to be proportional to $\log_2 3$ by a factor representing the frequency of generating the control actions: $H_\infty(\mathbf{u}) = \log_2 3 / 0.4 = 4$ b/s.

Then we turned to human experiments to estimate the entropy rate of the actual human control output (section 4.4). The entropy rate was estimated using a numerical method applied to the time series of the control signal: the coarse-grained correlation entropy $h_2(m, \epsilon)$ (4.29). The equivalence with Shannon’s entropy rate, $H_\infty(\mathbf{u}_\epsilon)$, and its convergence were demonstrated based on the assumption that human controllers resemble intermittency when stabilizing unstable systems [see section 4.1.1]. The recorded information rates from our experiments (Fig. 16) represent the amount of information that the human controller generates relative to the difficulty level of the task. Two situations were evaluated: when different amounts of time delay were present in the system, and when the degree of instability of the task was varied. The upper bound of the mutual information rate, represented by the estimated entropy rate, was observed to depend on the human ability to perform the task.

6.1.2 Information-Transmission Rate and Human Performance

The efficiency of human performance and its limitations were analyzed by associating the estimated upper bound of the information-transmission rate from human experiments with the minimum information rate required by the controller to stabilize the feedback control system (Fig. 16). If the former quantity was larger than the theoretically-derived lower bound, then the human was assumed to be able to stabilize the unstable system given a certain degree of instability of the task and/or time delay in the system. Thus, the estimated information rate provides not only a qualitative, but also a quantitative measure of performance.

When time delay was present in the system, the estimated information-transmission rate was observed to decrease with the amount of time delay. Consequently, the quality of human performance seems to degenerate when time delay affects the control task, and the ITR provides a quantitative measure of this effect. Particularly, the difference between the estimated information rate from human experiments and the minimum information rate required by the task indicates whether the human controller can stabilize the feedback system and how this performance varies with time delay.

By considering the minimum information rate that would be required by an LTI controller to stabilize the feedback system (given by Theorem 2), we can identify the situation when the human controller would be superior to an LTI system. Our experimental results [Fig. 16(a)] show that the human controller exceeds the performance of an LTI controller for time delays larger than 400 ms. This is apparent when the estimated ITR generated by manual control lies below the lower bound required by an LTI controller to stabilize the system (Theorem 2) and above the lower bound set for any type of controller (Theorem 1).

The increase of the minimum information rate required for feedback stabilization with the degree of instability of the plant (4.6) demands that the human controller deliver information at a higher rate. The estimated information rates from experiments reflect this tendency. The recorded information-rate curve for successful readings [Fig. 16 (b)] did increase exponentially with the degree of instability of the task from 3.15 b/s for a 20 m long pendulum to 8.35 b/s for a 3 m long pendulum.

Our initial expectations of the variation of the information-transmission rates with time delay and the degree of instability of the control task stated in Fig. 1, thus seem to be confirmed by our experimental results. Regarding the prediction of the limitations of the human controller with the aid of information-transmission rate, one would expect the information rates to decay below the lower bounds set by the stability criterion for closed-loop systems in order to illustrate insufficient information delivery to the control task. However, our empirical estimations did not fall below these lower bounds with the exception of the above-mentioned lower bound set by LTI controllers.

Nevertheless, it may still be possible to use the information-transmission rate method to predict the limitations of the human operator. Our observations indicate that successful readings of the entropy rate estimation are not always guaranteed, especially when the task is very difficult to control (Table 3). Therefore, we can assume a successful reading of the information rate to be a *sufficient condition* to guarantee control of an unstable system. On the other hand, unsuccessful readings may illustrate a situation when the capabilities of the human controller reached their limit. The causes of these unsuccessful readings are mainly correlated with insufficient data as will be discussed in section 6.3.4.

The analysis of human performance with information theory can also be a tool for assessment of *learning*. The capabilities of the human controller are expected to improve with practice, and our approach of measuring human performance after certain time intervals can reflect the different stages of learning.

6.1.3 Comparison with Other Related Studies

Information-theoretic approaches have also been used in the study of other HMI tasks. For example in tracking tasks, the maximum information rates of 9 b/s in continuous tracking and 11 b/s in discrete tracking were confirmed in [31]. It appears that discrete-type behavior yields a higher information rate than the corresponding continuous motion of the human operator. Therefore, it is not surprising that human operators prefer to adopt an intermittent manual control strategy when the control task is difficult to perform, e.g., tasks with high degree of instability, and/or time delay [94].

We derived an *upper bound* of the rate of information transmission of 4 b/s in the control of highly unstable systems based on bang-bang characteristics of human operators. This approximation is lower than those found in tracking tasks. However, this result is expected provided that balancing of the one-dimensional unstable system was performed near the limits of controllability with the constraint imposed by the three-level switch for the control signal. The resulting frequency range of operation is not the optimal range for information transmission via manual control [31, 135].

In our previous work [116] related to the same study, we also derived the *lower bound* of the information rate based on empirical results obtained from another investigation [5]. Ten subjects were recruited in that study to balance an inverted pendulum with one dimensional control and an adjustable moment of inertia. At the lowest level of the moment of inertia tested in the experiment, all subjects were still able to balance the inverted pendulum, but found it hard (at the “limits of controllability”). The value of the unstable pole corresponding to this level of moment of inertia was 0.47. Using the inequality (4.6) from Theorem 1, we estimated a lower bound of approximately 3 b/s. Although the experiment setup was different from our own (as we described in section 4.4.1), the lower bound of the information rate was equivalent with our result obtained for the highest degree of instability (i.e. the 3 m long pendulum). This consistency can be expected because both experiments yielded a similar value for the unstable pole.

Our experimental measurements provided estimations of the maximum information-transmission rate similar to the ones reported in tracking tasks. These results are believed to be more representative of actual human performance because human operators were not restricted to a three-level switch when exerting their control commands. Subjects were free to choose their own control strategy to maneuver the joystick in order to achieve the best performance. An average value of 8.35 b/s was estimated for the highest degree of instability considered in our experiments (Fig. 16). However, an overall maximum information rate of 8.6 b/s was recorded when balancing the one-dimensional inverted pendulum.

Many studies agree that human performance degrades with the amount of time delay [137, 138, 139]. Even Fitts law [30, 140] predicts this result by dividing the index of difficulty (ID) of the task by the movement time (MT) to compute the information rate. When

time delay affects the task, the ID remains unchanged, while MT increases causing the overall information rate to decrease. However, only very few studies have reported on *how* information-transmission rate actually varies with time delay. In a study that involved hitting a target on a screen with a mouse, the information rates were observed to decrease with time delay [1]. The results are reproduced in Table 4, and they are comparable with our empirical estimations of the information-transmission rate. For the largest time delay tested, both studies report an average rate of information transmission of approximately 2.3 b/s.

Table 4: Reported information-transmission rates from [1].

Time Delay [ms]	8.3	25	75	225
ITR [b/s]	4.3	4.1	3.5	2.3

6.1.4 On Bi-Directional Information Transmission in HMI

In this study of closed-loop human-machine interaction, we focused on the direction of information transmission from human to machine, through the human motor pathway. We did not explicitly address the information flow in the other direction - from machine to human through the sensory pathway, because the motor pathway is normally the bottleneck of information flow in the loop. Studies showed that the information capacity of the sensory pathway is much larger than that of the motor pathway. For example, it was estimated that the information capacity of the human eye (vision) is approximately 4.3×10^6 b/s [36] and that of the fingertip (vibrotactile sensation) is of an order-of-magnitude of 100 b/s [141], while the observed maximum rate of human information processing via one dimensional movement was limited by about 10 b/s [41, 31]. Therefore, for this study, the informational constraint and noise in the sensory pathway are negligible when compared with those in the motor pathway.

6.2 EFFECTS OF BANDWIDTH AND POWER SPECTRUM ON INFORMATION TRANSMISSION

The human controller as an information processor was observed to generate information at a certain rate relative to the dynamics of the task (i.e. degree of instability of the plant) and to variations in the task (i.e. time delay in the feedback system). Simultaneously, we examined the bandwidth and the power spectrum of the manual control signal in order to learn about the correlations between the adopted manual control strategy and the rate of information exchange in an HMI task.

6.2.1 Effect of Time Delay

When time delay affected the control task, we assumed from inequality (4.38) that the human should adapt its control movements to a smaller bandwidth in order to sustain a certain performance. Although this behavior may contravene the instincts of an untrained human controller (who tends to compensate for the effect of time delay by making faster movements [94]), the prediction capabilities of a human controller, who gets familiar with the task, will help him/her to adjust to the imposed bandwidth constraint in order to ensure stability. This result was indeed confirmed by our experimental observations illustrated in Fig. 18, where human operators were able to confine their control movements to a low-pass filter whose bandwidth decreased as time delay increased.

Moreover, the shape of the power spectrum of the control signal exhibits a peak in the low-frequency range that not only becomes more dominant, but also shifts closer to the DC value with increased time delay. A much smaller peak can also be seen for large time delays: at 2.8 Hz for 200 ms; at 2 Hz for 400 ms; and at 1.5 Hz for 600 ms. Our results seem to be consistent with other studies [135, 142] on how the frequency distribution changes in the power spectrum with increasing time delay.

It is apparent that both the bandwidth and the information-transmission rate of manual control decrease with increasing time delay in concordance with our hypothesis formulated in Fig. 1(a). Moreover, the restriction of the bandwidth size to smaller values with increasing

amount of time delay is expected to have an effect on the ability of the human controller to convey information. Human operators adopt a control strategy based on a smaller set of possible movements corresponding to the narrow bandwidth. Moreover, these control signals are exerted in the low-frequency range of the power spectrum. These factors imply that the ability of the human controller to transfer information should decrease with time delay. Additionally, we seem to be able to predict this variation of the information-transmission rate with the amount of time delay based on the shape of the power spectrum of the control signal by computing the entropy rate H_{PS} given by expression (4.39).

6.2.2 Why is the Bandwidth of Manual Control restricted to 2 Hz ?

When no time delay is introduced in the HIL system, the human controller has the freedom to choose control movements without any apparent bandwidth restrictions as suggested by the inequality (4.38). What would be the maximum bandwidth of manual control in this case? We know that it has to be finite in accordance with the finite “available bandwidth” in the range of approximately 2 Hz which was reported in literature [5, 103, 135]. This range can be explained by factoring the neuromuscular time delay of the human sensorimotor system in our inequality (4.38). A maximum bandwidth of approximately 2 Hz for manual control tasks can be derived for a neuromuscular lag of 150 ms [22]. This amount of time delay is in concordance with the results reported by many other studies [142, 143, 144, 145, 146, 147, 148, 149, 150]. It should be noted from Fig. 17 that our estimated bandwidth from human experiments for all tested scenarios is consistent with the 2 Hz bandwidth.

6.2.3 Effect of Degree of Instability

When the degree of instability of the control task was increased, we predicted that the bandwidth of the controller should increase according to inequality (4.37). At the same time, the human controller was expected to generate information at a higher rate in order to comply with the increasing lower bound ITR_{min} imposed by degree of instability of the control task (4.6). These results were anticipated in our hypothesis illustrated in Fig. 1(b).

The demand for fast corrective movements when stabilizing an unstable system is not surprising and can also be deduced analytically by an alternative approach. For example, Middleton [130] derived the step response of an unstable system in time domain and proved that a long rise time of the system’s response implies large overshoot. Fast movements are therefore required to avoid undesirable overshoot.

Furthermore, high-speed control signals involve high-frequency components in the power spectrum, and thus seem to infer a larger bandwidth [22]. However, the estimated bandwidth from our experiments rather indicates a decreasing trend as the degree of instability increased [Fig. 17(b) and Fig. 18]. There are three possible explanations for this result.

First, the subjects encountered difficulties balancing the inverted pendulum with the highest degrees of instability (i.e. 3 and 5 m long pendulum). We recorded very few successful readings of the information rate in this case, which may also imply that human controllers did not keep up with the demand of generating high-frequency control movements to satisfy the bandwidth requirement. A reason for this limitation of the human controller may originate in the attempt of the human to optimize its corrective movements when stabilizing the plant by minimizing the effect of signal-dependent noise [151]. We know that signal-dependent noise is characteristic for manual control, and it is amplified for high-speed movements.

Second, the inequality (4.37) imposes a lower bound on the bandwidth of the closed-loop system. We have seen that these results are directly affected by the bandwidth of the control signal. The human can thus exercise any control movements that satisfy this lower bound, but he/she is not required to generate control signals that would increase the bandwidth with each increasing difficulty index of the task. The human controller may generate (unnecessary) high-frequency control movements for a task with a low degree of instability than in the case of one with a high degree of instability. The results in Fig. 16 may illustrate this hypothesis: a bandwidth of 3.5 Hz was noted for a 20 m long pendulum, and bandwidths of less than 3 Hz were observed for the 3 m and 5 m long pendulums. This allows the human operators to select control movements with which they are comfortable, and that still achieve a good performance in the sense of the conveyed information-transmission rates. To exemplify this scenario, we illustrated in Fig. 21 how a signal with power spectrum $|U_1(f)|^2$ has a bandwidth f_1 that is less than the bandwidth f_2 of another signal with power spectrum $|U_2(f)|^2$. The

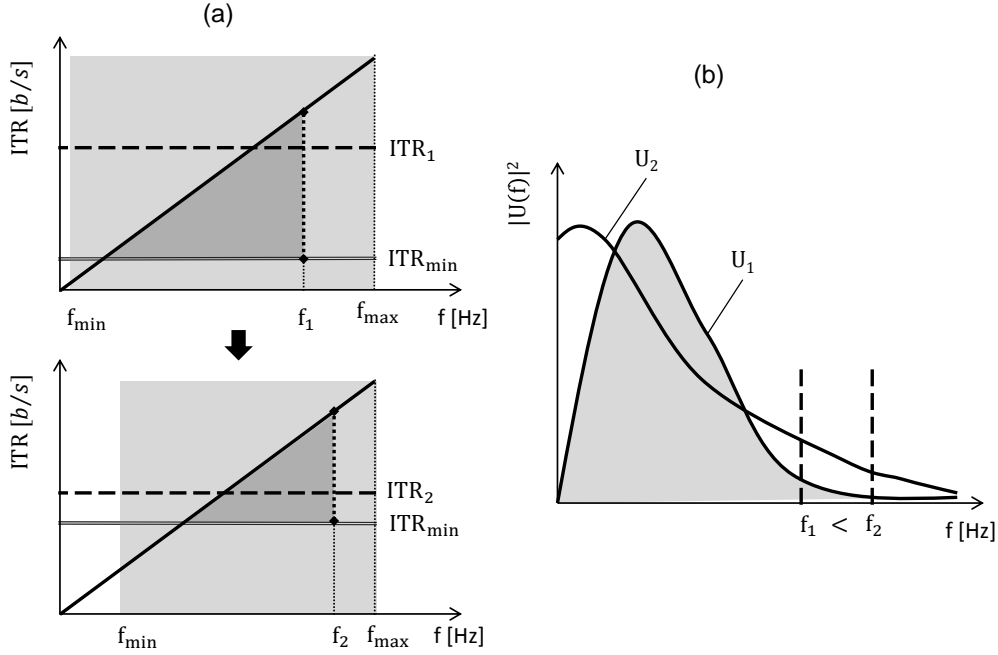


Figure 21: Example of power spectrum with lower bandwidth ($f_1 < f_2$), which yields a higher information-transmission rate ($ITR_1 > ITR_2$): illustration of ITR vs. bandwidth (a); and the frequency distribution in the power spectra of the two control signals (b).

latter case is assumed to correspond to a higher degree of instability of the task than the former case. Furthermore, it may also be possible to achieve higher information-transmission rates in the former case (i.e. $ITR_1 > ITR_2$).

Third, the inequality that establishes the variation of the minimum bandwidth with the degree of instability of the control task (4.37) is designed for an LTI feedback system and its frequency response is assumed to be a low-pass filter. We observed earlier that the human controller exhibits non-LTI behavior when the task is difficult to control (recall the estimated information rates in Fig. 16 relative to the two lower bounds corresponding to an LTI and a non-LTI controller). Moreover, the frequency response of the feedback system is a band-pass filter rather than a low-pass filter. Hence, the inequality (4.37) based on the above-mentioned assumptions may not apply in this case under the derived form. Further investigation is required to address this issue.

The frequency distribution in the power spectrum reveals that the subjects indeed generated overall higher frequency control commands to stabilize the inverted pendulum. This can be observed in the shape of the power spectrum [Fig. 17(b)], which shows a significant peak around 0.5 Hz that shifts away from the DC component with higher degree of instability of the task (i.e. as the pendulum length became shorter).

The power spectrum of the control signal was used to compute the entropy rate H_{PS} described by equation (4.39) in order to evaluate how far we can predict the variation of the information-transmission rate with the degree of instability of the task (Fig. 20). When the degree of instability of the task was increased, the human adjusted the control strategy by attempting to deliver higher frequency movements more consistently [Fig. 17(b)]. However, the overall bandwidth was observed to decrease slightly up to a certain limit (Fig. 18). These trends are reflected in the computation of the entropy rate H_{PS} , which was observed to increase initially, but then decreased for higher values of the degree of instability. The difference between this result and the estimated information rates (Fig. 16) can be explained by two possible factors. First, the power spectra was derived as an average over all subjects, while the information rate was averaged only over successful readings of the entropy rate (as shown in Table 3). Second, the nonlinear correlations in the control signal, which are attained by the mutual information rate, were lost when computing the power spectrum.

So far, our analysis provided an *understanding of why the human operators had to adjust* their control strategy to overcome time delay and/or high degrees of instability of the task, based on bandwidth constraints imposed by the plant dynamics. Moreover, we *observed how the human adapted* correspondingly based on the power spectrum analysis of the control signal. However, we still have to address *why the subjects chose to adapt in such a manner*. A possible answer is provided by the preference of the human subjects to rely on intermittent control in order to compensate for internal neuromuscular limitations. We will discuss this aspect in the next section.

6.3 ON INTERMITTENCY IN THE CONTROL OF UNSTABLE SYSTEMS

6.3.1 Balancing an Inverted Pendulum with Intermittent Control

Balancing an inverted pendulum, as well as controlling any unstable system, is an interactive task that requires the human operator to continuously generate corrective movements. The interplay between closed-loop (with sensory feedback) and open-loop (without sensory feedback) control mechanisms is essential in this case. Sensory information is needed by human operators to ensure long-term balancing of the inverted pendulum. However, the human is restricted to implementing ballistic corrective movements to stabilize the plant due to constraints such as time delay (human- and task related) and high degree of task instability. A hybrid control strategy is therefore necessary, and *intermittent control* was shown to combine the advantages of closed-loop- and open-loop control: serial actions are pre-planned using accumulated sensory feedback and are executed ballistically. The synergy of open-loop control and closed-loop control was also emphasized in human postural control [86, 152, 153].

When do human operators prefer intermittent control?

The difficulty of the task is associated with the difference between the time interval available for the human to generate a control command (i.e. time constant of the task which varies inversely with the degree of instability) and the time interval required for the sensorimotor system to generate a control signal (i.e. includes the sensory feedback delay, the time delay for motor planning and execution, muscular contraction latency, and any additional delay in the system).

If the time constant of the system is large enough and no additional time delays are present in the system, then the human operator seeks to generate control commands that are as smooth and continuous as possible. This result is not necessarily surprising. Continuous control is known to be superior over intermittent control in terms of performance and disturbance rejection [88, 91, 99].

However, a task with high degree of instability is a consequence of a small time constant of the system. Among the overall “set” of possible corrective movements, the human operator is therefore restricted to choosing fast movements for system stabilization [5, 107, 114]. High-speed movements are associated with signal-dependent noise [111], which is an important component of intermittent control. It has been suggested that the nervous system relies on such multiplicative noise to drive the feedback system at the limits of stability in order to increase the maneuverability of the task [6]. A benefit of this strategy is that corrective movements are generated at all time scales (including those shorter than the delay), such that the inverted pendulum can be statistically stabilized: fluctuations in the pendulum angle resemble a random walk with approximately zero mean value ($E[\theta] \approx 0$).

Intermittent control was also observed for bandwidth-limited applications where time delays that are introduced in the feedback loop by other sources than the human make continuous control difficult [101, 154, 155]. Moreover, an intermittent interval provides time to complete mental calculations required to construct a control action or time to send/receive information over a network channel. Furthermore, intermittent control simplifies prediction capabilities when the intermittent interval is greater than or equal to the time delay [80], [100, section 4.2], [102].

Intermittency in manual control can also benefit system identification. The human operator can gain better understanding about the relationship between the generated control signal (input to the plant) and the behavior of the system (output of the plant) by observing the effect of his/her control actions during the intermittent interval. During continuous control this causality may become ambiguous, and it may be difficult to associate the output of the plant to either the dynamics of the machine or the human action [156].

Why do human operators prefer intermittent control?

As an unstable system, the inverted pendulum falls at an exponential rate when no corrective movement is applied. When possible, continuous control is expected to be more effective than intermittent control in stabilizing the inverted pendulum. However, intermittent periods of no activity (i.e. intermittent intervals) offer important advantages [88]:

- temporary elimination of (signal-dependent) noise during the intermittent intervals;
- enhanced causal relationship between human action and system output, which can improve the development of an internal (mental) model of the control task;
- the ability to gain more information about the dynamics of the task when the controlled system is probed by high-frequency movements (i.e. estimation of the impulse response);
- the capability to maintain a high level of attention and to allow fatigue-resistant control by offering the possibility of computational and muscular recovery.

Moreover, mental computation associated with motor planning and execution can be reduced when impulse-like force patterns are generated rather than smooth continuous trajectories [114]. Intermittent control is consistent with regard to this aspect.

Other authors explained the occurrence of intermittent control as the result of human operators attempting to optimize their manual control movements [151]. The multiplicative noise component in manual control, which is characteristic of intermittent control, was not assumed in their model, but was derived using a maximum-likelihood estimation method applied for an optimal control algorithm to explain experimental data obtained from the manual balancing of an inverted pendulum.

6.3.2 Identifying Intermittent Control

Intermittent control exhibits certain characteristics that can be identified through various methods. In this section we describe a few of these methods and relate them to our experimental results.

Our observations indicated that the power spectrum of the control signal, when stabilizing an inverted pendulum with time delay and/or high degree of instability, exhibited a peak centered around 0.5 – 1 Hz (Fig. 16). This result is consistent with the results obtained by Loram et al. [5], where the power spectrum of the velocity of the pendulum angle [Fig. 22(a)] and the power spectrum of the velocity of corrective movements [Fig. 22(b)] exhibited peaks at approximately 0.5 Hz, and 1 Hz, respectively. A peak in the power spectrum of the velocity of movement located in the range 0.7–2 Hz was observed to be a characteristic of intermittent control in a variety of manual tasks, especially in manual tracking of visual targets [82, 91,

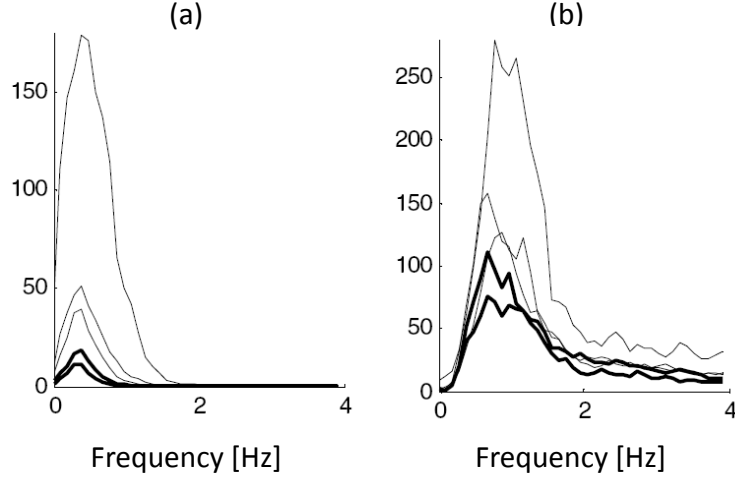


Figure 22: Power spectra of both the velocity of the inverted pendulum angle (a) and the velocity of the hand movement (b) exhibit peaks in the range of 0.5–1 Hz (adapted from [5]).

[93, 95, 157] and voluntary arm movements with and without visual feedback [95]. Such a peak in this range in the power spectrum represents a lack of smoothness in the hand trajectory. Moreover, these frequency components are not present in the visual stimulus, and are thus a product of the human control process.

Cabrera and Milton [6, 98, 158] conducted a set of experiments with human subjects balancing a stick in three dimensions. Both the movement of the hand and the movement of the the stick were recorded using reflective markers and motion-capture cameras. They analyzed the fluctuations of the quantity $\Delta z/l$, where l was the length of the pendulum, and $\Delta z = l \cos \theta$, with θ indicating the angle of the stick relative to the vertical upright position. The log-log plot of the power spectra for the fluctuations $\Delta z/l$ exhibit two scaling regions with slopes $-1/2$, and -2.5 , respectively [Fig. 23(a)]. The scaling with coefficient $-1/2$ was shown to be evidence of on-off intermittency [159, 160, 161].

The time intervals δt between the occurrence of the corrective movements were identified as laminar phases (refer to [6] for a detailed definition). The probability distribution of the laminar phases $P(\delta t)$ is shown in Fig. 23(b) on the log-log scale. The scaling of $P(\delta t)$ with exponent $-3/2$ is also considered to be a characteristic of on-off intermittency [162, 163].

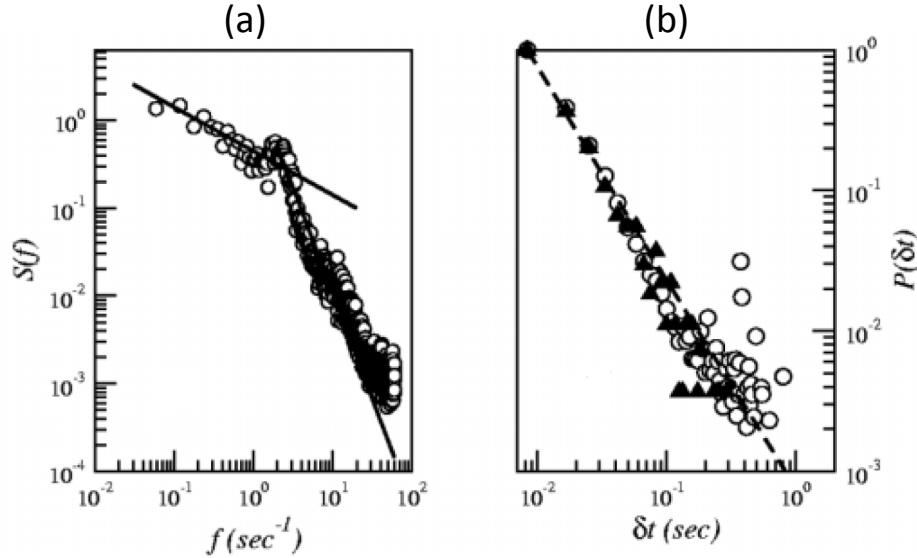


Figure 23: (a) The power spectrum of $\Delta z/l$ -fluctuations on log-log scale is characterized by two power law regimes with exponents $-1/2$ (upper line) and -2.5 (lower line). (b) Normalized laminar-phase probability distribution, $P(\delta t)$. The dashed line represents a power law with exponent $-3/2$. Figures adapted from [6].

While the above-mentioned studies investigated intermittent control by identifying discontinuities in the movement trajectory, other studies focused on methods to distinguish between continuous and intermittent control. These methods [86, 102, 164] exploit the non-LTI characteristics of intermittent control and assume that continuous control can be reproduced by an LTI system. Various frequency analysis methods were then applied for system identification [165, 166]: if the human response could not be represented by an LTI system, then the continuous control hypothesis was discarded. Relying on such mechanisms should come with a caveat, because time-variant behavior was already shown to be reproduced by an LTI system with colored noise [112].

6.3.3 Intermittent Control and the Correlation Entropy h_2

We discussed in section 4.4.5 the adequacy of using the entropy rate formula for dynamical systems, $h_2(m, \epsilon)$, in order to quantify the complexity of manual control. From the perspective that manual control can be reproduced by a dynamical system, its reconstructed state vectors - represented by the delay vectors $\mathbf{u} = [u(k), u(k - \tau), \dots, u(k - (m - 1)\tau)]^T$, where $k = (m - 1)\tau + 1, \dots, N$, may provide additional insights on manual control.

The inter-sample lag τ was estimated by the first minimum of the mutual information, and the average values were shown in Table 2 for each scenario. By multiplying these values with the sampling period $\Delta t = 10$ ms, our observations reflect time intervals that are comparable with the lag between consecutive movements in intermittent control (i.e. in the range of 250 – 500 ms [82, 83, 87, 88, 89, 90, 91, 92]). Hence, the parameter τ could provide a possible measure of the intermittent interval in manual control.

The rate of convergence of $h_2(m, \epsilon)$ with increasing m was proven to relate to the strength of correlations in the system [67], thus providing a possible approximation of the memory of the system. Our empirical results indicated that convergence was achieved for $m = 3$ in most scenarios. We can associate this value of m with the number of past states needed to generate the current control signal similar to a Markov chain of order m .

Furthermore, the time interval covered by the delay vector (3.19), which is defined by the product $m\tau$, can also be regarded as the time horizon over which prediction is exercised by the human. Based on the results from Table 2, this time interval was observed to increase gradually when more time delay was present in the system.

6.3.4 Limitations of the h_2 Estimation Method

The information-transmission rate was successfully estimated only when a plateau was exhibited in the entropy rate plot of $h_2(m, \epsilon)$. The convergence of the entropy rate was difficult to assess in the case of large time delays (i.e. 600 ms) and when the length of the pendulum was very short (i.e. 3 m). Due to the increased task difficulty, the human operators dropped the inverted pendulum before the end of the complete trial (i.e. a trial was maximum 60 s long), and they generated an insufficient amount of data samples for the estimation method.

Therefore, one of the main limitations of our entropy rate estimation method is the requirement of large amount of data. To a certain degree, this is a downside of any paradigm used to estimate any quantities similar to probability distributions. It has been suggested [4] that the minimum length of the time series, denoted by N_{min} , should satisfy $N_{min} > \epsilon^{-D}$ for a consistent result, where D is the dimension of the attractor of the dynamical system, and ϵ defines the refinement of its state space. However, it should be noted that our procedure to estimate the entropy rate needs overall less data than any method used to estimate the mutual information rate, which requires the estimation of higher-dimensional probability distributions.

Spurious spread of the curves in the entropy rate plot was also noted when the human controller did not exercise a consistent control strategy over the period of a trial or, more importantly, over all ten trials recorded for each scenario. Possible factors that contributed to this effect were attention drift and ongoing learning capabilities. While the former accounted for mistakes, the latter reflected the improvement of control over time during the experiment. We tried to apply our entropy rate estimation method to each trial separately to track the learning capabilities of the human operator during the time span of the experiment. However, the outcomes were not successful due to lack of sufficient data.

6.4 IS MANUAL CONTROL STOCHASTIC OR DETERMINISTIC?

Throughout our analysis of the human manual controller we applied interdisciplinary concepts from information theory and dynamical systems. While the former field focuses on **stochastic systems**, where quantities are described by probability distributions, the latter refers to **deterministic dynamical systems** which are described by a set of deterministic (difference or differential) equations and initial conditions. In our study, the lower bound of the mutual information rate is computed from the stochastic systems approach [21]. However, our method to estimate the upper bound of the mutual information rate (using the correlation entropy h_2) from experiments originates in the analysis of deterministic dynamical systems. Is there a contradiction in our approach?

We assumed intermittent control to reflect discrete-type dynamics in order to ensure equivalence between the entropy rate for stochastic systems and the entropy rate for dynamical systems. However, what happens if we discard this assumption? Specifically, if we assume the human to generate continuous dynamics, and we observe the correlation entropy h_2 to converge, does this imply that the human controller system is a deterministic system? This would create an inconsistency in our method regarding the lower and the upper bound of information-transmission rate. Therefore, we would have to address the question: is human manual control deterministic or stochastic?

Given the complexity and variability of the human neuromuscular system, the answer to this question may not have a clear answer [167]. Although there are many methods to distinguish between stochastic and deterministic systems [4, 168], the results are not always conclusive. This usually applies to experimental data, where the amount of data is finite and the stationarity property is assumed in order to apply various methods to characterize the data.

We want to show in this section that intermittency can be reproduced by both stochastic and deterministic systems. We then provide an example of a class of continuous stochastic systems with intermittency characteristics for which the entropy of dynamical systems (i.e. correlation entropy h_2) converges to a constant (not necessary zero) value. Therefore, we may conclude that the general belief according to which the entropy plot applied to stochastic systems evaluating in continuum should diverge to infinity may not be applied to a specific class of systems that exhibit intermittency.

On-off intermittency can be observed in **both stochastic and deterministic systems** [159, 160, 163]. The study by Cabrera and Milton [6, 97, 98] used a stochastic differential equation to reproduce intermittency. The human controller was modeled using time delay and multiplicative white Gaussian noise. The resulting stochastic differential equation replicated the power-law scaling with exponents $-1/2$ and -2.4 in the power spectra of $\Delta z/l$, and the power-law scaling with exponent $-3/2$ in the probability distribution of the laminar phases. These were shown to be signs of intermittency (Fig. 23).

Similar scaling of the power spectra with exponent $-1/2$ for systems exhibiting intermittency was obtained by Fujisaka and Yamada for a multiplicative noise (stochastic)

model [169], and a chaotic (deterministic) map [161]. Other studies also reported the power-law scaling of the power spectrum with exponent $-1/2$ for both stochastic and deterministic models [159, 160]. Furthermore, the probability distribution of the laminar phase was also shown to resemble a power-law distribution with exponent $-3/2$ for both stochastic and deterministic systems with intermittent behavior [163].

Convergence of h_2 for systems exhibiting on-off Intermittency

In the case of a dissipative system, chaos is associated with a strange attractor of a non-integer fractal dimension (i.e. Hausdorff dimension), and with a positive value for the Kolmogorov-Sinai entropy, h_{KS} , which represents a measure of the disorder in a dynamical system. Moreover, the Kolmogorov-Sinai entropy was shown to be a lower bound to the sum of the positive Lyapunov exponents [170]. Positive-valued estimates of the properties of the strange attractor, such as the fractal dimension, Lyapunov exponents, and the Kolmogorov-Sinai entropy, are believed to identify low-dimensional chaotic systems. In the case of Hamiltonian systems there is no attractor, and the fractal dimension of the trajectory in the phase space has a rather unclear meaning [171]. However, the Kolmogorov-Sinai entropy maintains its role in characterizing chaos [172, 173]. We recall from section 4.4.4 the following classification of dynamical systems evolving in continuum that are valid for both dissipative and Hamiltonian systems:

- (deterministically) periodic or quasi-periodic if $h_{KS} = 0$;
- deterministically chaotic if $h_{KS} = \text{constant} \neq 0$;
- stochastic process if $h_{KS} \rightarrow \infty$.

It should be noted that the correlation entropy h_2 developed by Grassberger and Procaccia [68, 69] yields the same behavior with h_{KS} . Moreover, the general belief states that the convergence of the correlation entropy to a positive constant is believed to represent a sufficient condition for assessing chaos in dynamical systems. The corresponding analogy for the Hausdorff dimension is the correlation dimension, D_2 . They are related according to the following expression: $D \leq D_2$.

Next, we will show that *continuous stochastic systems that exhibit on-off intermittency* are able to generate a convergent correlation dimension (D_2) and convergent correlation entropy (h_2). A series of studies by Provenzale and Osborne [168, 120, 174] provided a counter-example to the general belief stated above. They considered a class of stochastic processes resembling “colored” random noise that were first introduced in [175]. The discrete-time series was defined by the standard Fourier series:

$$X(t_i) = \sum_{k=1}^{N/2} \xi_k \cos(\omega_k t_i + \phi_k) \quad (6.1)$$

where $i = 1, \dots, N$, $t_i = i\Delta t$, and N is the length of the time series. The phases ϕ_k were random variables, and the coefficient ξ_k was related to the power spectrum $P(\omega_k)$ such that

$$\xi_k = \sqrt{P(\omega_k)\Delta\omega} \quad (6.2)$$

where $\Delta\omega = 2\pi/T$, and $T = N\Delta t$. The power spectrum was fixed to be a power law distribution $P(\omega) = C\omega^{-\alpha}$ with exponent α , and C was a constant to yield unit variance for the time series. The phases were randomly, uniformly distributed on the interval $(0, 2\pi)$.

The correlation dimension D_2 was estimated to be a constant positive value, and it was observed to depend on the scaling exponent α of the power spectrum [120, Table I.]. Therefore, the recorded values for the correlation dimension were related to the fractal properties of the stochastic system, rather than to any deterministic dynamical system. The strange attractor of a deterministic system with $D_2 \geq 1$ is continuous and differentiable along the direction of motion, but can be “fractal” in other directions perpendicular to the direction of motion. Such fractal curves (e.g. the Brownian motion) are continuous and non-differentiable [121]. The method developed by Grassberger and Procaccia to estimate h_2 does not take into account the ordering of the points in the time series. Therefore, it cannot distinguish between differentiable and non-differentiable curves, which translate to strange attractors and fractal random curves, respectively [120].

Furthermore, the correlation entropy h_2 converged to zero regardless of the spectral exponent α [174]. The rate of convergence was shown to be dependent on the length of the time series (i.e. number of data points) and the value of α . Contrary to the expectation

that the correlation entropy should diverge to infinity for stochastic systems, the estimated correlation entropy converges to a constant value.

Another study [176] analyzed the time series of trajectories from three satellite-tracked buoys in the Pacific Ocean for a period of a year. They reported a finite-valued correlation dimension ($D_2 \approx 1.4$) and a constant non-zero correlation entropy ($h_2 \approx 0.2$ bits per day). Although this result could indicate the presence of a low dimensional attractor, they found that the signals were nondeterministic and fractal. Furthermore, the power spectra resembled a power law distribution with exponent $\alpha = 3$.

Against initial and general belief, the correlation entropy converges to a constant for continuous stochastic systems as well. This seems to be the case for fractal curves that originate from stochastic systems when the power spectrum is shaped by a power law distribution with randomly distributed phases. This implies that the estimation of a finite non-diverging value for the correlation entropy does not necessarily imply that the time series is generated by a deterministic dynamical system. Therefore, there does not seem not to be a conflict in using the correlation entropy to characterize the human controller with stochastic properties. Future investigation on this topic will address this issue.

7.0 CONCLUSION

Our study has proposed a framework combining information- and control-theoretic approaches to address a difficult and fundamental question in human-machine interaction: What is the human capability in manual control of systems with complex unstable dynamics? Specifically, we quantified the human performance in terms of information-transmission rate measured in bits per second. We demonstrated our method for an example of stabilizing an inverted pendulum.

We derived that, for a human operator to control an unstable system, the minimum information-transmission rate of manual control required to stabilize the feedback system depends on the degree of instability of the task (i.e. length of the inverted pendulum). For the particular case of an LTI controller, we also have to factor in the lower bound any time delays and nonminimum-phase zeros of the plant.

We suggested a method to estimate the information-transmission rate from human experiments based on time series analysis. We found that this quantity varied within subjects with the degree of instability of the task and the time delay present in the closed-loop system. Specifically, the information-transmission rate of human operators decreased with time delay and increased with the degree of instability of the task. Our results were validated relative to other representative studies on manual control.

The comparison between the information-rate measurements from human experiments and the lower bound, that was derived theoretically, was shown to reflect a quantitative measure of human performance and to predict its limitations. The same comparison showed that the manual control strategy exceeded the characteristics of an LTI system. Thus, a representation of the human controller by a nonlinear and, possibly, time-varying system seems more adequate.

Furthermore, we presented the restrictions upon the bandwidth of the control signal based on the dynamics of the plant. Our analysis showed that the ability of the human controller to convey information seems to be associated with the distribution of the frequency components in the power spectrum rather than only the size of the bandwidth.

Our investigation evaluated both the potential and the limitations of manual control. Through our results and analysis, we hope to raise more interest in understanding the neural computation and sensorimotor integration of control movement.

APPENDIX A

INVERTED PENDULUM DYNAMICS

In this section we derive the equation of the inverted pendulum (4.1), which is shown in Fig. 24. The description of the parameters is given in Table 5. The dynamics of the inverted pendulum was derived using the Lagrangian method.

Let V denote the potential energy:

$$V = mg\frac{L}{2} \cos \theta,$$

and let T represent the translational and rotational kinetic energy of the system:

$$\begin{aligned} T &= \frac{1}{2}m (\dot{x}_1^2 + \dot{x}_1^2) + \frac{1}{2}J\dot{\theta}^2 \\ &= \frac{1}{2}m \left\{ \left[\frac{d}{dt} \left(\frac{L}{2} \sin \theta + x_0 \right) \right]^2 + \left[\frac{d}{dt} \left(\frac{L}{2} \cos \theta \right) \right]^2 \right\} + \frac{1}{2}J\dot{\theta}^2 \\ &= \frac{1}{2}m \left[\left(\frac{L}{2} \dot{\theta} \cos \theta + \dot{x}_0 \right)^2 + \left(\frac{L}{2} \dot{\theta} \sin \theta \right)^2 \right] + \frac{1}{2}J\dot{\theta}^2 \\ &= \frac{1}{2}m\dot{x}_0^2 + \frac{1}{2}m\frac{L^2}{4}\dot{\theta}^2 + m\dot{x}_0\dot{\theta}\frac{L}{2} \cos \theta + \frac{1}{2}J\dot{\theta}^2. \end{aligned}$$

where the notation $\dot{x} = dx/dt$ was adopted for the first time-derivative of x , and $\ddot{x} = d^2x/dt^2$ for the second time-derivative of x . The Lagrangian is then defined as:

$$\begin{aligned} L_g &= T - V \\ &= \frac{1}{2}m\dot{x}_0^2 + m\frac{L^2}{8}\dot{\theta}^2 + m\dot{x}_0\dot{\theta}\frac{L}{2} \cos \theta + \frac{1}{2}J\dot{\theta}^2 - mg\frac{L}{2} \cos \theta. \end{aligned} \tag{A.1}$$

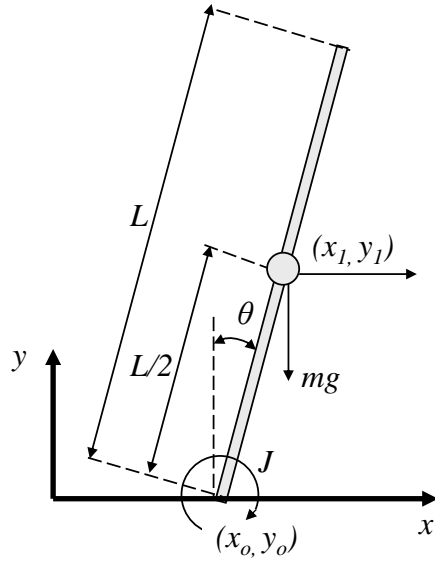


Figure 24: Inverted pendulum system.

The equation that describes the dynamics of the inverted pendulum system was obtained by computing the Euler-Lagrange equation:

$$\frac{\partial L_g}{\partial \theta} - \frac{d}{dt} \left(\frac{\partial L_g}{\partial \dot{\theta}} \right) = 0 \quad (\text{A.2})$$

Table 5: Description of the inverted pendulum parameters.

Parameter	Description
(x_0, y_0)	Coordinates of the bottom tip of the pendulum
(x_1, y_1)	Coordinates of the center of gravity of the pendulum
θ	Angle of the pendulum
L	Length of the pendulum
m	Mass of the pendulum
J	Moment of inertia of the pendulum

which yields the following:

$$\frac{\partial L_g}{\partial \theta} = -m\dot{x}_0\dot{\theta}\frac{L}{2}\sin\theta + mg\frac{L}{2}\sin\theta \quad (\text{A.3})$$

$$\begin{aligned} \frac{\partial L_g}{\partial \dot{\theta}} &= m\frac{L^2}{4}\dot{\theta} + m\dot{x}_0\frac{L}{2}\cos\theta + J\dot{\theta} \\ \frac{d}{dt}\left(\frac{\partial L_g}{\partial \dot{\theta}}\right) &= m\frac{L^2}{4}\ddot{\theta} + m\ddot{x}_0\frac{L}{2}\cos\theta - m\dot{x}_0\dot{\theta}\frac{L}{2}\sin\theta + J\ddot{\theta} \end{aligned} \quad (\text{A.4})$$

Substituting (A.3) and (A.4) into (A.2), we obtain:

$$\left(J + m\frac{L^2}{4}\right)\frac{d^2\theta}{dt^2} + m\frac{L}{2}\cos\theta\frac{d^2x}{dt^2} = mg\frac{L}{2}\sin\theta. \quad (\text{A.5})$$

where the moment of inertia $J = mL^2/12 \text{ kg} \cdot \text{m}^2$ corresponds to the rotation of the pendulum about its center of gravity (x_1, y_1) . After rearranging the terms in (A.5), we obtain the inverted pendulum expression (4.1) given in section 4.1.2.

APPENDIX B

EXPERIMENTAL DATA

Table 6 shows the total number of data samples recorded for each subject during each tested scenario. If a subject was to successfully stabilize the inverted pendulum during the entire length of the trial for all the trials, then a total of 600 seconds would be the maximum time interval recorded for a specific scenario. This number is computed considering that there were 10 trials with a duration of 60 seconds each.

Table 6: Duration of recorded data [seconds] for 12 subjects.

Pendulum length [m]	20					12	8	5	3
Time delay [ms]	0	100	200	400	600	0			
Subject A	600	600	600	380	291	600	564	548	339
Subject B	587	567	409	183	148	600	425	91	48
Subject C	600	598	600	387	255	600	600	600	371
Subject D	559	529	570	493	253	535	564	510	167
Subject E	589	476	530	402	447	545	482	544	343
Subject F	600	600	540	377	204	600	593	573	256
Subject G	590	536	540	239	147	510	551	351	219
Subject H	585	600	568	298	210	600	594	516	223
Subject I	600	572	515	351	145	599	592	486	175
Subject J	600	600	600	435	270	588	443	488	252
Subject K	558	570	505	413	217	539	563	344	126
Subject L	600	600	483	353	178	555	499	368	110

The following table provides the recorded values for τ using the first minimum of the delayed mutual information. We values marked with italic reflect the values for which the entropy-rate estimation was not successful. These values were not taken into consideration when the average values for τ were computed. The average values for τ computed from Table 7 were rounded to the closest integer when illustrated in Table 2.

Table 7: Values of τ [samples] for 12 subjects.

Pendulum length [m]	20					12	8	5	3
	0	100	200	400	600	0			
Subject A	14	13	15	16	18	15	11	<i>9</i>	<i>12</i>
Subject B	17	19	19	<i>22</i>	<i>22</i>	15	16	<i>17</i>	<i>51</i>
Subject C	13	18	12	19	21	6	10	11	10
Subject D	13	14	16	16	20	13	14	14	<i>15</i>
Subject E	20	15	14	17	18	14	14	14	<i>13</i>
Subject F	17	18	16	16	19	16	15	14	15
Subject G	15	13	14	17	<i>22</i>	12	15	<i>14</i>	<i>13</i>
Subject H	16	20	19	18	22	21	14	15	17
Subject I	15	17	15	18	<i>19</i>	17	16	13	<i>16</i>
Subject J	17	21	20	19	20	18	19	20	18
Subject K	12	14	17	15	20	13	13	13	13
Subject L	15	18	18	17	<i>20</i>	15	14	15	<i>16</i>
Average	15.33	16.67	16.25	17.1	19.75	14.58	14.25	14.33	15

BIBLIOGRAPHY

- [1] I. S. MacKenzie and C. Ware, “Lag as a determinant of human performance in interactive systems,” in *Proceedings of the INTERACT '93 and CHI '93 Conference on Human Factors in Computing Systems*. New York, NY, USA: ACM, 1993, pp. 488–493.
- [2] C. E. Shannon, “A mathematical theory of communication,” *Bell Systems Technical Journal*, vol. 27, pp. 379–423 and 623–656, 1948.
- [3] M. Bodson, “Fun control experiments with matlab and a joystick,” in *Proc. IEEE Conf. Decision and Control*, vol. 3, Maui, HI, USA, Dec. 2003, pp. 2508–2513.
- [4] H. Kantz and T. Schreiber, *Nonlinear Time Series Analysis: Second Edition*. Cambridge, UK: Cambridge University Press, 2004.
- [5] I. D. Loram, P. J. Gawthrop, and M. Lakie, “The frequency of human, manual adjustments in balancing an inverted pendulum is constrained by intrinsic physiological factors,” *Journal of Physiology*, vol. 577, pp. 417–432, Nov. 2006.
- [6] J. L. Cabrera and J. G. Milton, “On-off intermittency in a human balancing task,” *Physical Review Letters*, vol. 89, no. 15, pp. 158 702–1–158 702–4, Oct. 2002.
- [7] “Da vinci surgery.” [Online]. Available: <http://www.davincisurgery.com/>
- [8] J. Marescaux, J. Leroy, M. Gagner, F. Rubino, D. Mutter, M. Vix, S. E. Butner, and M. K. Smith, “Transatlantic robot-assisted telesurgery,” *Nature*, vol. 413, pp. 379–380, 2001.
- [9] S. Butner and M. Ghodoussi, “Transforming a surgical robot for human telesurgery,” *IEEE Transactions on Robotics and Automation*, vol. 19, no. 5, pp. 818 – 824, oct. 2003.
- [10] R.-E. Precup, L. Kovacs, T. Haidegger, S. Preitl, A. Kovacs, B. Benyo, E. Borbely, and Z. Benyo, “Time delay compensation by fuzzy control in the case of master-slave telesurgery,” in *6th IEEE International Symposium on Applied Computational Intelligence and Informatics (SACI)*, may 2011, pp. 305 –310.

- [11] R. Muradore, D. Bresolin, L. Geretti, P. Fiorini, and T. Villa, “Robotic surgery,” *IEEE Robotics Automation Magazine*, vol. 18, no. 3, pp. 24–32, sept. 2011.
- [12] “Subteran robotics: Cave crawler.” [Online]. Available: http://www.cs.cmu.edu/~groundhog/robots_cc.html
- [13] “Redzone robotics.” [Online]. Available: <http://redzone.com>
- [14] “Darpa robotics challenge.” [Online]. Available: http://www.darpa.mil/Our_Work/TTO/Programs/DARPA_Robotics_Challenge.aspx
- [15] “Subteran robotics: Mine observational locomotion experimenter (mole).” [Online]. Available: <http://www.usmra.com/MOLEUltraLight/MOLEUltrLight.htm>
- [16] E. Ackerman, “Japan earthquake: irobot sending packbots and warriors to fukushima dai-1 nuclear plant,” 2011. [Online]. Available: <http://spectrum.ieee.org/automaton/robotics/industrial-robots/irobot-sending-packbots-and-warriors-to-fukushima>
- [17] “Mars exploration rovers mission.” [Online]. Available: <http://marsrover.nasa.gov/home/index.html>
- [18] “Mars science laboratory.” [Online]. Available: http://www.nasa.gov/mission_pages/msl/index.html
- [19] E. Guizzo, “Fukushima robot operator writes tell-all blog,” 2011. [Online]. Available: <http://spectrum.ieee.org/automaton/robotics/industrial-robots/fukushima-robot-operator-diaries>
- [20] N. Martins, M. Dahleh, and J. Doyle, “Fundamental limitations of disturbance attenuation in the presence of side information,” *Automatic Control, IEEE Transactions on*, vol. 52, no. 1, pp. 56–66, jan. 2007.
- [21] N. C. Martins and M. A. Dahleh, “Feedback control in the presence of noisy channels: ‘Bode-like’ fundamental limitations of performance,” *IEEE Transactions on Automatic Control*, vol. 53, no. 7, pp. 1604–1615, Aug. 2008.
- [22] M. F. Lupu, M. Sun, and Z. H. Mao, “Bandwidth limitations in human control tasks,” in *2nd IASTED International Conference on Robotics*, Pittsburgh, PA, SUA, Nov. 2011.
- [23] T. B. Sheridan, *Humans and Automation: System Design and Research Issues*. New York, NY, USA: Wiles Series in Systems Engineering and Management, 2002.
- [24] R. Parasuraman, T. B. Sheridan, and C. D. Wickens, “A model for types and levels of human interaction with automation,” *IEEE Transactions on Systems, Man, and Cybernetics—Part A: Systems and Humans*, vol. 30, no. 3, pp. 286–297, May 2000.

- [25] T. Tsuji and Y. Tanaka, “Tracking control properties of human-robotic systems based on impedance control,” *IEEE Transactions on Systems, Man, and Cybernetics—Part A: Systems and Humans*, vol. 35, no. 4, pp. 523–535, 2005.
- [26] R. Kikuuwe, T. Yamamoto, and H. Fujimoto, “A guideline for low-force robotic guidance for enhancing human performance of positioning and trajectory tracking: It should be stiff and appropriately slowmodel-based human-centered task automation: A case study in acc system design,” *IEEE Transactions on Systems, Man, and Cybernetics—Part A: Systems and Humans*, vol. 38, no. 4, pp. 945–957, 2008.
- [27] T. B. Sheridan and W. R. Ferrell, *Man-Machine Systems: Information, Control, Decision Models of Human Performance*. Cambridge, MA, USA: MIT Press, 1974.
- [28] W. E. Hick, “On the rate of gain of information,” *Quarterly Journal of Experimental Psychology*, vol. 4, pp. 11–26, 1952.
- [29] R. Hyman, “Stimulus information as a determinant of reaction time,” *Journal of Experimental Psychology*, vol. 45, pp. 188–196, 1953.
- [30] P. M. Fitts, “The information capacity of the human motor system in controlling the amplitude of movement,” *Journal of Experimental Psychology*, vol. 47, no. 6, pp. 381–391, Jun. 1954.
- [31] T. O. Kvalseth, “Test of the 10 bits/sec channel-capacity hypothesis for human tracking,” *Applied Mathematical Modeling*, vol. 3, no. 4, pp. 307–308, Aug. 1979.
- [32] Z.-H. Mao, H.-N. Lee, R. J. Sclabassi, and M. Sun, “Information capacity of the thumb and the index finger in communication,” *IEEE Transactions on Biomedical Engineering*, vol. 56, no. 5, pp. 1535–1545, May 2009.
- [33] M. Hannula, “Information transmission capacity of the nervous system of the arm—an information and communication engineering approach to the brachial plexus function,” Ph.D. dissertation, University of Oulu, Finland, 2003.
- [34] K. Gold, “An information pipeline model of human-robot interaction,” in *Proc. 4th ACM/IEEE International Conference on Human-Robot Interaction*, La Jolla, CA, USA, Mar. 2009, pp. 85–92.
- [35] H. Jacobson, “The informational capacity of the human ear,” *Science*, vol. 112, no. 2901, pp. 143–144, Aug. 1950.
- [36] —, “The informational capacity of the human eye,” *Science*, vol. 113, no. 2933, pp. 292–293, Mar. 1951.
- [37] G. A. Miller, “Human memory and storage of information,” *IRE Trans. Information Theory*, vol. IT-2, no. 3, pp. 129–137, Sep. 1956.

- [38] J. R. Pierce and J. E. Karlin, “Reading rates and the information rate of the human channel,” *Bell System Technical Journal*, vol. 36, pp. 497–516, Mar. 1957.
- [39] S. C. Seow, “Information theoretic models of hci: A comparison of the hick-hyman law and fitts’ law,” *Human-Computer Interaction*, vol. 20, no. 3, pp. 315–352, Aug. 2005.
- [40] R. J. Jagacinski and J. M. Flach, *Control Theory for Humans: Quantitative Approaches to Modeling Performance*. Mahwah, NJ, USA: Lawrence Erlbaum Associates, 2003.
- [41] J. I. Elkind and L. T. Sprague, “Transmission of information in simple manual control systems,” *IRE Transactions on Human Factors in Electronics*, vol. HFE-2, no. 1, pp. 58–60, Mar. 1961.
- [42] R. Balakrishnan and I. S. MacKenzie, “Performance differences in the fingers, wrist, and forearm in computer input control,” in *Proc. ACM Conf. Human Factors in Computing Systems*, Atlanta, GA, USA, Mar. 1997, pp. 303–310.
- [43] H. Quastler, Ed., *Information Theory in Psychology: Problems and Methods*. Glencoe, Illinois: The Free Press, 1955.
- [44] D. Ward, “Adaptive computer interfaces,” Ph.D. dissertation, University of Cambridge, Cambridge, 2001.
- [45] N. Elia, “When Bode meets Shannon: control-oriented feedback communication schemes,” *IEEE Transactions on Automatic Control*, vol. 49, no. 9, pp. 1477–1488, Sep. 2004.
- [46] T. Schreiber. (1996) Efficient neighbor searching in nonlinear time series. [Online]. Available: <http://citeseerx.ist.psu.edu/viewdoc/summary?doi=10.1.1.35.2471>
- [47] —, “Measuring information transfer,” *Physical Review Letters*, vol. 85, no. 2, pp. 461–464, Jul. 2000.
- [48] C. J. Cellucci, A. M. Albano, and P. E. Rapp, “Statistical validation of mutual information calculations: comparison of alternative numerical algorithms,” *Physical Review E*, vol. 71, p. 066208, jun 2005.
- [49] A. M. Fraser, “Information and entropy in strange attractors,” *IEEE Transactions on Information Theory*, vol. 35, no. 2, pp. 245–262, 1989.
- [50] P. Grassberger, “Finite sample corrections to entropy and dimension estimates,” *Physics Letters A*, vol. 128, no. 67, pp. 369 – 373, 1988.
- [51] —, “Entropy estimates from insufficient samplings,” 2003. [Online]. Available: <http://www.citebase.org/abstract?id=oai:arXiv.org:physics/0307138>
- [52] R. M. S, “Estimating the errors on measured entropy and mutual information,” *Physica D*, vol. 125, pp. 285–294, 1999.

- [53] J.-F. Bercher and C. Vignat, “Estimating the entropy of a signal with applications,” *IEEE Transactions on Signal Processing*, vol. 48, no. 6, pp. 1687–1694, 2000.
- [54] M. Lungarella, T. Pegors, D. Bulwinkle, and O. Sporns, “Methods for quantifying the informational structure of sensory and motor data,” *Neuroinformatics*, vol. 3, no. 3, pp. 243–262, 2005.
- [55] M. Lungarella and O. Sporns, “Mapping information flow in sensorimotor networks,” *PLOS Computational Biology*, vol. 2, no. 10, pp. 1301–1312, 2006.
- [56] J. A. Vastano and H. L. Swinney, “Information transport in spatiotemporal systems,” *Physical Review Letters*, vol. 60, no. 18, pp. 1773–1776, May 1988.
- [57] A. M. Fraser and H. L. Swinney, “Independent coordinates for strange attractors from mutual information,” *Physical Review A*, vol. 33, no. 2, pp. 1134–1140, Feb. 1986.
- [58] D. Prichard and J. Theiler, “Generalized redundancies for time series analysis,” *Physica D: Nonlinear Phenomena*, vol. 84, no. 3-4, pp. 476–493, Jul. 1995.
- [59] M. Small, *Applied Nonlinear Time Series Analysis: Applications in Physics, Physiology and Finance*. Hackensack, NJ, USA: World Scientific Publishing Co. Pte. Ltd., 2005.
- [60] J. Escudero, R. Hornero, and D. Abasolo, “Interpretation of the auto-mutual information rate of decrease in the context of biomedical signal analysis. application to electroencephalogram recordings,” *Physiological Measurement*, vol. 30, pp. 187–199, 2009.
- [61] R. Quiñan Quiroga and S. Panzeri, “Extracting information from neuronal populations: information theory and decoding approaches,” *Nat Rev Neurosci*, vol. 10, no. 3, pp. 173–185, Mar. 2009.
- [62] O. Kwon and J.-S. Yang, “Information flow between stock indices,” *EPL*, vol. 82, pp. 68003–p1–p4, Jun. 2008.
- [63] S. K. Baek, W.-S. Jung, O. Kwon, and H.-T. Moon, “Transfer entropy analysis of the stock market,” Sep. 2005. [Online]. Available: <http://arxiv.org/abs/physics/0509014>
- [64] K. Hlavackova-Schindler, M. Palus, M. Vejmelka, and J. Bhattacharya, “Causality detection based on information-theoretic approaches in time series analysis,” *Physics Reports*, vol. 441, no. 1, pp. 1–46, 2007.
- [65] A. Kolmogorov, “New metric invariant of transitive dynamical systems and endomorphisms of lebesgue spaces,” *Doklady Akademii Nauk SSSR*, vol. 119, no. N5, pp. 861–864, 1958.
- [66] A. G. Sinai, “On the concept of entropy of a dynamical system,” *Doklady Akademii Nauk SSSR*, vol. 124, pp. 768–771, 1959.

- [67] A. Cohen and I. Procaccia, “Computing the kolmogorov entropy from time signals of dissipative and conservative dynamical systems,” *Physical Review A*, vol. 31, no. 3, pp. 1872–1882, Mar. 1985.
- [68] P. Grassberger and I. Procaccia, “Measuring the strangeness of strange attractors,” *Physica D*, vol. 9, no. 1-2, pp. 189–208, Oct. 1983.
- [69] —, “Estimation of the kolmogorov entropy from a chaotic signal,” *Physical Review A*, vol. 28, no. 4, pp. 2591–2593, Oct. 1983.
- [70] P. Gaspard and X.-J. Wang, “Noise, chaos and (ϵ, τ) -entropy per unit time,” *Physics Reports*, vol. 235, no. 6, pp. 291–343, 1993.
- [71] T. M. Cover and J. A. Thomas, *Elements of Information Theory: Second Edition*. New York, USA: Wiley, 2006.
- [72] M. S. Pinsker, *Information and Information Stability of Random Variables and Processes*. San Francisco, CA, USA: Holden-Day, INC., 1964.
- [73] R. M. Gray and J. C. Kiefer, “Mutual information rate, distortion, and quantization in metric spaces,” *IEEE Transactions on Information Theory*, vol. 26, no. 4, pp. 412–422, Jul. 1980.
- [74] A. Renyi, “On measures of information and entropy,” in *Proceedings of the 4th Berkeley Symposium on Mathematics, Statistics and Probability*, vol. 1, 1960, pp. 547–561.
- [75] R. Frigg, “In what sense is the kolmogorov entropy a measure for chaotic behaviour? bridging the gap between dynamical systems theory and communication theory,” *Brit. J. Phil. Sci.*, vol. 55, pp. 411–434, 2004.
- [76] Y. Hirata, K. Judd, and D. Kilminster, “Estimating a generating partition from observed time series: Symbolic shadowing,” *Physical Review E*, vol. 70, p. 016215, jul 2004.
- [77] F. Takens, *Detecting Strange Attractors in Turbulence*. New York: Springer, 1981, vol. 898.
- [78] M. B. Kennel, R. Brown, and H. Abarbanel, “Determining embedding dimension for phase-space reconstruction using a geometrical construction,” *Physical Review A*, vol. 45, no. 6, pp. 3403–3411, 1992.
- [79] C. Rhodes and M. Morari, “The false nearest neighbors algorithm: An overview,” *Computers and Chemical Engineering*, vol. 21, Supplement, pp. S1149 – S1154, 1997.
- [80] R. A. Schmidt and T. D. Lee, *Motor Control and Learning: A Behavioral Emphasis*, 4th ed. Champaign, IL: Human Kinetics, 2005.

- [81] R. Huys, B. E. Studenka, N. L. Rheaume, H. N. Zelaznik, and V. K. Jirsa, “Distinct timing mechanisms produce discrete and continuous movements,” *PLoS Comput Biol*, vol. 4, no. 4, p. e1000061, 04 2008.
- [82] K. J. W. Craik, “Theory of the human operator in control systems,” *British Journal of Psychology. General Section*, vol. 38, no. 3, pp. 142–148, 1948.
- [83] M. A. Vince, “The intermittency of control movements and the psychological refractory period,” *British Journal of Psychology*, vol. 38, no. 3, pp. 149–157, Mar. 1948.
- [84] R. T. Bye and P. D. Neilson, “The bump model of response planning: Variable horizon predictive control accounts for the speedaccuracy tradeoffs and velocity profiles of aimed movement,” *Human Movement Science*, vol. 27, no. 5, pp. 771 – 798, 2008.
- [85] H. Pashler and J. C. Johnston, *Attentional limitations in dual-task performance*. Hove, England: Psychology Press, 1998.
- [86] I. D. Loram, C. van de Kamp, H. Gollee, , and P. J. Gawthrop, “Identification of intermittent control in man and machine,” *J. R. Soc. Interface*, vol. 9, no. 74, pp. 2070–2084, 2012.
- [87] F. Navas and L. Stark, “Sampling or intermittency in hand control system dynamics,” *Biophysical Journal*, vol. 8, no. 2, pp. 252 – 302, 1968.
- [88] I. D. Loram, H. Gollee, M. Lakie, and P. J. Gawthrop, “Human control of an inverted pendulum: Is continuous control necessary? is intermittent control effective? is intermittent control physiological?” *The Journal of Physiology*, vol. 589, no. 2, pp. 307–324, 2011.
- [89] I. D. Loram, C. N. Maganaris, and M. Lakie, “Human postural sway results from frequent, ballistic bias impulses by soleus and gastrocnemius,” *The Journal of Physiology*, vol. 564, no. 1, pp. 295–311, 2005.
- [90] I. D. Loram and M. Lakie, “Human balancing of an inverted pendulum: position control by small, ballistic-like, throw and catch movements,” *The Journal of Physiology*, vol. 540, no. 3, pp. 1111–1124, 2002.
- [91] A. B. Slifkin, D. E. Vaillancourt, and K. M. Newell, “Intermittency in the control of continuous force production,” *Journal of Neurophysiology*, vol. 84, no. 4, pp. 1708–1718, 2000.
- [92] S. Hanne-ton, A. Berthoz, J. Droulez, and J. Slotine, “Does the brain use sliding variables for the control of movements?.” *Biological Cybernetics*, vol. 77, no. 6, p. 381, 1997.
- [93] R. C. Miall, D. J. Weir, and J. F. Stein, “Intermittency in human manual tracking tasks,” *Journal of Motor Behavior*, vol. 25, no. 1, pp. 53–63, 1993.

- [94] M. F. Lupu, M. Sun, D. Askey, R. Xia, and Z. H. Mao, “Human strategies in balancing an inverted pendulum with time delay,” in *32nd Annual International Conference of the IEEE EMBS*, Buenos Aires, Argentina, 2010, pp. 5246–5249.
- [95] J. A. Doeringer and N. Hogan, “Intermittency in preplanned elbow movements persists in the absence of visual feedback,” *Journal of Neurophysiology*, vol. 80, no. 4, pp. 1787–1799, 1998.
- [96] Y. Asai, Y. Tasaka, K. Nomura, T. Nomura, M. Casadio, and P. Morasso, “A model of postural control in quiet standing: Robust compensation of delay-induced instability using intermittent activation of feedback control,” *PLoS ONE*, vol. 4, no. 7, p. e6169, July 2009.
- [97] J. L. Cabrera, R. Bormann, C. Eurich, T. Ohira, and J. G. Milton, “State-dependent noise and human balance control,” *Fluctuation and Noise Letters*, vol. 4, no. 1, pp. 107–117, 2004.
- [98] J. L. Cabrera, C. Luciani, and J. Milton, “Neural control on multiple time scales: insights from human stick balancing,” *Condensed Matter Physics*, vol. 9, no. 2, pp. 373–383, 2006.
- [99] P. J. Gawthrop, I. D. Loram, and M. Lakie, “Predictive feedback in human simulated pendulum balancing,” *Biological Cybernetics*, vol. 101, pp. 131–146, Aug. 2009.
- [100] P. J. Gawthrop and L. Wang, “Intermittent model predictive control,” *Proceedings of the Institution of Mechanical Engineers, Part I: Journal of Systems and Control Engineering*, vol. 221, no. 7, pp. 1007–1018, 2007.
- [101] P. Gawthrop and L. Wang, “Intermittent predictive control of an inverted pendulum,” *Control Engineering Practice*, vol. 14, no. 11, pp. 1347–1356, November 2006.
- [102] P. Gawthrop, I. Loram, M. Lakie, and H. Gollee, “Intermittent control: a computational theory of human control,” *Biological Cybernetics*, vol. 104, pp. 31–51, 2011.
- [103] G. Stein, “Respect the unstable,” *IEEE Control Systems Magazine*, vol. 23, no. 4, pp. 12–25, Aug. 2003.
- [104] R. J. Peterka and P. J. Loughlin, “Dynamic regulation of sensorimotor integration in human postural control,” *Journal of Neurophysiology*, vol. 91, no. 1, pp. 410–423, 2004.
- [105] A. R. Potvin, J. A. Doerr, J. T. Estes, and W. W. Tourtellotte, “Portable clinical tracking-task instrument,” *Medical and Biological Engineering and Computing*, vol. 15, no. 4, pp. 391–397, Jul. 1977.
- [106] H. K. Khalil, *Nonlinear Systems*. Upper Saddle River, NJ: Prentice Hall, 2002.

- [107] M. F. Lupu, “Human strategies in the control of time critical unstable systems,” Master’s thesis, Swanson School of Engineering, University of Pittsburgh, Pittsburgh, PA, USA, 2010.
- [108] D. T. McRuer, “Human dynamics in man-machine systems,” *Automatica*, vol. 16, pp. 237–253, may 1980.
- [109] D. T. McRuer and E. S. Krendel, “The man-machine system concept,” *Proceedings of the IRE*, vol. 50, pp. 1117–1123, may 1962.
- [110] D. T. McRuer and H. R. Jex, “A review of quasi-linear pilot models,” *IEEE Transactions on Human Factors in Electronics*, vol. 8, pp. 231–249, september 1967.
- [111] C. M. Harris and D. M. Wolpert, “Signal-dependent noise determines motor planning,” *Nature*, vol. 394, pp. 780–784, aug 1998.
- [112] S. Baron, D. L. Kleinman, and W. H. Levison, “An optimal control model of human response part i: Theory and validation,” *Automatica*, vol. 6, no. 3, pp. 357–369, May 1970.
- [113] J. H. Braslavsky, R. H. Middleton, and J. S. Freudenberg, “Feedback stabilization over signal-to-noise ratio constrained channels,” *IEEE Transactions on Automatic Control*, vol. 52, pp. 1391–1403, august 2007.
- [114] L. R. Young and J. L. Meiry, “Bang-bang aspects of manual control in high-order systems,” *IEEE Transactions on Automatic Control*, vol. 10, no. 3, pp. 336–341, Jul. 1965.
- [115] G. A. Bekey, “The human operator as a sampled-data system,” *IRE Transactions on Human Factors in Electronics*, vol. HFE-3, no. 2, pp. 43–51, Sep. 1962.
- [116] M. F. Lupu, M. Sun, R. Xia, and Z.-H. Mao, “Rate of information transmission in human manual control of an unstable system,” *IEEE Trans. on Systems, Man, and Cybernetics: Human-Machine Systems*, vol. 43, no. 2, pp. 259–263, Mar. 2013.
- [117] T. Kapitaniak, *Chaos in systems with noise*. Teaneck, N.J.: World Scientific Publishing Co., 1988.
- [118] E. A. Jonckheere and B.-F. Wu, “Chaotic disturbance rejection and bode limitation,” in *American Control Conference, 1992*, june 1992, pp. 2227 –2231.
- [119] E. Jonckheere, A. Hammad, and B.-F. Wu, “Chaotic disturbance rejection a kolmogorov-sinai entropy approach,” in *Decision and Control, 1993., Proceedings of the 32nd IEEE Conference on*, dec 1993, pp. 3578 –3583 vol.4.
- [120] A. Osborne and A. Provenzale, “Finite correlation dimension for stochastic systems with power-law spectra,” *Physica D*, vol. 35, pp. 357–381, 1989.

- [121] L. Zunino, D. Prez, A. Kowalski, M. Martn, M. Garavaglia, A. Plastino, and O. Rosso, “Fractional brownian motion, fractional gaussian noise, and tsallis permutation entropy,” *Physica A: Statistical Mechanics and its Applications*, vol. 387, no. 24, pp. 6057 – 6068, 2008.
- [122] J. Theiler, “Spurious dimension from correlation algorithms applied to limited time series data,” *Physical Review A*, vol. 34, p. 2427, 1986.
- [123] R. Hegger, H. Kantz, T. Schreiber, and E. Olbrich, “Tisean (time series analysis,” 2007. [Online]. Available: http://www.mpipks-dresden.mpg.de/~tisean/Tisean_3.0.1
- [124] R. Hegger, H. Kantz, and T. Schreiber, “Practical implementation of nonlinear time series methods: The tisean package,” *CHAOS*, vol. 9, pp. 413–436, 1999.
- [125] H. W. Bode, *Network Analysis and Feedback Amplifier Design*. New York: D. van Nostrand, 1945.
- [126] I. M. Horowitz, *Synthesis of Feedback Systems*. New York: Academic Press, 1963.
- [127] J. S. Freudenberg and D. P. Looze, *Frequency domain properties of scalar and multi-variable feedback systems*. Berlin: Springer-Verlag, 1988.
- [128] W. S. Levine, *The Control Handbook: Control System Advanced Methods*. Florida: CRC Press: Taylor & Francis Group, 2011.
- [129] R. H. Middleton and G. C. Goodwin, *Digital Control and Estimation. A Unified Approach*. Englewood Cliffs, NJ: Prentice-Hall, 1990.
- [130] R. H. Middleton, “Trade-offs in linear control system design,” *Automatica*, vol. 27, no. 2, pp. 281–292, 1991.
- [131] M. M. Seron, J. H. Braslavsky, and G. C. Goodwin, *Fundamental Limitations in Filtering and Control*. New York: Springer-Verlag, 1997.
- [132] P. Iglesias, “An analogue of bode’s integral for stable non linear systems: Relations to entropy,” in *Proc. 40th IEEE Conf. on Decision and Control*, Orlando, FL, USA, 2001, pp. 3419–3420.
- [133] G. Zang and P. Iglesias, “Nonlinear extension of bode’s integral based on an information-theoretic interpretation,” *Systems and Control Letters*, vol. 50, pp. 11–19, 2003.
- [134] S. Yu and P. G. Mehta, “Bode-like fundamental performance limitations in control of nonlinear systems,” *IEEE Trans. on Automatic Control*, vol. 55, no. 6, pp. 1390–1405, 2010.

- [135] R. Chan and D. S. Childress, “On information transmission in human-machine systems: Channel capacity and optimal filtering,” *IEEE Transactions on Systems, Man, and Cybernetics*, vol. 20, no. 5, pp. 1136–1145, Sep. 1990.
- [136] L. F. Chaparro, *Signals and Systems using Matlab*. Burlington, MA, USA: Academic Press, 2011.
- [137] C. B. Gibbs, “Controller design: Interactions of controlling limbs, time-lags and gains in positional and velocity systems,” *Ergonomics*, vol. 5, pp. 385–402, 1962.
- [138] T. B. Sheridan and W. R. Ferrell, “Remote Manipulative Control with Transmission Delay,” *Human Factors in Electronics, IEEE Transactions on*, vol. HFE-4, no. 1, pp. 25–29, Sep. 1963.
- [139] I. S. MacKenzie, “Fitts’ law as a research and design tool in human-computer interaction,” *Hum.-Comput. Interact.*, vol. 7, no. 1, pp. 91–139, Mar. 1992.
- [140] P. M. Fitts and J.R.Peterson, “Information capacity of discrete motor responses,” *Journal of Experimental Psychology*, vol. 67, no. 2, pp. 103–112, 1964.
- [141] K. J. Kokjer, “The information capacity of the human fingertip,” *IEEE Transactions on Systems, Man, and Cybernetics—Part A: Systems and Humans*, vol. 17, no. 1, pp. 100–102, Jan. 1987.
- [142] A. J. M. Foulkes and R. C. Miall, “Adaptation to visual feedback delays in a human manual tracking task,” *Experimental Brain Research*, vol. 131, pp. 101–110, 2000.
- [143] P. D. Neilson, N. J. O’Dwyer, and M. D. Neilson, “Stochastic prediction in pursuit tracking: an experimental test of adaptive model,” *Biological cybernetics*, vol. 58, pp. 113–122, 1988.
- [144] R. C. Miall, D. J. Weir, D. M. Wolpert, and J. F. Stein, “Is the cerebellum a smith predictor?” *Journal of Motor Behavior*, vol. 25, no. 3, pp. 203–216, Sep. 1993.
- [145] E. Brenner, J. B. J. Smeets, and M. H. E. de Lussanet, “Hitting moving targets - continuous control of the acceleration of the hand on the basis of the targets velocity,” *Experimental Brain Research*, vol. 122, pp. 467–474, 1998.
- [146] P. G. Morasso, L. Baratto, R. Capra, and G. Spada, “Internal models in the control of posture,” *Neural Networks*, vol. 12, no. 7-8, pp. 1173–1180, 1999.
- [147] B. Krekelberg and M. Lappe, “Neuronal latencies and the position of moving objects,” *Trends in Neurosciences*, vol. 24, no. 6, pp. 335 – 339, 2001.
- [148] R. Nijhawan, “Neural delays, visual motion and the flash-lag effect,” *Trends in Cognitive Sciences*, vol. 6, no. 9, pp. 387 – 393, 2002.

- [149] J. Schlag and M. Schlag-Rey, “Through the eye, slowly: Delays and localization errors in the visual system.” *Nature Reviews Neuroscience*, vol. 3, no. 3, p. 191, 2002.
- [150] C. D. Wickens, J. G. Hollands, R. Parasuraman, and S. Banbury, *Engineering Psychology and Human Performance*, 4th ed. Pearson Education, Oct. 2012.
- [151] C. W. Eurich and K. Pawelzik, “Optimal control yields power law behavior,” in *Proceedings of the 15th international conference on Artificial neural networks: formal models and their applications - Volume Part II*, ser. ICANN’05. Berlin, Heidelberg: Springer-Verlag, 2005, pp. 365–370.
- [152] C. W. Eurich and J. G. Milton, “Noise-induced transitions in human postural sway,” *Phys. Rev. E*, vol. 54, pp. 6681–6684, Dec 1996.
- [153] J. J. Collins and C. J. D. Luca, “Random walking during quiet standing,” *Phys. Rev. Letters*, vol. 73, no. 5, pp. 764–767, Aug 1994.
- [154] P. J. Gawthrop and L. Wang, “Event-driven intermittent control,” *International Journal of Control*, vol. 82, no. 12, pp. 2235–2248, 2009.
- [155] E. Ronco, T. Arsan, and P. Gawthrop, “Open-loop intermittent feedback control: practical continuous-time gpc,” *Control Theory and Applications, IEEE Proceedings -*, vol. 146, no. 5, pp. 426–434, sep 1999.
- [156] H. v. d. Kooij and F. C. T. v. d. Helm, “Observations from unperturbed closed loop systems cannot indicate causality,” *The Journal of Physiology*, vol. 569, no. 2, pp. 705–705, 2005.
- [157] R. Miall and J. Jackson, *Experimental Brain Research*, vol. 172, pp. 77–84, 2006.
- [158] J. L. Cabrera and J. G. Milton, “Stick balancing: Onoff intermittency and survival times,” 2004.
- [159] S. C. Venkataramani, T. M. A. Jr., E. Ott, and J. C. Sommerer, “On-off intermittency: Power spectrum and fractal properties of time series,” *Physica D: Nonlinear Phenomena*, vol. 96, no. 14, pp. 66–99, 1996.
- [160] S. Miyazaki and H. Hata, “Universal scaling law of the power spectrum in the on-off intermittency,” *Phys. Rev. E*, vol. 58, pp. 7172–7175, Dec 1998.
- [161] H. Fujisaka, H. Ishii, M. Inoue, and T. Yamada, “Intermittency caused by chaotic modulation. ii,” *Progress of Theoretical Physics*, vol. 76, no. 6, pp. 1198–1209, 1986.
- [162] H. Fujisaka and T. Yamada, “A new intermittency in coupled dynamical systems,” *Progress of Theoretical Physics*, vol. 74, no. 4, pp. 918–921, 1985.
- [163] J. F. Heagy, N. Platt, and S. M. Hammel, “Characterization of on-off intermittency,” *Phys. Rev. E*, vol. 49, pp. 1140–1150, Feb 1994.

- [164] H. Gollee, A. Mamma, I. Loram, and P. J. Gawthrop, “Frequency-domain identification of the human controller,” *Biological Cybernetics*, vol. 106, no. 6-7, pp. 359–372, 2012.
- [165] L. Ljung, Ed., *System identification (2nd ed.): theory for the user*. Upper Saddle River, NJ, USA: Prentice Hall PTR, 1999.
- [166] R. Pintelon, J. Schoukens, and J. Wiley. (2001) *System identification a frequency domain approach*.
- [167] C. Werndl, “Are deterministic descriptions and indeterministic descriptions observationally equivalent?” *Studies In History and Philosophy of Science Part B: Studies In History and Philosophy of Modern Physics*, vol. 40, no. 3, pp. 232 – 242, 2009.
- [168] A. Provenzale, L. Smith, R. Vio, and G. Murante, “Distinguishing between low-dimensional dynamics and randomness in measured time series,” *Physica D*, vol. 58, pp. 31–49, 1992.
- [169] T. Yamada and H. Fujisaka, “Intermittency caused by chaotic modulation. i,” *Progress of Theoretical Physics*, vol. 76, no. 3, pp. 582–592, 1986.
- [170] Y. B. Pesin, “Characteristic lyapunov exponents and smooth ergodic theory,” *Russian Math. Surveys*, vol. 32, pp. 55–112, 1977.
- [171] G. Benettin, D. Casati, L. Galgani, A. Giorgilli, and L. Sironi, “Apparent fractal dimensions in conservative dynamical systems,” *Physics Letters A*, vol. 118, pp. 325–330, Nov. 1986.
- [172] V. I. Arnold and A. Avez, *Ergodic problems of classical mechanics*. New York: W. A. Benjamin Inc, 1968.
- [173] A. J. Lichtenberg and M. A. Leiberman, *Regular and stochastic motion; 2nd ed.*, ser. Appl. Math. Sci. New York, NY: Springer, 1992.
- [174] A. Provenzale, A. Osborne, and R. Soj, “Convergence of the k2 entropy for random noises with power law spectra,” *Physica D*, vol. 47, pp. 361–372, 1991.
- [175] S. Panchev, *Random functions and turbulence*, ser. International series of monographs in natural philosophy. Pergamon Press, 1971.
- [176] A. Osborne, A. K. Jr., A. Provenzale, and L. Bergamasco, “A search for chaotic behavior in large and mesoscale motions in the pacific ocean,” *Physica D: Nonlinear Phenomena*, vol. 23, no. 13, pp. 75 – 83, 1986.